Temp=-239

DOE/NASA/0131-1
NASA CR-168139

Experimental and Theoretical Study of Combustion Jet Ignition

(NASA-CR-168139) EXPERIMENTAL AND THEORETICAL STUDY OF COMBUSTION JET IGNITION Final Report (California Univ.) 138 p HC A07/MF A01 CSCL 21E

N84-10054

Unclas
G3/07 42339

Daih-Yeon Chen, Ahmed F. Ghoniem,
and Antoni K. Oppenheim
University of California

March 1983

Prepared for
NATIONAL AERONAUTICS AND SPACE ADMINISTRATION
Lewis Research Center
Under Grant NAG 3-131

DEPARTMENT OF ENERGY
Office of Basic Engineering Research
Under Contract W-7405-ENG-48

and

NATIONAL SCIENCE FOUNDATION
Under Grant CPE-8115163

DOE/NASA/0131-1
NASA CR-168139

Experimental and Theoretical Study of Combustion Jet Ignition

Daih-Yeon Chen, Ahmed F. Ghoniem,
and Antoni K. Oppenheim
University of California
Berkeley, California

March 1983

Prepared for
National Aeronautics and Space Administration
Lewis Research Center
Cleveland, Ohio 44135
Under Grant NAG 3-131

Department of Energy
Office of Basic Engineering Research
Under Contract W-7405-ENG-48

and

National Science Foundation
Under Grant CPE-8115163

TABLE OF CONTENTS

NOMENCLATURE

a - Transformed length in the transformed plane for 0.5 H in the physical plane

f - Fractional volume of burned medium in a cell

h_c - Side length of a cell

H - Width of jet exit

i - $\sqrt{-1}$

m - Index for any vortex blob

$\bar{n}_f$ - Unit vector normal to the flame front

P - Non-dimensional pressure

$\bar{r}$ - Position vector (=x+iy) non-dimensionalized by H

$\bar{r}_f$ - Non-dimensional position vector of flame front

r_o - Blob core radius

R_e - Reynolds number ($=\frac{\rho_u U_o H}{\mu}$)

s_c - Strength of combustion generated volumetric source

S_u - Non-dimensional burning rate

t - Time non-dimensionalized by H / U_o

t_i - Time instant for starting combustion

t_o - Time instant for starting ignition

t_p - Time instant for peak pressure

Δt - Non-dimensional time increment

u - X-component velocity in the physical plane

$\bar{u}$ - Velocity vector non-dimensionalized by the jet inlet velocity U_o

U_m - X-component velocity in the transformed plane

U_o - Jet inlet velocity

v - Y-component velocity in the physical plane

V_b - Volume of burned medium

V_c - Volume of a cell

V_m - Y-component velocity in the transformed plane

V_u - Volume of unburned medium

W_b - Complex potential of a blob

W_{bg} - Complex potential of a blob image

W_c - Complex potential of a combustion generated volumetric source

W_{cg} - Complex potential of a combustion generated volumetric source image

W_m - Complex potential of any vortex blob

W_s - Complex potential of a source

x - X coordinate in the physical plane

y - Y coordinate in the physical plane

Z - Complex position coordinate (=x+iy) in the physical plane

ζ - Complex position coordinate in the transformed plane

ζ_b - Complex position coordinate of a blob in the transformed plane

ζ_c - Complex position coordinate of a combustion generated source in the transformed plane

λ - Wave length

μ - Viscosity

ρ_b - Density of burned medium

ρ_u - Density of unburned medium

σ - Standard deviation ($=\sqrt{\frac{2t}{R_e}}$)

ω - Vorticity ($=\nabla\times\vec{u}$)

ω_b - Vortex strength of a blob

∇ - Non-dimensional del operator

∇^2 - Non-dimensional Laplacian operator

$\frac{D}{Dt}$ - Non-dimensional substantial derivative

CHAPTER 1

INTRODUCTION

One of the keys to our energy future is to develop a lean combustion engine that can operate stably and economically using lean mixtures and producing clean emissions[1]. The concept that a lean combustion engine offers distinct advantages[2], both with respect to pollution as well as efficiency, is well known, as attested by the development of stratified charge engines. However, efforts to achieve satisfactory performance under extra-lean conditions have been so far unsuccessful. Most of the difficulties encountered in this connection can be ascribed to an overly localized ignition process. That is, the rate of burning the charge depends on the flame propagation speed, which in lean mixtures is just too slow for satisfactory operation. Thus, attempts to develop a lean combustion engine invariably result in problems associated with excessive emissions of unburned hydrocarbons due to poor flame propagation. To make matters worse, the bulk quenching[3] and the wall quenching effects[4] enhance the emission index of unburned hydrocarbons. These deficiencies can be overcome by the use of multi-point ignition sources since high overall rates of burning in a lean charge can be attained by having the combustion initiated at a multitude of sites distributed throughout the mixtures. The multi-point ignition can be achieved by impregnating the charge with active radicals which enhance the induction process and speed up the onset of exothermic reactions. This can be accomplished by the use of combustion jet ignition system which delivers and distributes the free radicals throughout the combustion chamber with turbulent jets.

The combustion jet ignition system is a promising means for enhanced ignition in I. C. engines with lean premixed charge[5]. The system generates jets of combustion products containing free radicals and discharges them into the combustible medium as ignition sources. These initial concentrations of free radicals serve as substitutes[6] for high initial temperature in the ignition of combustible mixtures. The use of jets of free radicals as ignition sources for combustible mixtures offers the following advantages[7]:

(a) a controllable depth of penetration, so that combustion can be started at any desired location within the charge,

(b) zonal pre-turbulization enhancing the combustion process, and

(c) a wide dispersion resulting in multi-point ignition.

Of particular interest to us is the fact that these three properties of combustion jet ignition can improve the thermal efficiency of the combustion processes in I. C. engines by promoting high overall rates of burning. To illustrate this improvement, consider the following example. In an idealized Otto engine, as shown in Figure 1, the constant volume combustion process 2-3 is where ignition and inflammation processes take place. Prior to the ignition process are the intake process 6-1 and the piston compression process 1-2. The intake valve can induce a significant amount of turbulence[8-9] which persists until ignition. The piston motion during the compression stroke also can induce turbulence, manifested primarily by the roll-up vortices[10-11]. These induced turbulences can strongly influence the ignition processes since they exist prior to ignition. After the inflammation process are the piston expansion process 3-4 and the exhaust processes 4-5 and 5-6. The higher the pressure of state 3, the higher will be the thermal efficiency of the Otto

cycle. The higher pressure of state 3 can be achieved by using the combustion jet ignition which promotes high overall rates of burning. Figure 2 shows the comparison of the pressure-time traces obtained in closed bomb experiments for conventional spark ignition, and combustion jet ignition. The third curve in Figure 2 shows theoretically calculated pressure-time trace for constant volume combustion using CEC-76 computer program[12]. The induction period (t_i-t_o) is shorter for combustion jet ignition than for conventional spark ignition. In addition, the combustion duration (t_p-t_i) is also shorter for combustion jet ignition than for conventional spark ignition. With shorter induction period and combustion duration, combustion jet ignition has higher peak pressure due to fast burning and less energy loss.

A combustion jet ignition system consists of the following five distinct processes:

1. The generation of combustion products containing free radicals.
2. The delivery and distribution of the free radicals by turbulent jets.
3. The induction period.
4. The ignition processes.
5. The inflammation processes.

The understanding of these five processes are crucial to the developments of the combustion jet ignition system, which is one of the proper means of controlled combustion to govern the action of free radicals. These five processes cover the studies of the mechanism of the generation, the delivery and distribution of free radicals, and of the role they play in controlling the combustion processes. Reported here are parts of

the studies:

1. Experimental study of the formation processes of the combustion jets of free radicals. A specially designed igniter with prechamber was used to build up and control the stagnation pressure upstream of the orifice.
2. Theoretical study of the formation processes of the turbulent jets by using Chorin's Random Vortex Method (RVM).
3. Theoretical study of the inflammation processes in the turbulent jets by using RVM implemented with the flame propagation algorithm.

CHAPTER 2

LITERATURE SURVEY

For the study of combustion jet ignition, surveys on both ignition studies and turbulent jets were performed. In this chapter, the literature survey on ignition studies will be presented first, followed by the literature survey on turbulent jets.

2.1 Ignition Studies

Ignition is the initiation of a self-sustained exothermic process of combustion. It is different from inflammation[13] which is the initiation and propagation of a self-sustained flame. Ignition is an essential ingredient of controlled combustion. In order to understand the mechanism of the ignition processes, several ignition systems are being actively investigated by researchers. Among those ignition methods, the following six were selected for literature survey here:

1. Shock Induced Ignition Method.
2. Conventional Spark Ignition Method.
3. Photochemical Ignition Method
4. Flame Jet Ignition Method.
5. Plasma Jet Ignition Method.
6. Combustion Jet Ignition Method.

2.1.1 Shock Induced Ignition Method

The reflected shock tube technique is widely used to obtain data for chemical reaction rates in the high temperature range. This technique provides a test environment of uniform temperature and pressure behind

reflected shock waves for studying the ignition processes. Many interesting and fundamental physical concepts of ignition processes have been reported from shock induced ignition studies[14-17]. These physical concepts of ignition processes are:

1. Ignition has two modes : (i) a constant pressure process representing the case of mild ignitio· . and (ii) an adiabatic process representing the case of strong ignition.
2. The demarkation line between these two modes on the pressure-temperature plane of initial conditions is called the strong ignition limit and is best correlated with the line $(\frac{\partial ln\tau}{\partial T})_P$ = constant for hydrocarbon-oxygen mixtures, where τ is induction period, T is temperature and P is pressure.
3. Higher energy release rates can generate blast waves within a smaller volume of gas in the course of ignition.
4. Higher temperature sensitivity of the induction time can cause a smaller fraction of the gas to be auto-ignited.
5. The dynamic properties of exothermic processes in combustion are due to the evolution of mechanical energy that is manifested by pressure waves which affect the flow field.

2.1.2 Conventional Spark Ignition Method

The conventional spark ignition system supplies energy between 10-50 mJ per electric spark event of a duration of approximately 1 ms and ignites homogeneous and stoichiometric or slightly rich air-fuel mixtures without difficulty. The processes of spark ignition depend on many parameters such as arc energy, peak voltage, duration of discharge, geometry of the spark gap, and the location of the spark relative to the

particular geometry of the compressed charge[5]. Generally, lean mixtures require additional precautions, such as increased electrode distances in the spark plug, prolonged duration, higher energy, etc. In a current detailed study of the new aspects on spark ignition[18-20], some interesting findings of spark ignition were summarized as follows:

1. The detailed structure of the spark event was divided into spark head and glow phases and separated by a transition region.
2. About 10% of the total energy is used to produce the spark plasma within 10 μs during the spark head phase for every spark event.
3. The power input in the spark head phase is very effective and of high importance in the ignition processes.
4. The temperature of the spark head phase is about 60000 K. This high temperature causes the initiation of combustion associated with the generation of a pressure wave in the thin spark channel ($\approx 3\ mm^3$) which starts to expand with supersonic velocity.
5. The temperature of the glow phase of the spark event seems to occur in a temperature range somewhat higher than 1000 K. The energy losses to the electrodes during this relatively long time ($\approx$ 1 ms) become more important. Therefore the glow phase of the spark cannot be as efficient as the spark head phase with regard to energy transferred to the gases.
6. The starting diameter of the spark channel for ignition is determined by the breakdown mechanism. It is possible to increase this starting diameter (or starting volume) by temporal redistribution of the energy of the Capacitor-Discharge ignition without changing the total energy supplied to the spark.

2.1.3 Photochemical Ignition Method

In the studies of chemical kinetics, photochemical techniques were developed to experimentally investigate the photolysis processes. By applying this technique to the studies of ignition processes[21-23], some observations were obtained as listed in the following:

1. Photochemical ignition does not impose a temperature rise but, instead, increases the concentrations of important reaction intermediates and shifts the thermodynamic state of the mixtures into the rapid reaction region via photodissociation.
2. The ignition and flame stabilization can be achieved by using vacuum ultraviolet radiation ($1.45 \times 10^{-5} < \lambda < 1.80 \times 10^{-5}$ cm)
3. The critical concentration of oxygen atoms for igniting a hydrocarbon-air mixture is of an order of 10^{14} atoms/cm^3. Higher initial oxygen atom concentrations can reduce the induction period and enhance flame propagation.
4. At input energies of interest to internal combustion engine systems and for plasmas generated in certain observed fuels, downstream effects of vacuum ultraviolet radiation make no significant contribution to large improvements in the flame initiation observed during ignition by hydrocarbon plasmas.

In addition to vacuum ultraviolet radiation, laser light which is in the visible and infrared regions of the spectrum was also successfully used to ignite the hydrocarbon-air mixtures. The laser beam is focused at a small point within the mixtures to achieve breakdown, thereby generating a plasma kernel, which is approximately 2 cm long and 0.5 cm in diameter, that acts as a site for the source of ignition. The investigations, carried out using an ASTM-CFR engine[24], demonstrated the

following results:

1. The laser ignition system has a more rapid pressure rise than the conventional spark ignition system for all air-to-fuel ratios tested.
2. The conventional spark ignition system would not run with an air-to-fuel ratio above 22.5:1, while with the laser system the maximum air-to-fuel ratio obtained was 27.8:1.
3. Laser systems can reduce specific fuel consumption and have less HC and CO emissions, but have more NO_x emissions.

2.1.4 Flame Jet Ignition Method

The flame jet ignition system can generate a jet of flames that penetrate deeply into the main charge to initiate the inflammation processes. The system initiates the combustion in the prechamber first and causes a pressure difference between the prechamber and main chamber which are connected by a channel. Before the completion of the combustion in the prechamber, the flames are injected, due to the pressure difference, into the main chamber through the inlet channel connected to the prechamber. Depending on the pressure difference, the diameter and the length of the inlet channel wall, the jet of flames can be either laminar or turbulent. As the jet of flames exits the inlet channel at a relatively high velocity, bulk quenching can occur. Furthermore, the jet of flames experiences shearing due to the effects of the channel walls. As a consequence, the jet of flames can be a jet containing a large number of small size turbulent flamelets or bulk quenched turbulent kernels if a high enough degree of turbulence can be achieved.

The flame jet ignition system distributes the jet of flames, which can be bulk quenched, throughout the combustion chamber to initiate the inflammation processes. The inflammation processes initiated by this system have been extensively studied by researchers[6,25-32], but the results of these studies are still controversial and need further investigation. Gussak *et al.*[26-28] define this inflammation process initiated by flame jets as the "LAG" process, *i.e.* avalanche activation of combustion process. Applying his so-called "LAG" process to prechamber engines, Gussak claimed the following:

1. The "LAG" process has nothing to do with the frontal mechanism of combustion. It is associated with the mechanism of bulk inflammation of a combustible mixture. It has an inflammtion delay period.
2. Though the temperature of flame jets is lower than that in the electric discharge of a spark ignition, nevertheless, flame jets can reliably ignite the mixture in the main chamber.
3. Flame jets can ignite a wider range of lean mixtures in the main chamber by a factor of 1.5-2.0 than a conventional electric spark can.
4. The main chemically active center in the combustion products of a rich methane-air mixture is atomic hydrogen.
5. A steady flame jet can stabilize and promote combustion of the main flow of a combustible medium in a combustion channel with no stabilizer. This steady flow of flame jets impinges perpendicular to the main flow at a small subcritical pressure difference (about half the critical value) between the prechamber and the main chamber.

6 For an optimal design of a prechamber system, the prechamber has a relative volume of 2-3% of the main chamber volume and is equipped with outlet channels whose relative cross section is 0.03-0.04 cm^2 per cm^3 prechamber volume. Under these optimal conditions, a mixture of equivalence ratio 1.4-2.5 in the prechamber can provide the highest specific power of the prechamber engine, minimum specific fuel consumption, maximum stability and the widest range of effective leaning of mixture in the main chamber.

Besides Gussak *et al.*, Wang *et al.*[32] in China have also studied flame jet ignition with an application to a simulated rotary combustion engine. They made the following statements:

1. By using lean mixtures, the flame jet igniter produces jets of flame which either ignite the mixture stream in the main chamber or extinguish at the mouth of the prechamber.
2. By using rich mixtures, the flame jet igniter produces jets of flame which become flamelets, traveling along the jet path line for some distance from the outlet. They either extinguish or flash to ignite the mixture stream in the main chamber suddenly.
3. Under the same stream velocity in the main chamber, flame jet ignition using lean mixture is due to high temperature effect, but flame jet ignition using rich mixture is due to active radicals effect.

Based on their theoretical chemical kinetic calculations of the ignition mechanism, Creighton *et al*[6,29,30] do not agree Gussak's theory for the "JAG" process engine. They claimed:

1. The flame propagation is dominated by diffusion of radicals which eliminates any induction period.
2. The buildup of radical concentrations governs the induction period, and the rate of fuel consumption is determined by the steady state radical concentrations.
3. The ignition temperature can be decreased by addition of radicals. This effect becomes especially noticeable when the initial CH_3 concentration is at a level exceeding 1% of the initial concentration of fuel.
4 The calculations show lower radical concentrations for the "LAG" process than those Gussak claimed, but the results are of the same order of magnitude.
5. The "LAG" process is a flame propagation process which does not depend on induction type chemistry. The flame produces enough radicals to achieve steady state radical concentrations ahead of flame.

Finally, Furukawa *et al*[31] in Japan investigated the controllability of the time required for combustion in the main chamber using turbulent flame jets. The results of their studies show that the flame jets first enter the main chamber and then start inflammation. As the orifice diameter decreases, the penetration speed of the leading front of the flame jets becomes higher. Moreover, the combustion duration in the main chamber tends to decrease rapidly for the rich mixture of propane-air and n-butane-air than others.

2.1.5 Plasma Jet Ignition Method

The plasma jet ignition method produces a high temperature plasma in a confined, recessed cavity provided with an orifice. The high temperature plasma is generated so rapidly that the cavity is pressurized, causing a jet of plasma to be discharged through the orifice into the combustible medium as an ignition source. The electric power supply for plasma jet ignition system discharges at a relatively low voltage and high current through the spark which is generated in a conventional manner by a high voltage, low current ignition system.

Considerable research work[33-41] has been done on the studies of plasma jets and their ignition characteristics. Some observations were obtained as listed in the following:

1. Plasma jets enter the main chamber in the form of a turbulent plume which is imbedded in a blast wave headed by a hemispherical shock wave.
2. The blast wave effects are dissipated by the time combustion starts. After a delay typically of an order of 1 msec, ignition takes place in the turbulent zone of the plume.
3. The depth of penetration of the jets is a function of their initial velocity.
4. The burning speed is initially quite high and decreases monotonically as the flame kernel expands.
5. With provisions made to fill the cavity with different feedstocks, the most effective for ignition were hydrocarbons, among which those initially in liquid state were particularly effective.

6. Plasma jets can ignite gaseous mixtures below the normal flammability limit.
7. A plasma jet ignition system requires relatively high electric power, *e.g.* 1 J.
8. The HC and NO emissions are increased and the CO emission is slightly decreased.

2.1.6 Combustion Jet Ignition Method

The combustion jet ignition system can generate jets of combustion products containing free radicals and discharge them into the combustible medium as ignition sources.

The combustion jet ignition method is very similar to the flame jet ignition method. The only difference between these two methods is that the latter method generates a jet of flames and the former method produces a jet of combustion products. The compositions of flame jets are incomplete combustion products containing flames, but the compostions of combustion jets are complete combustion products. In order to study the flame jet ignition mechanism, one has to understand the effect of the degree of incompleteness of combustion products on ignition processes. In doing so, a study of combustion jet ignition, which uses a jet of completely combusted products, has to be performed first. Then the degree of incompleteness for jets of combustion products is varied to study flame jet ignition.

The combustion jet ignition method is also very similar to the EGR ignition method which distributes a virtually infinite number of ignition sources throughout the fresh charge to initiate combustion in bulk at a proper rate of burning. The EGR ignition system is a system using a

sufficiently large amount of exhaust gases to ignite their mixture with the fresh charge. Such a system has been developed, up to commerical application, by Onishi *et al.*[42] with a remarkable proof of clean emissions and higher thermal efficiency.

Up to now there is no literature showing the characteristics of the combustion jet ignition method. But, with the knowledge obtained from both flame jet ignition and EGR ignition studies, a special combustion jet igniter with a prechamber for generating combustion jets has been developed at University of California at Berkeley. The igniter can also generate jets of flames with varying degrees of incomplete combustion for studying flame jet ignition.

2.2 Turbulent Jets

Turbulent jets are the major means of controlled combustion for the delivery and distribution of free radicals, which are essential intermediate constituents. They serve as multi-point ignition sources to improve the thermal efficiency of the combustion processes in a lean combustible mixture. In order to understand the fluid mechanic properties of turbulent jets, a survey of turbulent jets was performed.

Turbulent jets have been extensively studied[43-50] both theoretically and experimentally. The theoretical studies of plane or axi-symmetric steady turbulent jets were performed traditionally using self-similar approximations[43-45]. A recent study[48] used the "pressure-correction" numerical method to approximate two-dimensional, time-dependent turbulent jets. For the case of steady turbulent jets with combustion, *e.g.* fuel jets[45,46], the plane or axi-symmetric fuel jets were approximated using self-similr method implemented with the Schwab-Zeldovich

transformation technique. All the studies discussed above do not show the detailed structure of turbulent jets such as the large-scale eddy structure of turbulent jets.

Turbulent jets have also been investigated experimentally. A variety of experimental data on plane and axi-symmetric turbulent jets without combustion have demonstrated the self-similar feature of turbulent jets[49]. More recent experimental interests are focused on the formation of the turbulent plume with and without combustion[50]. This experimentally observed turbulent plume has been actively investigated by many researchers as mentioned in sections 2.1.4 and 2.1.5, in an attempt to use it as an ignition tool. A detailed experimental study of the axi-symmetric turbulent jets with and without combustion has shown the existence of the large-scale eddy structure of turbulence[47]. The large-scale eddy structure of turbulent jets, as shown in Figure 3, is organized in the form of a staggered array of vortices of alternating circulation. This large-scale eddy structure of turbulent jets, as with other large-scale eddy structures in other turbulent shear flows, dominates the mixing and entrainment processes.

CHAPTER 3

EXPERIMENTAL SETUP

The experimental setup, as shown in Figure 4 in the form of a block diagram, consists of the following systems for a combustion jet ignition study:

1. Combustion Jet Igniter
2. Main Chamber
3. Flow Mixing System
4. Optical System
5. Electric Spark System
6. Trigger Line

3.1 Combustion Jet Igniter

The combustion jet igniter, as shown in Figure 5, was designed to generate jets of combustion products containing free radicals and discharge them into the combustible medium as ignition sources. The igniter has a cylindrical chamber, so-called prechamber, of 1.59 cm in diameter and 4.37 cm in length. The volume of the prechamber is 6.43 cm^3 and can be varied by adding insert sleeves. The prechamber is fitted with gas inlet, purge outlet and jet orifice. The mixtures, coming from the flow mixing device, flow into the prechamber through the gas inlet located at the top of the prechamber. The mixtures can be purged from the prechamber through the purge outlet located at the side wall near the orifice plate. After continuous purging of the prechamber for about 3 minutes, the fresh mixtures are ignited, with both gas inlet and purge outlet valves closed. Ignition in the prechamber is achieved using an electric spark.

The electric spark occurs near the orifice plate between the valve rod head and the electrode protruding from the side wall of the inserted sleeve. The high electric voltage is applied through the high voltage lead to the valve rod. The valve rod head sits on the teflon seat housed in the orifice plate. The orifice plate housing the teflon seat can be interchanged to provide variable-sized orifice diameters.

The motion of the valve rod is controlled by a fast acting 19-SD-40 solenoid. To close the valve, the valve rod is pushed down to seal the orifice by spring force. To open the valve, the valve rod is quickly pulled up by magnetic force induced by the solenoid. The motion of the valve rod is measured by a Bently Nevada displacement transducer of which a calibration curve is shown in Figure 6.

Before the electric spark occurs, the gas inlet and the purge outlet valves are closed with a pressure tight seal, while the orifice is sealed by the valve rod head which is pushed down by a spring. Once the mixtures in the prechamber are ignited and combusted, the prechamber is pressurized by combustion products. The pressure of the prechamber is measured by a Kistler Model # 601 pressure transducer and recorded on a Tektronix Model # 549 storage oscilloscope. The completely combusted products can be discharged into the main chamber through the orifice in the form of jets. This is done by activating the solenoid to open quickly the valve after the peak pressure is reached.

By properly adjusting the timing for opening the valve before combustion is completed, *i.e.*, before peak pressure is reached, the combustion jet igniter can generate jets of flames which are different from jets of combustion products. In order to be able to study the difference between combustion jet ignition and flame jet ignition, a "spik-

ing circuit", as shown in Figure 7, was designed. This allowed the valve to be opened sooner enabling the incomplete combustion products to be discharged into the main chamber if desired. This spiking circuit powers the solenoid by initially raising the voltage across the solenoid coils to 150 volts to overcome the coil's impedence. Once the spiking circuit is triggered, the current flows charge the capacitor and cut the high voltage, leaving 30 volts to keep the solenoid energized. This spiking circuit reduces the activation time, the time required for the solenoid to opening the valve, to 1 ms and cut the total opening time to 6 ms.

3.2 Main Chamber

The main chamber is a cylindrical, stainless steel explosion vessel fitted with optical glass windows 9 cm in diameter with a distance of 9 cm between their inner faces. The volume of the explosion vessel is 572 cm^3, and its viewing cross-sectional area is 64 cm^2. The explosion vessel is fitted with four instrument plugs, one of which is at the top of the vessel and fitted with the combustion jet igniter as shown in Figure 8. Two additional plugs were used for purging and filling the vessel. The last plug was fitted with a Kistler Model # 601 pressure transducer, the pressure signal from which was recorded on a Tektronix Model # 549 storage oscilloscope. The jets of combustion products, coming from the orifice of the prechamber, enter the main chamber fitted with optical glass windows suitable for Schlieren photography. The formation processes of combustion jets in the main chamber, filled with air at atmospheric pressure and temperature, were recorded on high-speed motion picture films. Moreover, if the main chamber is filled with a combustible medium, then the ignition and inflammation processes of the medium caused by combustion jets can be investigated.

3.3 Flow Mixing System

In order to measure the compositions of mixtures used in the prechamber, a continuous flow mixing device was used for the sake of safety and easy operation. A schematic diagram of this system is shown in Figure 9. This system is an modified version of the continuous flow mixing apparatus designed by Kamel[51], which used hypodermic needles to measure flow rates. The advanced system uses jewel orifices to measure flow rates. The flow is insured to be choked flow at the jewel orifice exit by maintaining a stagnation pressure upstream of the orifice at least twice as large as the orifice downstream pressure. Under the critical flow conditions, the mass flow rate through the jewel orifice is a linear function of the upstream stagnation pressure and independent of the orifice downstream pressure. This linear dependence of critical mass flow rate on the orifice upstream stagnation pressure was calibrated for each jewel orifice using a "Precision" Wet Test Meter. The calibration curves for H_2, O_2 and C_3H_8 gases are shown respectively in Figures 10, 11 and 12.

In an attempt to obtain better accuracy of mixture compositions, the continuous flow mixing system with 3 orifices was calibrated again using HP 5750B Gas Chromatograph. The calibration curves are shown in Figures 13, 14 15 and 16. In obtaining these curves, the upstream stagnation pressures of any two orifices were maintained constant but that of the third orifice was allowed to vary. The lowest upstream stagnation pressure of these three orifices was verified as being at least twice the downstream pressure of the orifices, thus insuring critical flow conditions for all orifices.

3.4 Optical System

Schlieren photography was used in all combustion jet ignition experiments to record the formation and the inflammation processes of combustion jets. The main chamber, *i.e.* explosion vessel, was placed in the collimated beam of light created by a conventional Z configuration Schlieren optical system, as shown in Figure 17. The mirrors used were 152 mm in diameter and of 1.22 meter focal length. At the focus of the second mirror was a circular aperture stop or a knife edge to discriminate the deflected light. Additional lenses and filters, not shown in Figure 17, were used to insure proper imaging and exposure of the turbulent plume in the explosion vessel. The Schlieren movies were taken using a 1000 watt Xenon continuous light source and a Hycam high speed camera filming at 5500 frames per second. The timing marks were made on the film by the camera every 1 ms.

3.5 Electric Spark System

The ignition circuit, as shown in Figure 18, used to energize the combustion jet igniter, is similar to the one used by Morganstern *et al*[52]. The device uses a transformer to increase the voltage from 110 volts A. C. to 700 volts A. C.. Then, a rectifier converts the signal to 500 volts D. C. for the primary loop of a standard auto ignition coil. The magnetic field generated by the D. C. voltage is then eliminated by cutting off the applied voltage with an S.C.R. transistor switch. This generates up to 40000 volts in the secondary loop of the ignition coil that can short-circuit the isolated spark gap and produce a spark in the prechamber.

3.6 Trigger Line

As shown in Figure 4, a trigger signal enters the Hycam camera to activate the motion of the film. When the camera attains its pre-set speed for film motion, it sends out 2 signals to trigger respectively the oscilloscope and the ignition circuit. Then, the ignition circuit produces a spark in the prechamber and the oscilloscope gets ready for receiving the pressure transducer signals. In addition, the built-in delay circuit in the oscilloscope sends out a delayed signal to trigger the spiking circuit to activate the solenoid to open the valve. The mixtures, with known compositions, are ignited by the electric spark and combusted to pressurize the prechamber. The valve remains closed until the peak pressure is reached at which time it opens. Once the valve is open, the jets of combustion products are generated and enter the main chamber equipped with optical glass windows for taking Schlieren movies. The formation and the inflammation processes are recorded on the Schlieren movie film by the camera. In addition, the displacement-time trace for valve motion and the pressure-time traces for the prechamber and the main chamber are recorded on the oscilloscope.

CHAPTER 4

EXPERIMENTAL RESULTS

A series of tests were conducted to study the formation process of combustion jets. The experimental data obtained in this study consists of high speed Schlieren movies of combustion jet formation in the main chamber with synchronized pressure and valve motion records. Of particular interest to us are the data of initial jet penetration speed which are listed in Table 1 These initial jet penetration speed were obtained from the linear regression analysis for the jet penetration depth data in the initial stage. The linear regression function for each test run is listed in Table 2. All of the results are grouped into 3 cases and are presented in the following sections.

4.1 Case I

This case used a C_3H_8/Air mixture of equivalence ratio φ = 1.0 in the prechamber to study the formation processes of combustion jets. The prechamber volume was 4.0 cm^3 and its orifice diameter was 3 mm.

Figure 19-a shows the pressure-time trace of combustion in the prechamber with all valves closed. The peak pressure for this test run is 19 psig. This pressure-time trace is used as a reference for comparison in this case study.

Figure 19-b presents the presure-time trace of combustion in the prechamber with valve opening starting at peak pressure. The spiking circuit shown in Figure 7 was not used in this test run. The displacement-time trace, which is an indication of valve motion, is aslo shown in Figure 19-b. The valve starts to open 4 ms after the electric

spark occurs and takes 7 ms to fully open. After the valve opens, the pressure decays at a rate faster than that of the reference pressure in Figure 19-a. The formation processes of the combustion jets for this test run are shown in Figure 20. The jets enter the main chamber, which is filled with air at atmospheric pressure and temperature, through the 3 mm orifice in the form of a turbulent plume. The turbulent plume develops as it travels downstream. There are no flame fronts or inflammation processes observed in this turbulent plume. This is because the turbulent plume consists only of completely combusted products. This is a typical case of combustion jets because the valve opens at or after the peak pressure.

4.2 Case II

In this case study, the spiking circuit was applied to reduce both the delay time required to start opening the valve and the valve opening duration. As shown in Figure 21-a, the prechamber was pressurized up to 24 psig with air, then the valve is suddenly opened using the solenoid applied with or without spiking circuit. The delay time required to start opening the valve is reduced from 4 ms to 2 ms and the valve opening duration was also cut from 7 ms to 4 ms. The prechamber pressure decays faster for the test run with spiking circuit than for that without the spiking circuit. This indicates that the air was discharged into the main chamber through the valve faster for the test run with spiking circuit. These reductions in the time periods for the discharge of the combustion jets into the main chamber are very important in the combustion jet ignition study.

This case again used a C_3H_8/Air mixture of φ = 1.0 to study the formation process of the combustion jet. The valve opening time is varied in

this case to investigate its effect on the turbulent plume formation processes and the jet penetration depth trace. As shown in Figure 21-b, the reference pressure-time trace for this case has a peak pressure of 19 psig. All the results, as shown if Figures 22-27 for this case study are presented in the form of pressure and valve motion records with jet penetration depth trace.

Figure 22 shows the experimental results for a test run with valve opening 3 ms after peak pressure is reached. This time delay for starting valve opening after the peak pressure was found to be consistent with the time period on the 16 mm movie film from the beginning time marker to the first frame of the jets. The pressure-time trace of this test run reproduced the reference pressure-time trace until the valve started opening. When the valve starts opening, the pressure is 11 psig and starts decaying with the production of the combustion jet. The time period for generating the combustion jet for this test run was 4 ms. The jet penetration depth data were obtained by measuring the length from the orifice to the turbulent plume tip which were recorded on the 16 mm Schlieren movie film. The regression line of the jet penetration depth data shows a penetration speed of 24.4 m/sec for the turbulent plume in the initial stage. But, when the turbulent plume travels closer to the bottom wall which is 9 cm from the orifice, its penetration speed decreases monotonically.

Figures 23 and 24 show the experimental results for two test runs with valve opening 2 ms and 1 ms respectively after peak pressure. The pressures at the moment the valve starts opening for these two test runs are 15 psig and 17 psig respectively which are higher than last test run shown in Figure 22. The time period of generating combustion jets for these two test runs is 5 ms. The initial penetration speeds of the tur-

bulent plume for these two test runs are 29.5 m/sec and 30.6 m/sec respectively, and decrease monotonically when they travel closer to the wall.

Figure 25 shows the experimental results for a test run with the valve opening exactly when peak pressure is reached. This peak pressure of 19 psig is the maximum pressure one can use to produce combustion jets for this case study. For this test run the time period for generating combustion jets is 6 ms and the intial penetration speed of the turbulent plume is 30.8 m/sec. The penetration speed again decreases when the turbulent plume travels closer to the wall. The jet penetration depth trace of this test run is compared with that of the test run shown in Figure 22. This comparison, as shown in Figure 26, demonstrated that this test run with higher initial stagnation pressure upstream of the orifice has higher initial penetration speed of combustion jets.

Figure 27 shows the experimental results for a test run with valve opening 2 ms before the reference peak pressure is reached. This is a test run with valve opening starting before combustion in the pechamber is completed. Therefore, combustion in the prechamber continues while the valve is opening. Finally, a peak pressure of 19 psig can be reached. The pressure at the moment the valve starts opening is 14 psig. The time period of generating combustion jets is 5 ms and the initial penetration speed of combustion jets is 27.7 m/sec for this test run. As the turbulent plume travels closer to the wall, its penetration speed decreases monotonically at a rate slower than all the previous test runs. It is interesting to note that the jet penetration depth trace for this test run is quite similar to that for last test run shown in Figure 25. This indicates that continued pressurization due to combustion in the prechamber after the valve

opens can maintain the initial jet penetration speed until the turbulent plume travels very close to the wall. Moreover, it is also found that flame fronts exist in the turbulent plume recorded on the 16 mm Schlieren movie film for this test run. Therefore, this test run should be considered as a test run of flame jets.

The results of this case study can be summarized as follows. The penetration speed of combustion jets is initially constant and decreases monotonically as the combustion jets travel closer to the wall. The constant penetration speed of combustion jets is proportional to the initial stagnation presure of the orifice for the same stoichiometric mixture. A flame jet can be generated with valve opening starting before the reference peak pressure is reached.

4.3 Case III

This case used a CH_4/Air mixture to study the formation process of the combustion. The equivalence ratio of the CH_4/Air mixture is varied in this case to investigate its effect on the turbulent plume formation process. The spiking circuit was also applied in this case.

Figures 28-a and 28-b show the reference pressure-time traces for the CH_4/Air mixture of equivalence ratios φ = 1.0 and φ = 1.2 respec tively. The peak pressure for φ = 1.0 is 18 psig and for φ = 1.2 is 11 psig.

The experimental data including the cinematographic Schlieren records of combustion jets for φ = 1.0 are shown in Figure 29 and 30. This test run of φ = 1.0 starts valve opening at the peak pressue of 18 psig. The time period of generating combustion jets is 5 ms. The initial penetration speed of combustion jets is 22.7 m/sec and decreases monotonically as they travel closer to the wall. The penetration depth trace of this

test run is compared with that of the test run shown in Figure 25. This comparison, as shown in Figure 31, demonstrates that combustion using a stoichiometric C_3H_8/Air mixture in the prechamber shows much higher initial penetration speed of combustion jets than that using a stoichiometric CH_4/Air mixture although the initial stagnation pressure difference between these two test runs is 1 psi. This interesting comparison needs further investigation.

The experimental data including the cinematographic Schlieren records of combustion jets for φ = 1.2 are shown in Figures 32 and 33. This test run of φ = 1.2 starts the valve opening at the peak pressure of 11 psig. The time period of generating combustion jets is 5 ms. The initial penetration speed of combustion jets is 31.6 m/sec and decreases monotonically but not until they are much closer to the wall than in previons cases. The penetration depth trace of this test run is compared with that of the test run shown in Figure 30. This comparison, as shown in Figure 34, demonstrates that combustion using a rich mixture in the prechamber tends to have higher initial penetration speed of combustion jets than that using a stoichiometric mixture although the former has lower initial stagnation pressure than the latter. This interesting observation needs further study.

The experimentaal data including the cinematographic Schlieren records of combustion jets for φ = 1.0 are shown in Figures 35 and 36. This test run starts opening the valve 1 ms after the electric spark. The combustion in the prechamber begins when the valve starts to open. Hence, the combustion cannot pressurize the prechamber up to a higher peak pressure. The peak pressure for this test run is 3 psig and the pressure at the moment the valve starts opening is 1 psig. The time period of

generating combustion jets is 10 ms. The initial penetration speed is 19.5 m/sec which is lower than any previous test runs. This initial penetration speed decreases monotonically when the turbulent plane travels closer to the wall. This is a test run of flame jets. Its jet penetration depth trace is compared with that of the test run shown in Figure 30. The comparison, as shown in Figure 37, indicates that although the initial stagnation pressure upstream of the orifice for flame jets is very low, flame jets have a comparable jet penetration speed as combustion jets. This interesting observation needs further study.

CHAPTER 5

THEORETICAL MODEL AND NUMERICAL TECHNIQUE

In order to interpret and understand the physical phenomena observed in the turbulent jet experiments and furthermore to explain the formation processes of the large-scale eddy structure of turbulent jets, the theoretical studies of the formation and inflammation processes of turbulent jets were performed using Chorin's Random Vortex Method implemented with the flame propagation algorithm. In this chapter, the theoretical models for the problems of turbulent jets with and without combustion are presented first, followed by descriptions of the numerical techniques used to solve the problems.

5.1 Theoretical Model

The problem of turbulent jets in this study is simplified by assuming:

1. The fluid is incompressible and two-dimensional;
2. The pressure of the entire flow field is constant;
3. Gravitational field is neglected; and
4. The decoupled energy equation is neglected.

With consideration of exothermic effects of combustion incorporated into the turbulent flow field, two more assumptions are further made as follows:

5. The flame with a specified constant normal burning relative velocity is an interface where chemical reactions occur infinitely fast between reactants and products having constant but different densities; and

6. The exothermic effects of combustion on the turbulent flow field are manifested by the dynamic effect of combustion generated volumetric sources, flashing over the flow field, and accompanied with the transformation of reactants into products.

After stating the above idealizations, the non-dimensional forms of mathematical models for the two cases without and with combustion are described in sections 5.1.1 and 5.1.2 respectively.

5.1.1 Turbulent Jets without Combustion

The non-dimensional governing equations, Navier-Stokes equations, for the 2-D, incompressible, free jet without combustion are:

Continuity equation $$\nabla \cdot \bar{u} = 0 \qquad (5.1)$$

Momentum equation $$\frac{D\bar{u}}{Dt} = -\nabla P + \frac{1}{R_e}\nabla^2 \bar{u} \qquad (5.2)$$

The initial and boundary conditions for the problem are physically specified as follows:

Initial conditions	$\bar{u} = (0,0)$	for the entire flow field	
Boundary conditions	$\bar{u} = (0,0)$	at the solid boundaries	(5.3)
	$\bar{u} = (0,1)$	at the inlet	

The problem with elliptical governing equations is well posed after all the peripheral boundary conditions and the initial conditions are specified.

If vorticity $\bar{\omega} = \nabla \times \bar{u}$ is used, then the mathematical model is transformed into the following governing equation:

$$\frac{D\bar{\omega}}{Dt} = \frac{1}{R_e}\nabla^2 \bar{\omega} \qquad (5.4)$$

with $\varpi = 0$ for the initial condition

$\varpi = finite$ at all the boundaries satisfying the boundary conditions listed in Equation (5.3) (5.5)

The problem of turbulent jets without combustion remaining to be solved is the governing equation (5.4) expressed in terms of ω with the initial conditions and boundary conditions listed in equation (5.5). The vorticity distributions, determining the turbulent jet flow field, at any time instant are unknowns in this mathematical model and were approximated by using Random Vortex Method. The procedures of obtaining vorticity distributions at any time instant by using Random Vortex Method will be discussed in section 5.2.

5.1.2 Turbulent Jets with Combustion

The mathematical model in section 5.1.1 is further extended to include the combustion processes. Using assumptions 4 and 5 mentioned in section 5.1, the complicated combustion processes are idealized as the transformation of reactants into products at the flame fronts with the combustion generated volumetric sources flashing over the whole flow field. Therefore, the exothermic effects of combustion are expressed in terms of the dynamic effects of combustion generated volumetric sources located at the flame fronts. In order to obtain the volumetric source distributions at any time instant, one has to know the locations of flame fronts which are described by the following flame propagation equation:

$$\frac{D\vec{r}_f}{Dt} = S_u \vec{n}_f \tag{5.6}$$

Now the mathematical model for turbulent jets with combustion can be set up by adding equation (5.6) into the mathematical model of section

5.1.1. The unknowns for the mathematical model with combustion are instantaneous flame front locations, *i.e.* volumetric source distributions, and instantaneous vorticity distributions which determine the turbulent jet flow field with combustion. The volumetric source distributions and vorticity distributions at any time instant in the flow field were approximated by using Random Vortex Method implemented with the flame propagation algorithm. The procedures of obtaining these distributions at any time instant will be discussed in section 5.2

5.2 Numerical Techniques

This section explains the numerical techniques and procedures used to approximate the solutions for the mathematical models listed in section 5.1. The section begins with the explanation of the Random Walk Concept and then performs the Schwarz-Christoffel Transformation which is needed to consider the invisicid interaction of the vortices. Finally, the section explains how the Random Vortex Method and the flame propagation algorithm were used to obtain the vorticity distributions and the volumetric source distributions at any time instant.

5.2.1 Random Walk Concept

The vorticity transport equation (5.4) indicates that if one follows the fluid element with a certain amount of vorticity, then he finds that the time rate of vorticity change is due to the vorticity diffusion. But in terms of the statistical point of view, Chorin proposed the Random Vortex Concept[53-57] to enable us to explain the equation (5.4) as the following idea. If one follows the fluid element with that specified amount of vorticity, then he finds that the motion of the fluid element with a specified amount of vorticity is random. Here the fluid element of finite core and

with a small amount of vorticity is called a vortex blob and its diffusion processes are explained in terms of random motion based on a Gaussian distribution. The mathematical background for the idea of random motion, the so-called random walk, is discussed as follows:

Consider initially imposing a fluid element with a specified amount of vorticity in an infinite motionless domain, then the vorticity transport equation is:

$$\frac{\partial \omega}{\partial t} = \frac{1}{R_e} \nabla^2 \omega \tag{5.7}$$

The solution for equation (5.7) with initial conditions $\omega = \delta$ (r), a delta function at the origin, and boundary conditions $\omega = 0$ at infinity is

$$\begin{aligned} \omega(r,t) &= \left(\frac{4\pi t}{R_e}\right)^{-\frac{1}{2}} \exp\left(-\frac{R_e r^2}{4t}\right) \\ &= \frac{1}{\sqrt{2\pi}\sqrt{\frac{2t}{R_e}}} \exp\left[-\frac{1}{2}\left(\frac{r}{\sqrt{\frac{2t}{R_e}}}\right)^2\right] \\ &= \frac{1}{\sqrt{2\pi}\,\sigma} \exp\left(-\frac{1}{2}\frac{r^2}{\sigma^2}\right) \end{aligned} \tag{5.8}$$

This solution is a zero mean Gaussian Distribution with one standard deviation $\sigma = \sqrt{\frac{2t}{R_e}}$. This distribution can be followed by the normal random variable, named the random walk of the vortex blob with vorticity ω. The normal random variable, *i.e.* random walk, is further assumed to be time-independent to facilitate the study of transient formation processes of turbulent jets. Therefore, the random walk, which assumes the Gaussian Distribution of zero mean and one standard deviation $\sigma = \sqrt{\frac{2t}{R_e}}$, at any time instant $t = m\Delta t$ can be obtained by m times the summation of random walks which follow the Gaussian distribution of zero mean and one standard deviation $\sigma = \sqrt{\frac{2\Delta t}{R_e}}$.

With the use of the random walk concept mentioned above, the displacement of a vortex blob was obtained at any time instant by adding the normal random displacement due to random walk to the expected displacement due to the inviscid interactions between vortex blobs. The procedures in obtaining the vorticity distributions at any time instant are discussed in section 5.2.3.

5.2.2 Schwarz-Christoffel Transformation

In order to facilitate the consideration of the inviscid interactions between vortex blobs or a vortex blob and a source, the Z-plane (physical plane) was transformed into the ζ-plane by performing the following Schwarz-Christoffel transformation:

$$\frac{dZ}{d\zeta} = \frac{1}{\pi}\frac{\sqrt{\zeta^2-1}}{\zeta}$$

where the Z-plane is non-dimensionalized by H and the ζ-plane by a. The Z-plane and ζ-plane were plotted in Figure 38 with points in the Z-plane being conformally mapped into those in the ζ-plane. As a result of this transformation, the uniform flow coming out of the inlet channel was mapped into a source located at the origin in the ζ-plane.

In the ζ-plane, the complex velocities for the following two-dimensional simple flows are modified[57] to be :

$\frac{dW_s}{d\zeta} = \frac{1}{\pi}\frac{1}{\zeta}$ for the source s located at the origin

$\frac{dW_b}{d\zeta} = \frac{-i\omega_b|\zeta-\zeta_b|}{2\pi Max(|\zeta-\zeta_b|, r_o)}\frac{1}{(\zeta-\zeta_b)}$ for any vortex blob b generated from walls

$\frac{dW_c}{d\zeta} = \frac{s_c|\zeta-\zeta_c|}{2\pi Max(|\zeta-\zeta_c|, r_o)}\frac{1}{(\zeta-\zeta_c)}$ for any volumetric source c generated from combustion

where ω_b is vortex strength and s_c is volumetric source strength. The volumetric source strength s_c, is determined[57] to be $\frac{1}{2}(\frac{\rho_u}{\rho_b} - 1)h_c^2\frac{df}{dt}$. The complex velocities here are non-dimensionalized by the uniform velocity U_0 at the inlet of the channel.

To determine the velocity of any vortex blob m induced by other vortex blobs, the source, combustion generated volumetric sources and their images due to the existence of the walls, the complex velocities for every simple flow are superimposed as follows:

$$\frac{dW_m}{d\zeta} = U_m - iV_m = \frac{dW_s}{d\zeta} + \sum_{b \neq m} \frac{dW_b}{d\zeta} + \sum_{bg} \frac{dW_{bg}}{d\zeta} + \sum_{c \neq m} \frac{dW_c}{d\zeta} + \sum_{cg} \frac{dW_{cg}}{d\zeta}$$

where bg stands for the image of vortex blob b and cg stands for the image of volumetric source c.

The induced velocity $\frac{\overline{dW}_m}{d\zeta}(= U_m + iV_m)$ of any vortex blob m is the velocity with which we follow to observe the random walk of this vortex blob m. This material velocity contributes to a displacement, so-called expected displacement in the statistical point of view, which is equal to $\frac{\overline{dW_m}}{d\zeta}$ times Δt. The total displacement during the time period Δt is approximated by adding a normal random displacement to this expected displacement.

5.2.3 Random Vortex Method

The Random Vortex Method has been successfully used to study the turbulent flows of different configurations. The detailed descriptions of this method can be found in references 53 and 57. Presented here are only the brief discussions of the use of this method to study turbulent jets.

As pointed out in section 5.2.1, the equation (5.4) statistically describes the motion of any wall generated vortex blob in the entire turbulent jet flow field. The motion of any vortex blob can be decomposed into two steps. First, the vortex blob undergoes an expected motion due to the inviscid interaction as discussed in section 5.2.2. Then, it has a random motion as described in section 5.2.1. While the expected displacement is calculated by the forward finite difference method as mentioned in section 5.2.2, the random displacement is determined by a randomly generated number from the computer.

In order to update the vorticity distribution at any time step, the equation (5.4) is applied to every vortex blob in the turbulent jet flow field to describe its motion. After the vorticity distribution is updated, satisfaction of the no-slip boundary conditions with generation of vorticity at the walls is checked for the next time step. The generated vorticity is quantized and deposited at the walls This newly generated quantized vorticity becomes vortex blob once it move into the flow field. The vorticity distribution with the newly generated quantized vorticity at the walls is updated again with the method mentioned above. These procedures of both checking the no-slip boundary conditions with generation of quantized vorticity and updating the vorticity distributions are repeated to obtain the vorticity distributions at any time step for turbulent jets.

This Random Vortex Method uses the Prandtl boundary layer assumptions to facilitate the calculations for the vortex blob interactions near the solid boundaries. The flow fields near the solid boundaries are called shear layer regions. The assumptions used in these shear layer regions are (1) $\frac{\partial v}{\partial x} \ll \frac{\partial u}{\partial y}$ and (2) $\frac{\partial^2}{\partial x^2} \ll \frac{\partial^2}{\partial y^2}$. Hence the properties of a vortex blob in these regions are simplified and the term vortex sheet[53] is

applied instead of vortex blob. The newly generated quantized vorticity is called vortex sheet and is allowed to move in the shear layer regions. The vortex sheet diffuses or randomly walks only in the direction perpendicular to the solid boundaries. In addition, the vortex sheet only influences other vortex sheets which are in the shadow region below it. These two properties of vortex sheets reduce a significant amount of computation time. Once vortex sheets move beyond the shear layer regions, they become vortex blobs. Conversely, vortex blobs will become vortex sheets if they move into the shear layer regions. A shear layer region thickness of 3 standard deviations was selected to give best accuracy in the calculations.

5.2.4 Flame Propagation Algorithm

The flame propagation algorithm was developed by Chorin[58] and successfully applied, with the use of the Random Vortex Method, to study the turbulent flow in a combustion tunnel[57]. The algorithm was designed mainly to trace the motion of the flame fronts. Similar to equation (5.4), equation (5.6) describes the motion of the flame fronts in the turbulent jet flow field. The motion of a flame front can be decomposed into two steps. First, the flame front moves in the direction of its normal with a relative velocity taken here as a constant, equal to the appropriate laminar burning velocity of the mixture, S_u . Secondly, the flame front moves with a velocity due to the inviscid interactions as discussed in section 5.2.2.

The motion of the flame front in the first step is due to consumption of the reactants and is called combustion. Combustion transforms reactants into products and generates volumetric sources located at the flame fronts. The combustion generated volumetric sources from the

previous time step are applied to influence the turbulent jet flow field at the current time step and then removed. Here, the exothermic effects of combustion on the turbulent jet flow field are manifested by the dynamic effects of combustion generated volumetric sources flashing over the entire flow field. The method of obtaining the combustion generated volumetric sources is incorporated in the procedures used in section 5.2.3 to update the vorticity distribution at any time step for turbulent jets with combustion.

The flame front is an interface where chemical reactions occur infinitely fast between reactants and products. In order to locate the flame fronts, the flow field is divided into square cells with length h_c. The fraction of volume occupied by products in a given cell is defined as follows:

$$f \equiv \frac{V_b}{V_b + V_u} = \frac{\bar{V}_b}{V_c} \quad \text{where } 0 \leq f \leq 1$$

Thus, $f = 0$ or 1 means that there are, respectively, either reactants or products in the cell, while $0<f<1$ applies to cells containing the flame front interface. Its particular geometry is deduced, depending on the f numbers in neighboring cells. A detailed explanation of the interface geometry can be found in references 57 and 58.

CHAPTER 6

THEORETICAL RESULTS

With the use of the Random Vortex Method implemented with the flame propagation algorithm, four cases of computer simulations for turbulent jets were conducted to study the formation and the inflammation processes of turbulent jets. The typical input data used at the start of calculations are listed in Table 3. The calculated results of these four cases are discussed in the following sections. The purposes of studying these four cases are explained respectively in the following:

1. Case I was designed to study the formation processes of the developing turbulent jets and the behavior of the large-scale eddy structure of turbulent jets at early time. This case simulates the formation processes of a turbulent plume created by the combustion jets, which are turbulent jets of combustion products, before ignition.
2. Case II was designed to study the behavior of the large-scale eddy structure of turbulent jets at later time. This case simulates the turbulent flow field of the developed combustion jets before ignition.
3. Case III was designed mainly to study the inflammation processes in the turbulent jets. This case illustrates the mechanism of the inflammation processes in turbulent jets with a single point ignition source located at the center of the jet exit.
4. Case IV was designed to study and simulate the inflammation processes initiated by a line source located at the jet exit.

6.1 Case I

This case was designed to study the formation processes of the turbulent plume observed in the experiments as discussed in Chapter 4. The calculated results are shown in Figures 40. Instantaneous vorticity distributions are shown on the left and instantaneous velocity vector fields are shown at six downstream locations of 0.5, 3.0, 5.5, 8.0, 10.5 and 13.0 from the jet exit. Nondimensionalized locations are based on the jet exit width.

At the beginning of the computation (Time = 0.00), the entire turbulent jet flow is potential flow, which satisfies the initial condition of zero vorticity in the mathematical model. In the Z-plane, this potential flow is formed by discharging the uniform flow through the inlet channel into the semi-infinite plane as shown in the left of Figure 39. But in the corresponding ζ-plane, the potential flow is formed by assuming a source located in the semi-infinite plane as shown in the right of Figure 39.

Then as the calculations begin, the vortex sheets are generated by satisfying the non-slip boundary conditions at the solid walls. These vortex sheets are transported into the potential flow field as so-called vortex blobs. Vortex blobs of the same sense form a vortex cloud which has characteristics of self-rotating and expanding, causing the flow to recirculate. The vortex blobs produced from the horizontal walls are in the same sense as those produced from the adjacent vertical walls. The former vortex blobs were entrained into the main stream of the turbulent jets and combined with the latter vortex blobs to form two self-rotating and expanding vortex clouds. These two developing vortex clouds, which are of opposite sense, move parallel to each other and form the first vortex pair.

As the calculations continue, the vortex clouds continue growing separately by coalescing with the newly generated vortex blobs of the same sense and hence augmenting the entrainment. These coalescing processes are shown in Figures 40-a,b with this first vortex pair moving downward and its vortex clouds becoming bigger and bigger. Finally, the random nature of the RVM causes the first vortex pair to become anti-symmetric. While the first anti-symmetric vortex pair is growing downstream of turbulent jets, the two incoming streams of vortex blobs are forced to move off the jet centerline and hence have time to form another anti-symmetric vortex pair before becoming entrained into the first vortex pair. This anti-symmetric effect of the vortex pair on forming another anti-symmetric vortex pair causes the vortex pairs to be staggered and forms a large-scale eddy structure of turbulent jets.

It is interesting to note that the first vortex pair triggers the formation of the large-scale eddy structure of turbulent jets. In this study of turbulent jets, the large-scale eddy structure of turbulence, as shown in Figures 40-c,d,e, is constructed by a series of vortex pairs, which are organized in the form of a staggered array of vortex clouds generating local recirculation flow patterns.

This large-scale eddy structure of turbulent jets dominates the formation processes of a turbulent plume. All the fluids coming from the exit of the inlet channel are caused to recirculate by the large-scale eddy structure. The fluids from the left part of the orifice recirculate in a clockwise sense and the other part in a counterclockwise sense. Moreover, the fluids from the region near the inlet channel walls recirculate faster than those from the region far from the inlet channel walls. Therefore, the fluids exiting from the inlet channel are kept together under

recirculation and form a turbulent plume. The penetration speed of this turbulent plume is determined by the strength of the first vortex pair heading the large-scale eddy structure of turbulent jets.

In this case calculations were performed only up to 21 time steps.This case study has demonstrated not only the formation processes of the first vortex pair and turbulent plume, but also the mechanism of developing a large-scale eddy structure. The continuation of calculations becomes very time-consuming and costly because of the large number of vortex blobs (about 4600) produced. In order to continue the calculations and to study the behavior of the large-scale eddy structure of turbulent jets at later times, one has to reduce the generation rate of vortex blobs. The effects of the non-slip horizontal walls on the turbulent jet flow fields are already known from this case study to enhance the development of the first vortex pair with a larger degree of randomness, and hence to augment the large-scale eddy structure of turbulent jets. The assumption of frictionless horizontal walls will be used in the studies of the following cases.

6.2 Case II

In designing this case, the horizontal walls, which were non-slip in the previous case, were assumed to be frictionless here. Hence, the generation of the vortex blobs from the horizontal walls was eliminated to facilitate the caculations. In an attempt to obtain a steady flow, the calculations for this case were conducted up to 66 time steps to simulate the turbulent flow field created by the developed combustion jets. The calculated results are shown in Figures 41 on a scale of 6/10 to those of Figures 40. Instantaneous vorticity distributions are shown on the left. Instantaneous velocity vector fields are shown on the right at six

downstream locations of 0.8, 4.8, 8.8, 12.8, 16.8, 20.8 from the jet exit. Nondimensionalized locations are based on the jet exit width.

Figures 41-a,b,c,d show the developing processes of the first vortex pair as explained in case I. The first vortex pair in this case is formed by two clouds, which are produced only from the vertical walls, of less randomness and smaller size. Therefore, the potential core region of the turbulent jets is longer in this case, and the large-scale eddy structure of the turbulent jets is formed further downstream

As the calculations continue, the two big vortex clouds, which are always associated with the existence of the non-slip solid boundaries, form an anti-symmetric first vortex pair and start introducing the second smaller vortex pair. Gradually, as shown in Figures 41-e,f,g, the second vortex pair develops into an anti-symmetric form due to the anti-symmetric effect of the first vortex pair. The second vortex pair also introduces the third vortex pair, while itself being entrained into the first vortex pair. The second vortex pair finally coalesces with the first vortex pair to form a bigger, more anti-symmetric first vortex pair. The third vortex pair hence becomes the second vortex pair and is influenced by the first vortex pair to become more anti-symmetric. As calculations continue further, the third, the fourth, and subsequent vortex pairs are formed, as shown in Figures 41-h,i,j,k,l,m,n, using the same mechanism as the second vortex pair. This series of vortex pairs is becoming bigger, more anti-symmetric due to the anti-symmetric effect resulting from the preceding vortex pair and by coalescing with the successive vortex pairs. The vortex pair formed near the jet exit finally will be entrained into the first vortex pair by coalescing itself with the preceding vortex pair. This process enables the development of the large-scale eddy structure, which

is organized in the form of a staggered array of vortex clouds, of greater amplitude further downstream. This large-scale eddy structure of turbulent jets dominates not only the entrainment and mixing processes but also the entire turbulent flow field.

6.3 Case III

This case was designed to study the mechanism of the inflammation processes in turublent jets. A single point ignition source was applied at the center of the jet exit at the beginning of the calculations. The results of calculations are shown in Figures 42 with the instantaneous vorticity distributions on the left and the instantaneous flame front locations on the right. The scale of these figures is same as that of Figures 41.

As the calculations begin, the large-scale eddy structure develops in a mechanism similar to that described in Case II. In addition, the formation of the large-scale eddy structure in this case is under the influence of the exothermic effects of combustion. The large-scale eddy structure for this case is augmented in such a way that the first vortex pair is bigger in size, and the potential core region is shorter in length. Hence, the inflammation processes can enhance the formation processes of the large-scale eddy structure of turbulent jets.

As discussed in Cases I and II, the large-scale eddy structure dominates the entire turbulent jet flow field. In this case, the large-scale eddy structure also demonstrates its control over the flame propagation processes. That is, the flame fronts, with a prescribed normal burning speed (S_u = 0.02), are carried by the turbulent flow field. Of particular interests is that the flame fronts are carried by the recirculatiing flow fields created by the large-scale eddy structure of turbulent jets.

Besides, the recirculation flow fields also keep the burnt mixture together to form a turbulent plume with combustion. The penetration speed of this turbulent plume is determined, instead of by the normal burning rate, primarily by the strength of the first vortex pair heading the large-scale eddy structure of turbulent jets enclosed within the flame fronts. Therefore, the inflammation processes and the flame shape for this case of relatively small normal burning speed are determined by the large-scale eddy structure, as well as where and when the ignition source occurs in the turbulent flow field.

This case performed calculations up to 21 time steps and illustrated the effects of inflammation on turbulence, and vice versa. For the sake of brevity, the case only used a single point ignition source located at the center of the jet exit to study the mechanisms of the inflammation processes in turbulent jets and the formation processes of a turbulent plume with combustion. The next case considers 5 point ignition sources to study the inflammation processes initiated by combustion jets. The 5 point ignition sources form a line ignition source at the jet exit.

6.4 Case IV

This case was designed with an attempt in mind to simulate the inflammation processes initiated by combustion jets. The case assumes that the mixtures coming out of the exit are complete combustion products. Moreover, the case assumes that no induction period is needed for the initiation and propagation of the self-sustained flames. In addition, this case assumes to have a line ignition source at the exit of turbulent jets. The calculations begin with the flames starting to propagate from the jet exit. The results of calculations are shown in Figures 43 with the instantaneous flame fronts superimposed on the instantaneous vorticity

distributions. The scale of these figures is the same as that of Figures 41.

As the calculations continue, the large-scale eddy structure develops by the same mechanism as described in Case III. The turbulent plume with combustion also develops in the same way as described in Case III. The large-scale eddy structure again can dominate the entire turbulent jet flow field and the inflammation processes in it.

As the calculations continue further, the large-scale eddy structure develops itself into a staggered array of vortex clouds which create local recirculation flows, causing the turbulent plume to have more wrinkled flame fronts. The recirculation flows also keep the burnt gases together, as they did in Case III, but producing a flame shape which is different from that in Case III. This illustrates that the flame shape and inflammation processes have a strong dependence on the number and the locations of the ignition sources deposited into turbulent jets. The penetration speed of a turbulent plume with combustion is also determined, instead of by the normal burning rate, primarily by the strength of the first vortex pair heading the large-scale eddy structure of turbulent jets enclosed within the flame fronts.

The case performed calculations up to 36 time steps and again illustrated the effects of the large-scale eddy structure on the flame shape and inflammation processes of turbulent jets.

CHAPTER 7

CONCLUSIONS

The conclusions for this combustion jet ignition study are summarized below:

1. A combustion jet ignition system was developed to generate turbulent jets of combustion products containing free radicals and to discharge them as ignition sources into the combustible medium.
2. Experimentally, the penetration speed of combustion jets has been found to be constant initially and decreases monotonically as turbulent jets of combustion products travel closer to the wall.
3. The initial penetration speed of combustion jets is proportional to the initial stagnation pressure upstream of the orifice for the same stoichiometric mixture.
4. Combustion using a C_3H_8/Air mixture in the prechamber shows higher initial penetration speed of combustion jets than that using a CH_4/Air mixture although the initial stagnation pressure difference between these two test runs is 1 psi. This is a primitive study and needs further investigation.
5. For combustion using a CH_4/Air mixture in the prechamber, the initial penetration speed of combustion jets is higher for rich mixture than for stoichiometric mixture although the former has lower initial stagnation pressure than the latter. This is a primitive study and needs further investigation.

6. The Random Vortex Method is a very useful tool for studying the large-scale eddy structure of turbulent jets.
7. The first vortex pair triggers the formation of the large-scale eddy structure of turbulent jets.
8. The large-scale eddy structure of turbulent jets is constructed by a series of vortex pairs, which are organized in the form of a staggered array of vortex clouds generating local recirculation flow patterns.
9. The large-scale eddy structure dominates the formation processes of turbulent jets or experimentally observed turbulent plumes.
10. The flame fronts are carried by the recirculating flow fields created by the large-scale eddy structure. In addition, the recirculation flow fields keep the burnt mixture together, forming a turbulent plume with combustion.
11. The large-scale eddy structure dominates the inflammation processes in turbulent jets.
12. The flame shape and inflammation processes have a strong dependence on the number and the locations of the ignition sources deposited into turbulent jets.

REFERENCES

1. Oppenheim, A. K., and Weinberg, F. J., "Combustion R & D: Key to Our Energy Future," Astronautics & Aeronautics, pp. 22-31, November 1974.

2. Oppenheim, A. K., "Prospects for Internal Combustion Engines among Advanced Energy Conversion Systems," Proceedings of the 13th Intersociety Energy Conversion Engineering Conference, Vol. **2**, pp. 1192-1200, SAE, Inc., Warrendale, Pa., 1978.

3. Smith, O. I., Westbrook, C. K., and Sawyer, R. F., "Lean Limit Combustion in an Expanding Chamber," 17th Symposium (International) on Combustion, The Combustion Institute, 1979.

4. Ishikawa, N., and Daily, J. W., "Model Engine Studies of Hydrocarbon Quenching," 17th Symposium (International) on Combustion, The Combustion Institute, 1979.

5. Dale, J. D., and Oppenheim, A. K., "Enhanced Ignition for I. C. Engines," SAE Paper 810146, 1981.

6. Guirguis, R. H., Oppenheim, A. K., Karasalo, I., and Creighton, J. R., "Thermochemistry of methane Ignition," Progress in Astronautics and Aeronautics, **76**, AIAA, New York, 134-153, 1981.

7. Oppenheim, A. K., Teichman, K., Hom, K., and Stewart, H. E., "Jet Ignition of an Ultra-Lean Mixture," SAE Paper 780637, 1978.

8. Lancaster, D. R., Krieger, R. B., Sorenson, S. C., and Hull, W L., "Effects of Turbulence on Spark-Ignition Engine Combustion," SAE Paper 760160, 1976.

9. Huebner, K. H., and McDonald, A. T., "Experimental Determination of Airflow Patterns in Piston Engines with Induction Swirl," SAE Paper 720026, 1972.

10. Oppenheim, A. K., Cheng, R. K., Teichman, K., Smith, O I., Sawyer, R F., Hom, K., and Stewart, H. E., "A Cinematographic Study of Combustion in an Enclosure Fitted with a Reciprocating Piston," Stratified Charge Engines, Institute of Mechanical Engineering Conference Publications 1976-11, 1976.

11. Daneshyar, H., Fuller, D. E., and Dekker, B. E. L., "Vortex Motion Induced by the Piston of an Internal Combustion Engine," Int. J. Mech. Sci., Vol. **15**, 1973.

12. Gordon, S., and McBride, B. J., "Computer Program for Calculation of Complex Chemical Equilibrium Compositions, Rocket Performance, Incident and Reflected Shocks, and Chapman-Jouguet Detonations," NASA SP-273, 1976.

13. Oppenheim, A. K., "Ignition Studies," LBL-5068, Lawrence Berkeley Laboratory, February 1982.

14. Oppenheim, A. K., Cohen, L. M., Short, J. M., Cheng, R. K., and Hom, K., "Shock Tube Studies of Exothermic Processes in Combustion," Shock Tube Research Society, Japan, 1975.

15. Vermeer, D. J., Meyer, J. W., and Oppenheim, A. K., "Auto-Ignition of Hydrocarbons Behind Reflected Shock Waves," Combustion and Flame **18**, 327-336, 1972.

16. Meyer, J. W., and Oppenheim, A. K., "On the Shock-Induced Ignition of Explosive Gases," 13th Symposium (International) on Combustion, The Combustion Institute, 1970.

17. Oppenheim, A. K., Cohen, L. M., Short, J. M., Cheng, R. K. and Hom, K., "Dynamics of the Exothermic Process in Combustion," 15th Symposium (International) on Combustion, The Combustion Institute, 1974.

18. Albert, H., Bloss, W. H., Herden, W., Maly, R., Saggau, B., and Wagner, E., "New Aspects on Spark Ignition," SAE Paper 770854, 1977.

19. Maly, R., and Vogel, M., "Initiation and Propagation of Flame Fronts in Lean CH_4-Air Mixtures by the Three Modes of the Ignition Spark," 17th Symposium (International) on Combustion, The Combustion Institute, 1979.

20. Maly, R., "Ignition Model for Spark Discharges and the Early Phase of Flame Front Growth," presented at the 18th Symposium (International) on Combustion, The Combustion Institute, 1980.

21. Cerkanowicz, A. E., and McAlevy III, R. F., "Photochemical Ignition and Combustion Enhancement in High Speed Flows of Fuel-Air Mixtures," AIAA Paper No. 73-216, 1973.

22. Cerkanowicz, A. E., "Radiation Augmented Combustion," Interim Report AFOSR-TR-79-1096, 1979.

23. Orrin, J. E., Vince, I. M., and Weinberg, F. J., "Ignition by Radiation from Plasmas," Combustion and Flame **37**, 91-93, 1980.

24. Dale, J. D., Smy, P. R., and Clements, R. M., "Laser Ignited Internal Combustion Engine-An Experimental Study," SAE Paper 780329, 1978.

25. Wyczalek, F. A., Harned, J. L., Maksymiuk, S., and Blevins, J. R., "EFI Prechamber Torch Ignition of Lean-Mixtures," SAE Paper 750351, 1975.

26. Gussak, L. A., "High Chemical Activity of Incomplete Combustion Products and a Method of Prechamber Torch Ignition for Avalanche Activation of Combustion in Internal Combustion Engines," SAE Paper 750890, 1975.

27. Gussak, L. A , "The Role of Chemical Activity and Turbulence Intensity in Prechamber-Torch Organization of Combustion of a Stationary Flow of a Fuel-Air Mixture," SAE Report, 1979.

28. Gussak, L. A., Karpov, V. P., and Tikhonov, Yu. V., "The Application of Lag-Process in Prechamber Engines," SAE Paper 790692, 1979.

29. Creighton, J. R., "A Critique of the Theory for Gussak's 'LAG Process' Engine," SAE Paper 790249, 1979.

30. Creighton, J. R., and Oppenheim, A. K., "Control of the Rate of Methane Oxidation by Quasi-Equilibrium Radical Concentrations," LLL Report, 1979.

31. Furukawa, Junichi, and Gomi, Tsutomu, "On the Propagation of Turbulent Jet-Flame in a Closed Vessel," SAE Paper 810777, 1981.

32. Wang, T. S., Zhang, Y. F., Zhao, H. F., Qi, Z. M., and Ren, A. F., "A Study of Ignition by Flame Torches," 18th Symposium (International) on Combustion, The Combustion Institute, 1980.

33. Weinberg, F. J., Hom, K., Oppenheim, A. K., and Teichman, K., "Ignition by Plasma Jet," Nature , Vol. **272**, pp. 341-343, 1978.

34. Cetegen, B., Teichman, K. Y., Weinberg, F. J., and Oppenheim, A. K., "Performance of a Plasma Jet Igniter," SAE Paper 800042, 1980.

35. Teichman, K. Y., "Study of Jet Ignition for Lean Mixtures," Ph. D. Thesis, University of California, Berkeley, 1978.

36. Cetegen, B. M., "Study of Performance of a Plasma Jet Igniter," M. S. Thesis, University of California, Berkeley, 1979.

37. Wyczalek, F. A., Frank, D. L., and Neuman, J. G., "Plasma Jet Ignition of Lean Mixtures," SAE Paper 750349, 1975.

38. Asik, J. R., Piatkowski, P., Foucher, M. J., and Rado, W. G., "Design of a Plasma Jet Ignition System for Automotive Application," SAE Paper 770355, 1977.

39. Orrin, J. E., Vince, I. M., and Weinberg, F. J., "A Study of Plasma Jet Ignition Mechanism," 18th Symposium (International) on Combustion, The Combustion Institute, 1980.

40. Harrison, A. J., and Weinberg, F. J., "Flame Stabilization by Plasma Jets," Proc. Roy. Soc. Lond. A. **321**, pp 95-103, 1971.

41. Hilliard, J. C., and Weinberg, F. J., "Effect of Nitrogen-Containing Plasmas on Stability, NO Formation and Sooting of Flames," Nature ,Vol. **259**, 1976.

42. Onishi, S., Jo, S. H., Shoba, K., Jo, P. D., and Kato, S., "Active Thermo-Atmosphere Combustion (ATAC) - A New Combustion Process for Internal Combustion Engines," SAE Paper 790501.

43. Schlichting, H., Boundary-Layer Theory, McGraw-Hill, Six Edition, 1966.

44. White, F. M., Viscous Fluid Flow, McGraw-Hill, 1974.

45. Kanury, A. F., Introduction to Combustion Phenomena, Gardon and Breach, Second Edition, 1977.

46. Lewis, B., and von Elbe, G., Combustion, Flames, and Explosions of Gases, Academic Press, Second Edition, 1961.

47 Dimotakis, P. E., Miake-Lye, R. C., and Papantoniou, D. A., "Structure and Dynamics of Round Turbulent Jets," GALCIT Report FM 82-01, 1982.

48. Hengrussamee, Dhawatchai, "Mixing of Hot Starting-Jets with Cold Surroundings," Ph. D. Thesis, Imperial College, London, 1975.

49. Abramovich, G. N., The Theory of Turbulent Jets, M.I.T., 1963.

50. Scorer, R. S., Environmental Aerodynamics, Ellis Horwood Limited, 1978.

51. Kamel, M. M., Lundstrom, E., and Oppenheim, A. K., "Apparatus for Continuous Flow Mixing of Explosive Gases," Jounal of Physics E., Vol. **1**, 1968.

52. Morganstern, B., Dale, J. D., Smy, P. R., and Clements, R. M., "Low Temperature Starting of a Diesel Engine Using Time Spark Discharge," Canadian Combustion Institute Meeting, 1981.

53. Chorin, A. J., and Marsden, J. E., A Mathematical Introduction to Fluid Mechanics, Springer-Verlag, New York, 1979.

54. Chorin, A. J., "Vortex Sheet Approximation of Boundary Layers," J. Comp. Phys., **27**, June 1978.

55. Chorin, A. J., "Vortex Models and Boundary Layer Instability," SIAM J. Sci. Stat. Comput., **1**, March 1980.

56. Chorin, A. J., "Numerical Studies of Slightly Viscous Flow," J. Fluid Mech., Vol. **57**, pp. 785-796, 1973.

57. Ghoniem, A. F., Chorin, A. F., and Oppenheim, A. K., "Numerical Modelling of Turbulent Flow in a Combustion Tunnel," Phil. Trans. R. Soc. Lond., **A 394**, 303-325, 1982.

58. Chorin, A. J., "Flame Advection and Propagation Algorithm," J. Comp. Phys., 1980. 6

Table 1

Jet Penetration Speed for Combustion Jets Experiments

Case	Figure	Mixture	φ	t_i (ms)	P_{0i}(psig)	V_i(m/sec)
II	22	C_3H_8/Air	1.0	+3	11	24.4
II	23	C_3H_8/Air	1.0	+2	15	29.5
II	24	C_3H_8/Air	1.0	+1	17	30.6
II	25	C_3H_8/Air	1.0	0	19	30.8
II	27	C_3H_8/Air	1.0	-2	14	27.7
III	30	CH_4/Air	1.0	0	18	22.7
III	33	CH_4/Air	1.2	0	11	31.6
III	36	CH_4/Air	1.0	*	1	19.5

φ - Equivalence ratio.

P_{0i} - Initial stagnation pressure upstream of the orifice.

V_i - Initial penetration speed.

t_i - Valve opening time after (+) or before (-) peak pressure.

* - Valve opening 1 ms after electric spark.

Table 2

Linear Regression Functions

(Y = AT + B)

Case	Figure	A(m/sec)	B(m)	r
II	22	24.38	2.53×10^{-3}	0.996
II	23	29.47	-9.20×10^{-5}	0.996
II	24	30.62	2.05×10^{-4}	0.996
II	25	30.80	3.26×10^{-4}	0.994
II	27	27.67	2.02×10^{-3}	0.999
III	30	22.69	3.02×10^{-3}	0.997
III	33	31.56	1.14×10^{-3}	0.999
III	36	19.50	9.49×10^{-4}	0.998

r - Correlation coefficient

Y - The estimated jet penetration depth

A - Slope of the least squares line of the jet penetration depth data

B - Y-intercept of the least squares line of the jet penetration depth data

T Time (second)

Table 3

Input Data for Turbulent Jets Calculations

Reynolds number	10000
Width of jet exit	1.0
Time increment	0.1
Space increment	0.2
Length of each vertical wall	0.2
Length of each horizontal wall	4.5
Side width of a cell	0.2
Normal burning speed	0.02
Density ratio (Reactants/Products)	6.0
Strength of a vortex blob	0.05
Minimum strength of a combustion generated source	0.001
Standard deviation	4.47×10^{-3}
Shear layer thickness	1.34×10^{-2}

FIGURE CAPTIONS

Fig. 1 Idealized Otto cycle

Fig. 2 Comparison of pressure-time traces

Curve 1 - Obtained in closed bomb experiments using conventional spark ignition

Curve 2 - Obtained in closed bomb experiments using combustion jet ignition

Curve 3 - Obtained from theoretical calculation for constant volume combustion using CEC-76 computer program

Fig. 3 Jet fluid field in the plane of symmetry of the jet. Reynolds number = 2500, d = 0.3 in, $0 < x/d < 35$ (from Dimotakis *et al*)

Fig. 4 Block diagram of experimental setup

Fig. 5 Schematic diagram of combustion jet igniter

Fig. 6 Calibration curve for a displacement transducer

Fig. 7 Schematic diagram of the spiking circuit

Fig. 8 Main chamber fitted with combustion jet igniter

Fig. 9 Schematic diagram of the continuous flow mixing device

Fig.10 Critical flow rate calibration curves for N_2-orifice

Fig.11 Critical flow rate calibration curves for O_2-orifice

Fig.12 Critical flow rate calibration curves for C_3H_8-orifice

Fig.13 Calibration curve of C_3H_8/O_2 for continuous flow mixing device

Fig.14 Calibration curves of N_2/O_2 for continuous flow mixing device

Fig.15 Calibration curves of C_3H_8/Air for continuous flow mixing device

Fig.16 Calibration curves of CH_4/Air for continuous flow mixing device

Fig 17 Schematic diagram of Schlieren optical system

Fig.18 Schematic diagram of ignition circuit for combustion jet igniter

Fig.19-a Pressure-time trace for combustion of C_3H_8/Air mixture (φ = 1.0) in the prechamber with all valves closed (Reference pressure-time trace for case I)

Fig.19-b Pressure-time and displacement-time traces for combustion of C_3H_8/Air mixture (φ = 1.0) in the prechamber with valve opening at peak pressure (without spiking circuit)

Fig 20 Cinematographic Schlieren records of combustion jets in the main chamber filled with air at atmospheric pressure and temperature (without spiking circuit)

Mixture : C_3H_8/Air (φ = 1.0)

Orifice diameter : 3 mm

Fig 21-a The effect of the spiking circuit on the valve motion and the pressue-time trace

Fig 21-b Pressure-time trace for combustion of C_3H_8/Air mixture (φ = 1.0) in the prechamber with all valves closed. (Reference pressure-time trace for case II)

Fig.22 Experimental data for a test run with valve opening 3 ms after peak pressure

Mixture : C_3H_8/Air (φ = 1.0)

Fig.23 Experimental data for a test run with valve opening 2 ms after peak pressure

Mixture : C_3H_8/Air (φ = 1.0)

Fig.24 Experimental data for a test run with valve opening 1 ms after peak pressure

Mixture : C_3H_8/Air (φ = 1.0)

Fig 25 Experimental data for a test run with valve opening at peak pressure

Mixture : C_3H_8/Air (φ = 1.0)

Fig.26 Comparison of jet penetration depth traces between two test runs with valve opening at peak pressure and 3 ms after peak pressure

Fig.27 Experimental data for a test run with valve opening 2 ms before peak pressure

Mixture : C_3H_8/Air (φ = 1.0)

Fig.28 Pressure-time traces for combustion of CH_4/Air mixture in the prechamber with all valves closed (Reference pressure-time traces for case III) (a) φ = 1.0 (b) φ = 1.2

Fig.29 Cinematographic Schlieren records of combustion jets in the main chamber filled with air at atmospheric pressure and temperature (with spiking circuit)

Mixture : CH_4/Air (φ = 1.0)

Orifice diameter : 3 mm

Valve opening : at peak pressure

Fig 30 Experimental data for a test run with valve opening at peak pressure

Mixture : CH_4/Air (φ = 1.0)

Fig.31 Comparison of jet penetration depth traces between two test runs with CH_4/Air mixtures and C_3H_8/Air mixtures

Fig.32 Cinematographic Schlieren records of combustion jets in the main chamber filled with air at atmospheric pressure and temperature (with spiking circuit)

Mixture : CH_4/Air (φ = 1.2)

Orifice diameter : 3 mm

Valve opening : at peak pressure

Fig.33 Experimental data for a test run with valve opening at peak pressure

Mixture : CH_4/Air (φ = 1.2)

Fig.34 Comparison of jet penetration depth traces between two test runs with CH_4/Air mixtures of equivalence ratios φ = 1.0 and φ = 1.2

Fig.35 Cinematographic Schlieren records of combustion jets in the main chamber filled with air at atmospheric pressure and temperature (with spiking circuit)

Mixture : CH_4/Air (φ = 1.0)

Orifice diameter : 3 mm

Valve opening : 1 ms after electric spark

Fig 36 Experimental data for a test run with valve opening 1 ms after electric spark

Mixture : CH_4/Air (φ = 1.0)

Fig 37 Comparison of jet penetration depth traces between two test runs with valve opening at peak pressure and 1 ms after electric spark

Fig.38 Schwarz-Christoffel transformation of Z-plane into ζ-plane

Left : Physical plane or Z-plane

Right : Transformed plane or ζ-plane

Fig 39 Streamline patterns of initial flow of turbulent jets in Z-plane (left) and ζ-plane (right)

Fig 40 Computer plots of turbulent jets without combustion for R_e = 10000

Left : Instantaneous vorticity distribution

Right : Instantaneous velocity field

(a) Time = 1 (b) Time = 6 (c) Time = 11 (d) Time = 16

(e) Time = 21

Fig.41 Computer plots of turbulent jets without combustion for R_e = 10000, assuming smooth horizontal walls

Left : Instantaneous vorticity distribution

Right : Instantaneous velocity field

(a) Time = 1 (b) Time = 6 (c) Time = 11 (d) Time = 16

(e) Time = 21 (f) Time = 26 (g) Time = 31 (h) Time = 36

(i) Time = 41 (j) Time = 46 (k) Time = 51 (l) Time = 56

(m) Time = 61 (n) Time = 66

Fig.42 Computer plots of turbulent jets with combustion for R_e = 10000, S_u = 0.02, smooth horizontal walls and a single point ignition source located at the center of the jet exit

Left : Instantaneous vorticity distribution

Right : Instantaneous flame front locations

(a) Time = 1 (b) Time = 6 (c) Time = 11 (d) Time = 16

(e) Time = 21

Fig.43 Computer plots of turbulent jets with combustion for R_e = 10000, S_u = 0.02 smooth horizontal walls and a line ignition source located at the jet exit

(a) Time = 1 (b) Time = 6 (c) Time = 11 (d) Time = 16

(e) Time = 21 (f) Time = 26 (g) Time = 31 (h) Time = 36

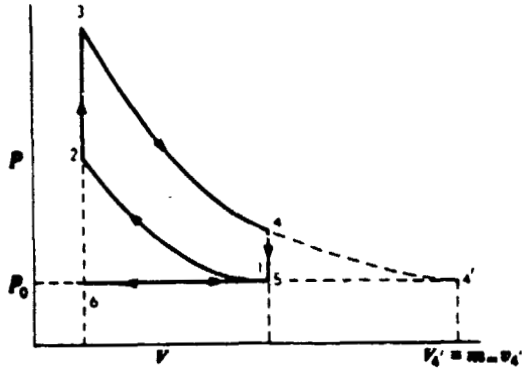

Process 1-2 : Isentropic compression stroke
Process 2-3 : Constant-volume combustion
Process 3-4 : Isentropic expansion stroke
Process 4-5 : Constant-volume and adiabatic exhaust blowdown
Process 5-6 : Constant-pressure and adiabatic exhaust stroke
Process 6-1 : Constant-pressure and adiabatic intake stroke

Figure 1

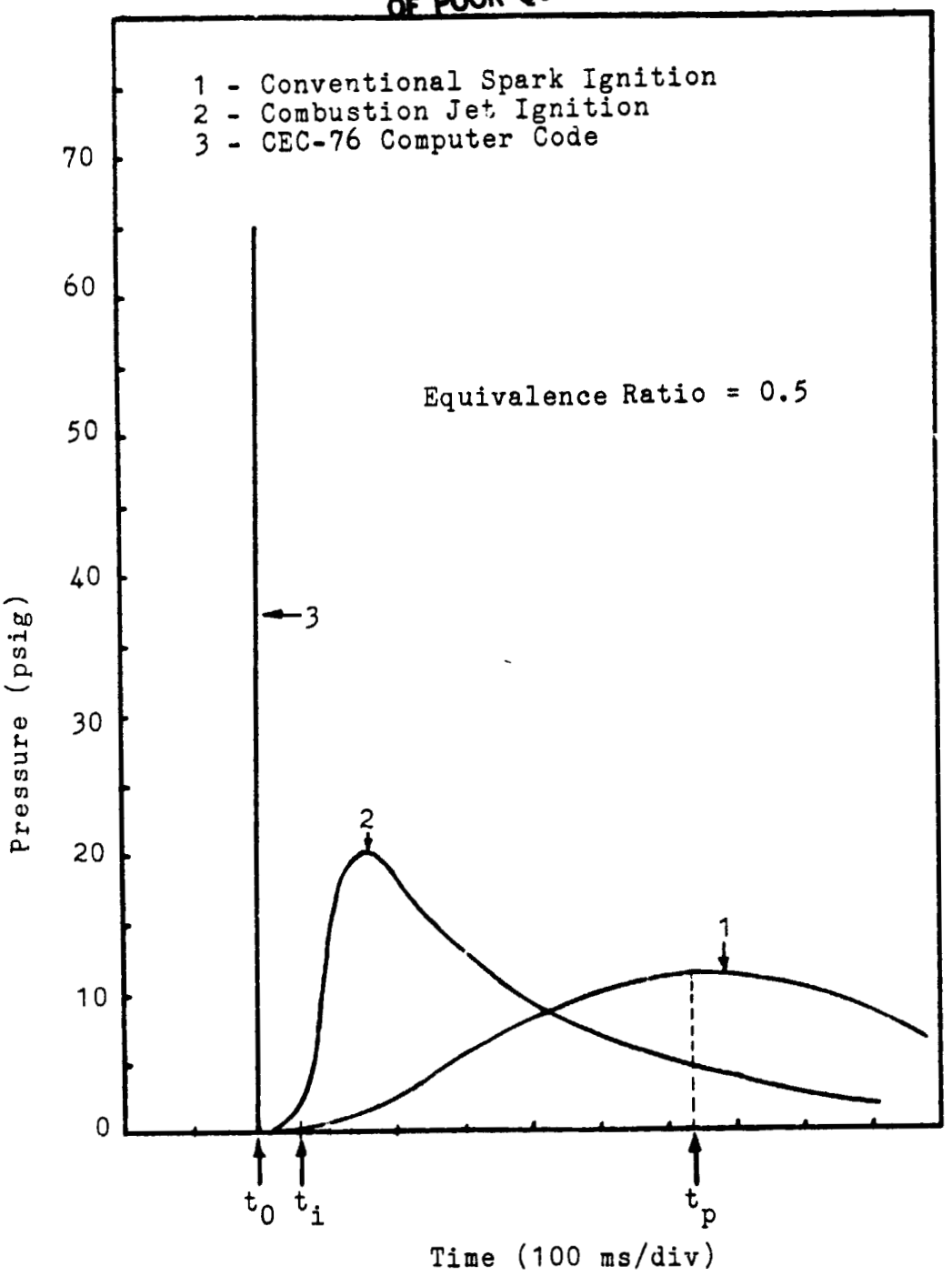

Figure 2

Figure 3

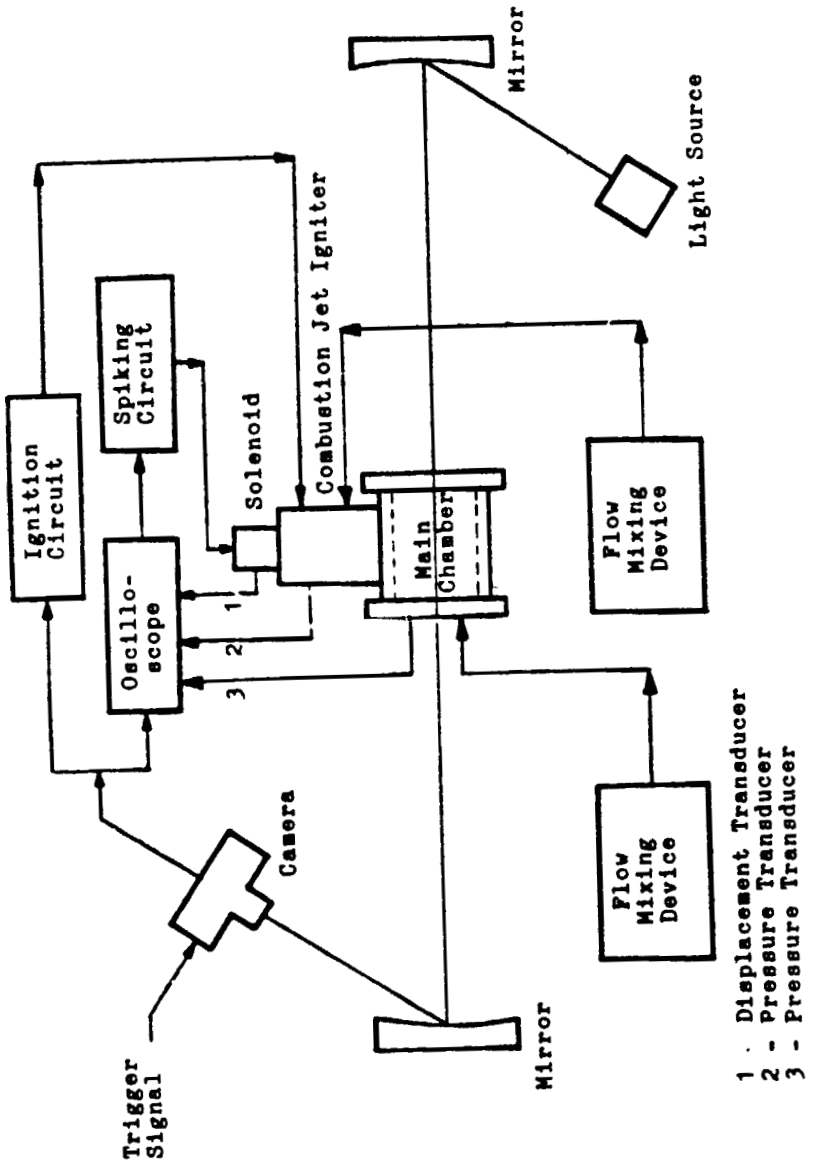

Figure 4

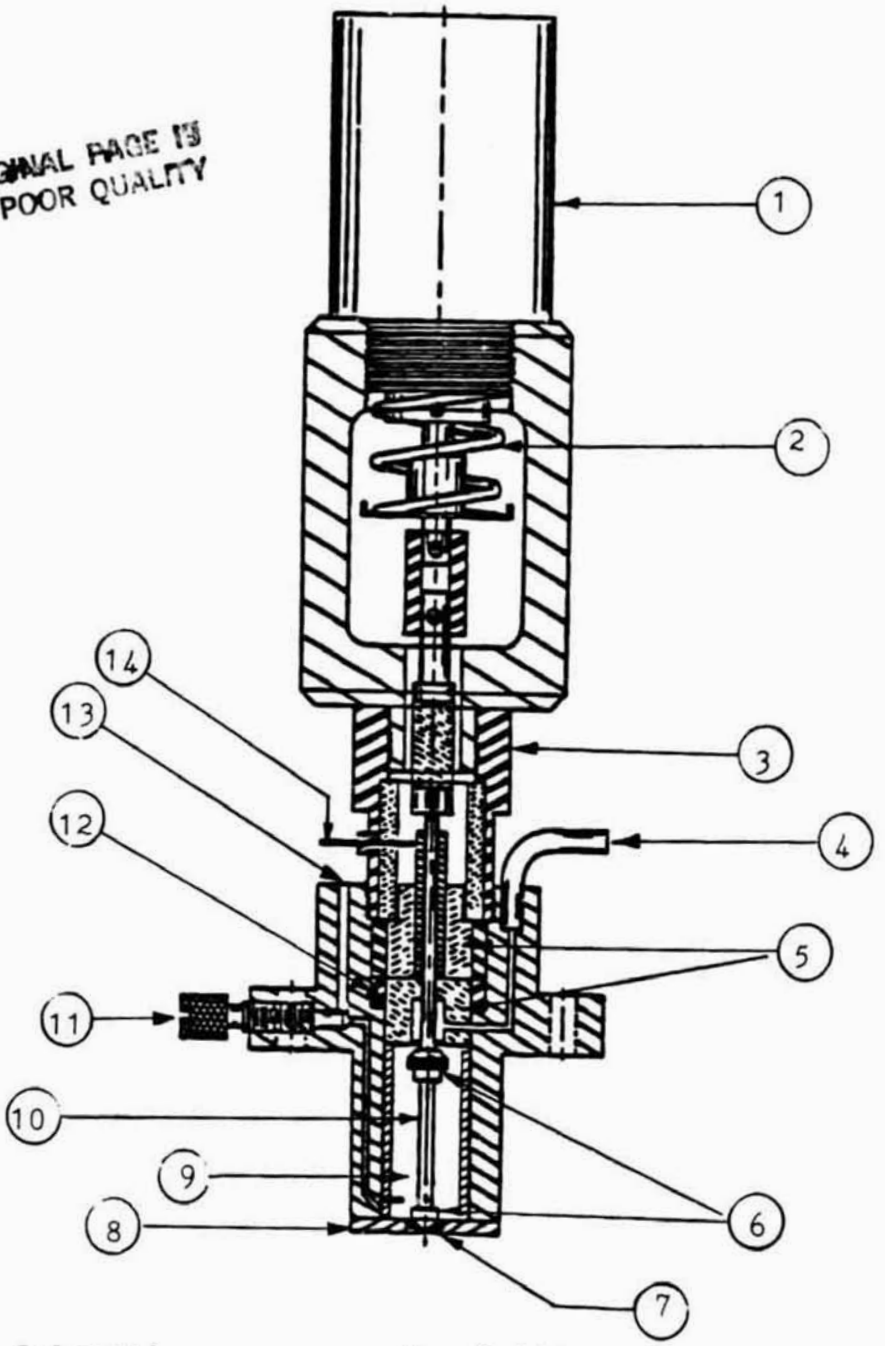

1 - Solenoid
2 - Spring
3 - Solenoid Support
4 - Gas Inlet
5 - Macor Guides
6 - Valves
7 - Tapered Orifice
8 - Orifice Plate
9 - Prechamber
10 - Valve Rod
11 - Shut Off Valve
12 - Alignment Slot and Key
13 - Purge Outlet
14 - High Voltage Lead

Figure 5

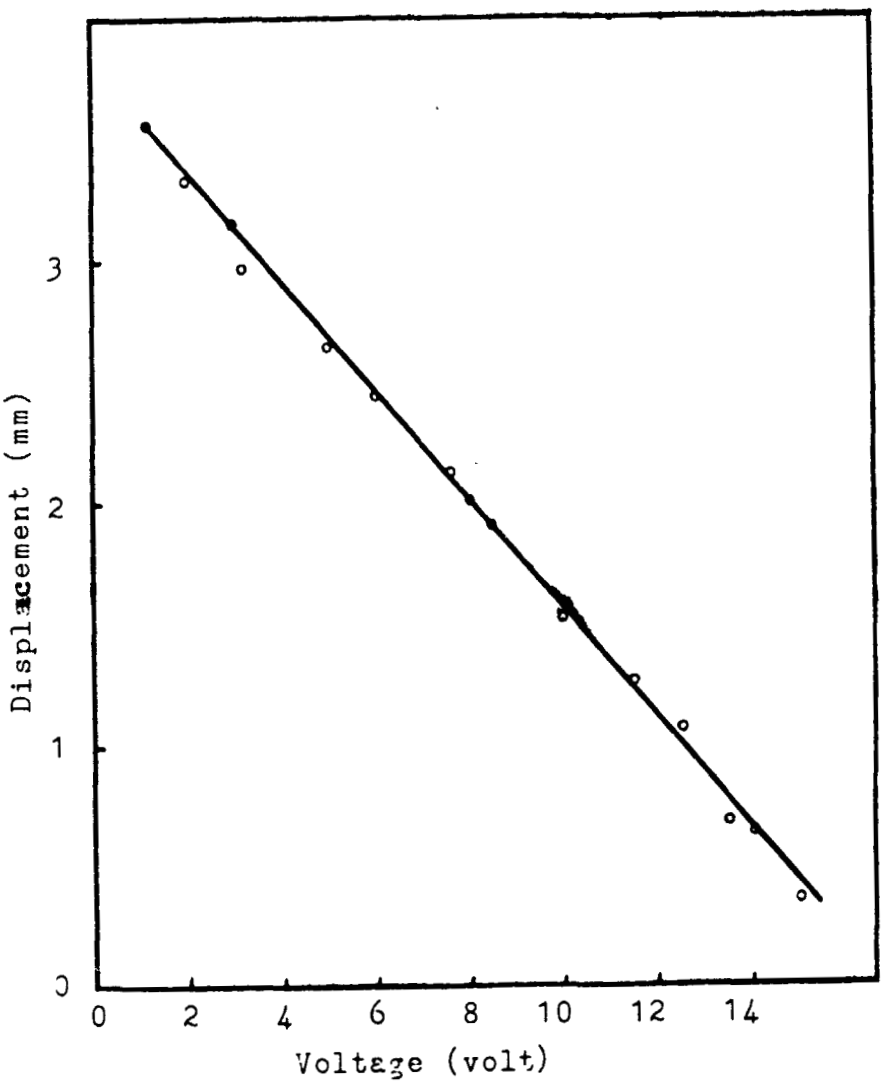

Figure 6

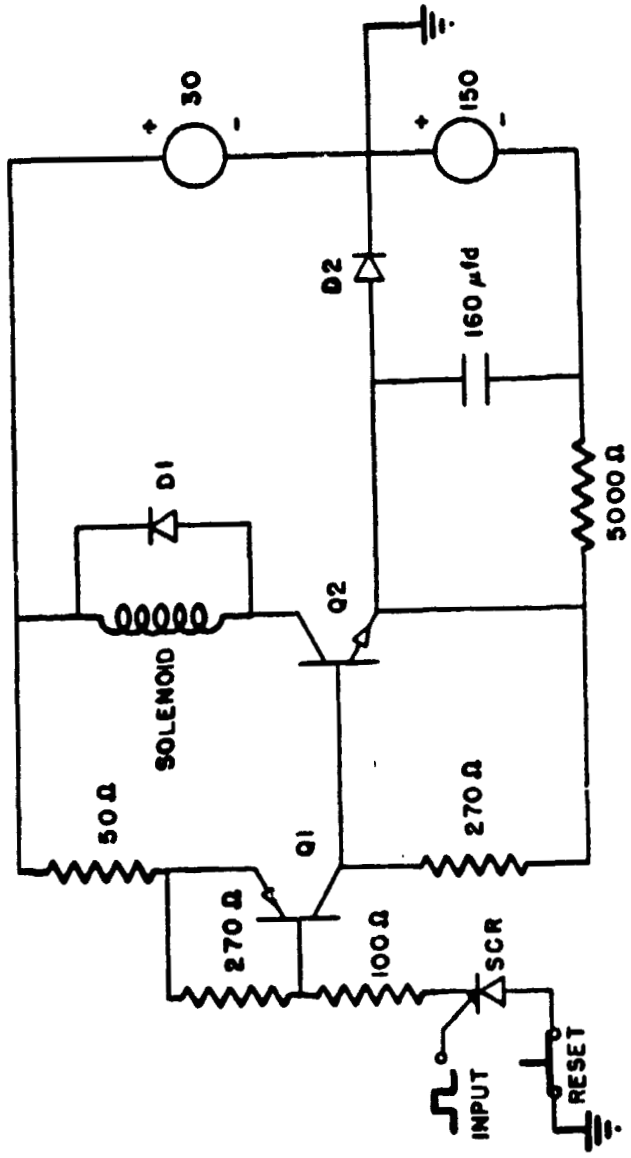

Figure 7

Figure 8

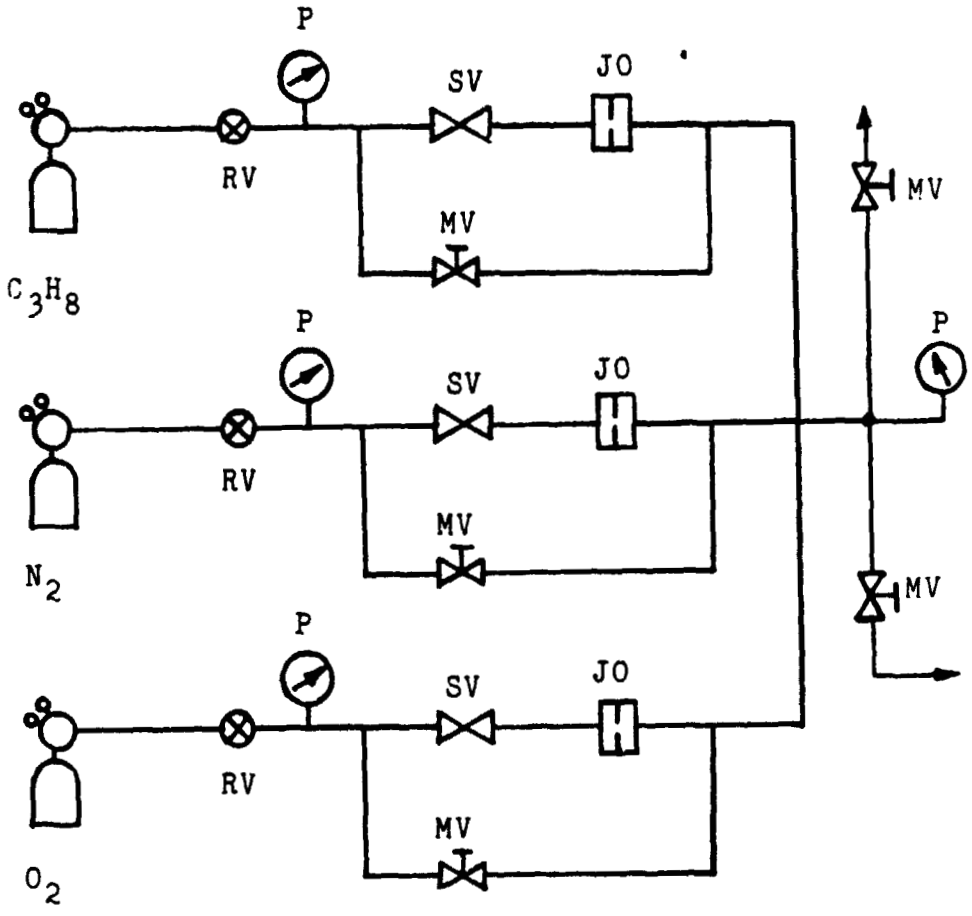

RV - Regulating Valve
MV - Manual Valve
SV - Solenoid Valve
JO - Jewel Orifice
P - Pressure Gauge

Figure 9

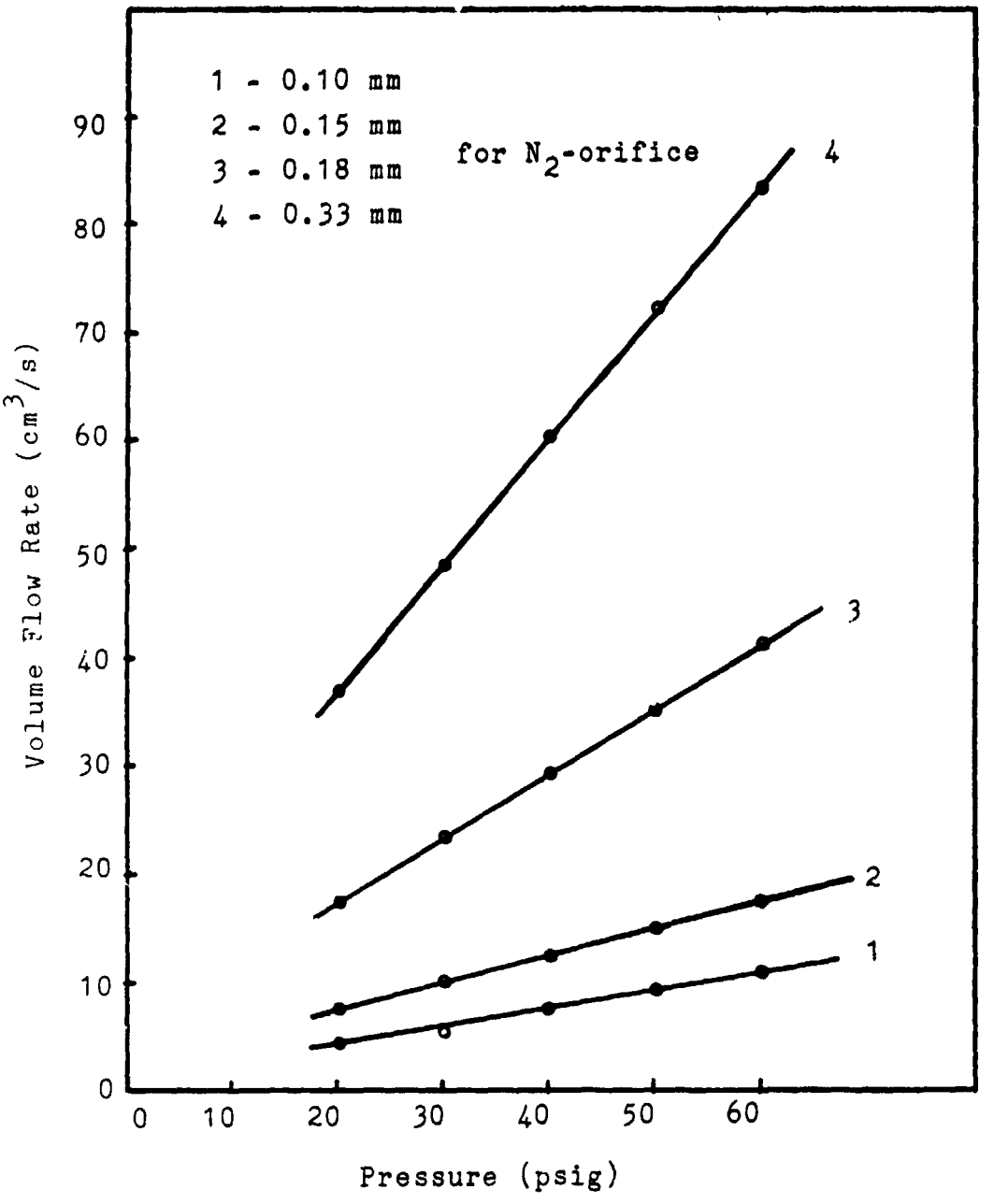

Figure 10

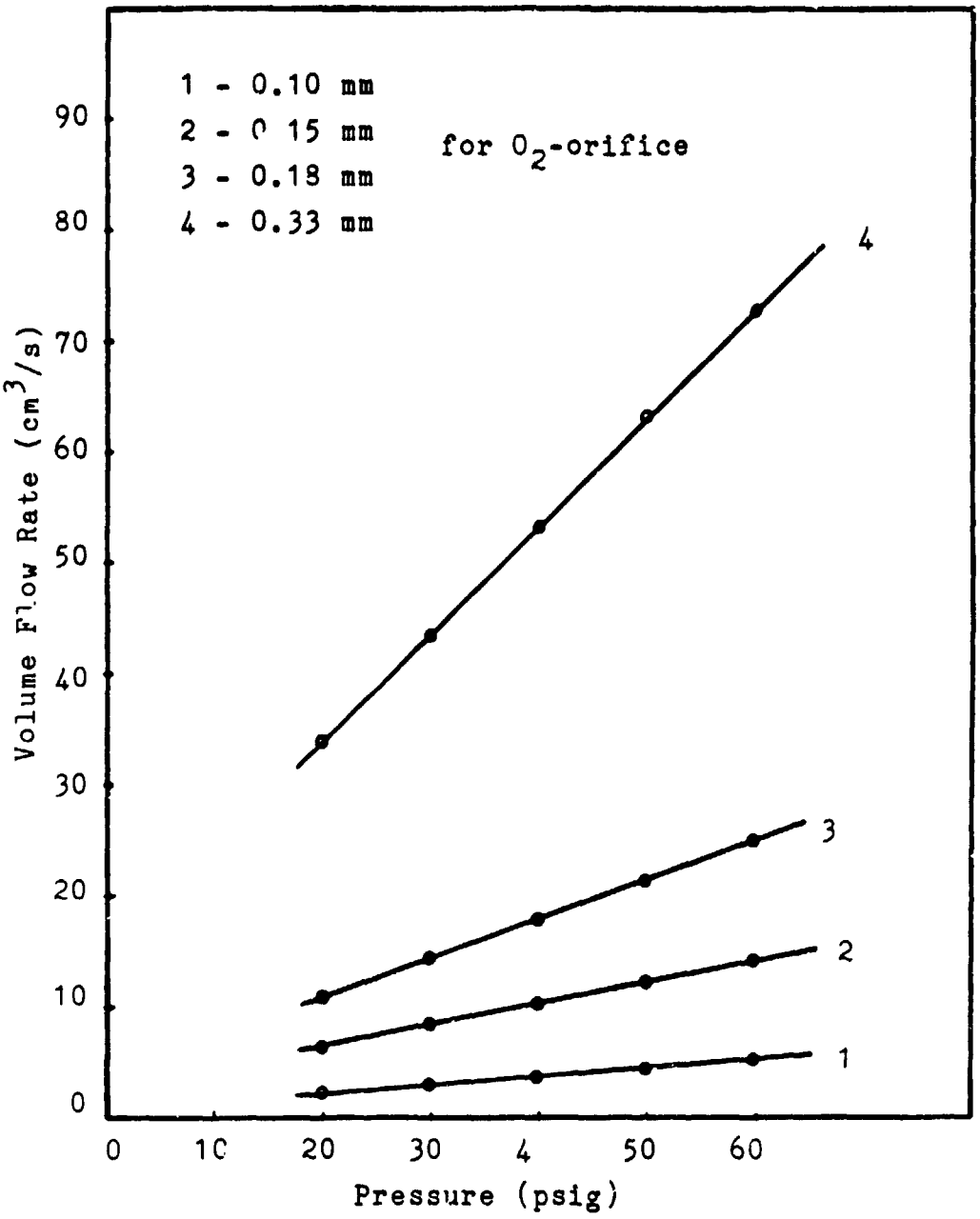

Figure 11

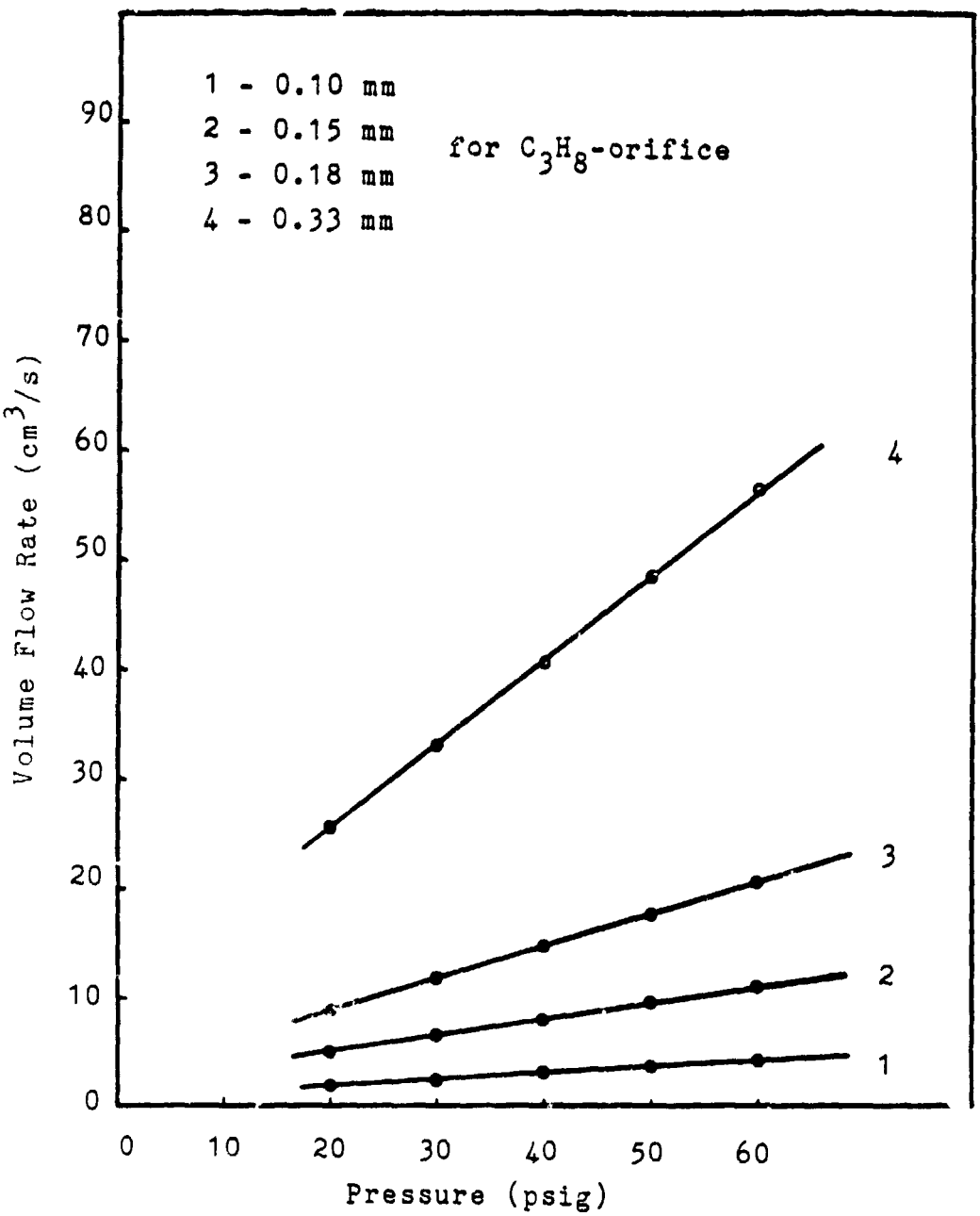

Figure 12

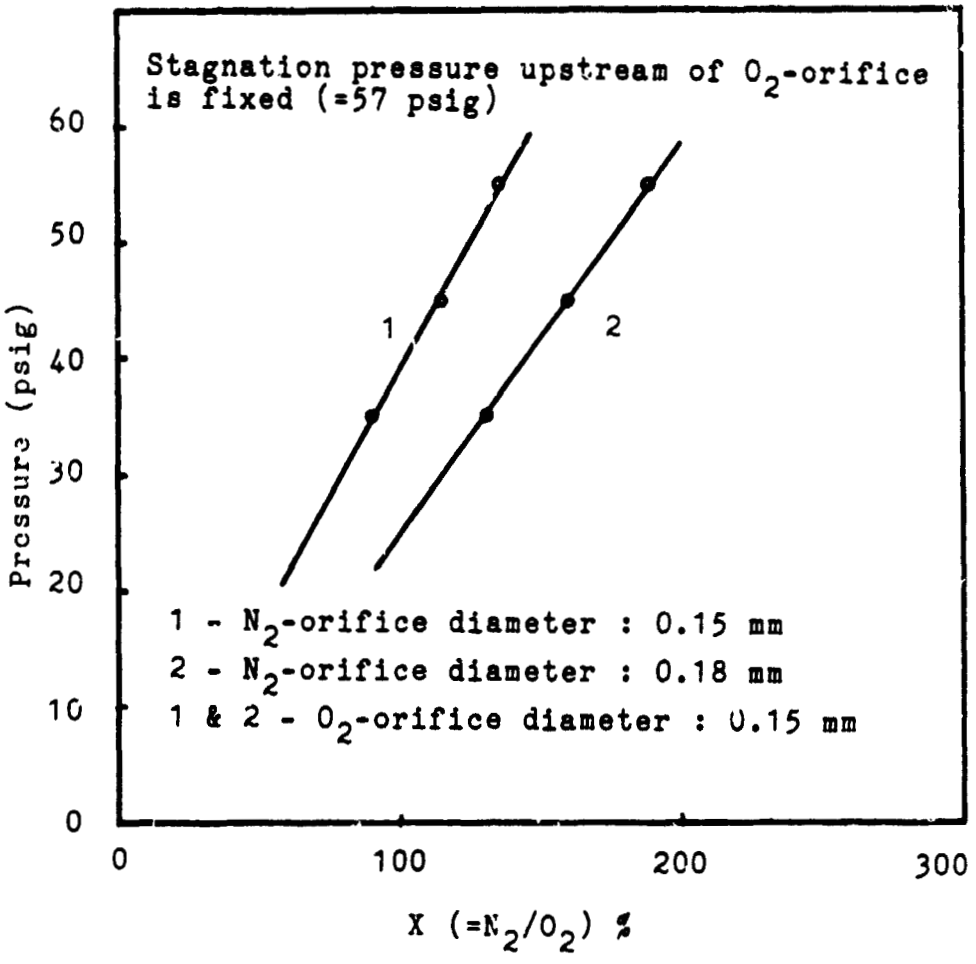

Figure 13

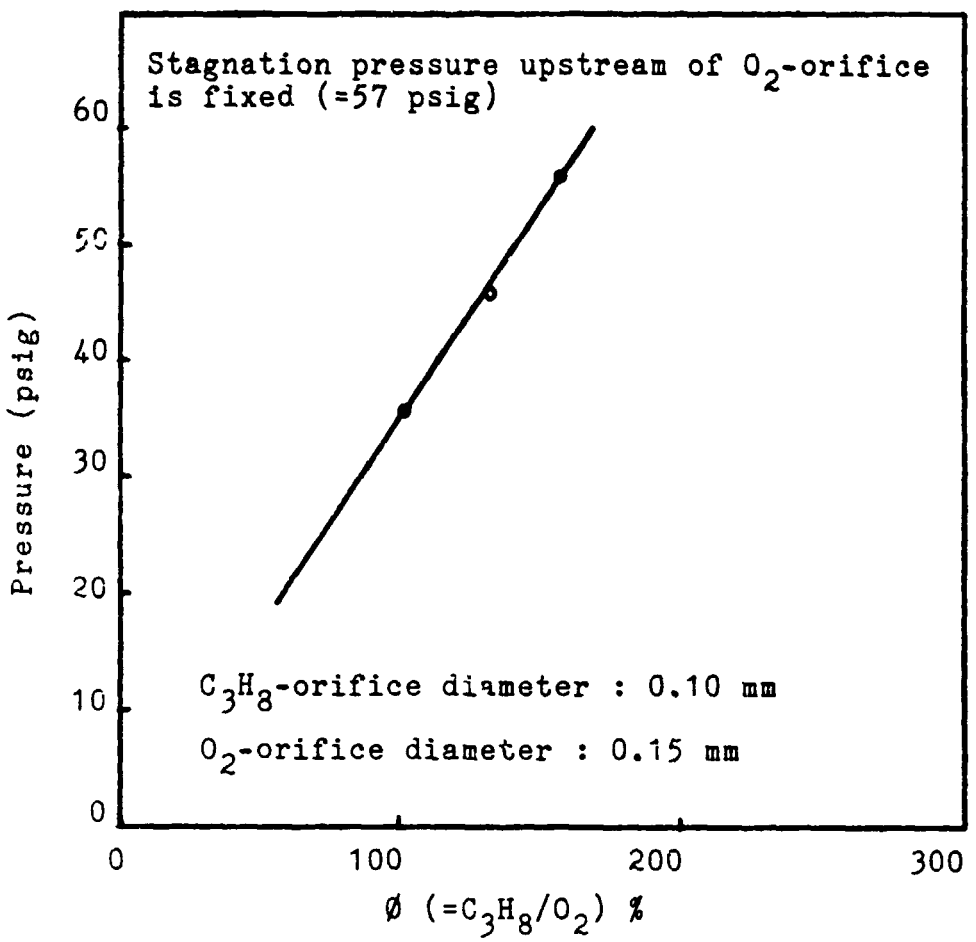

Figure 14

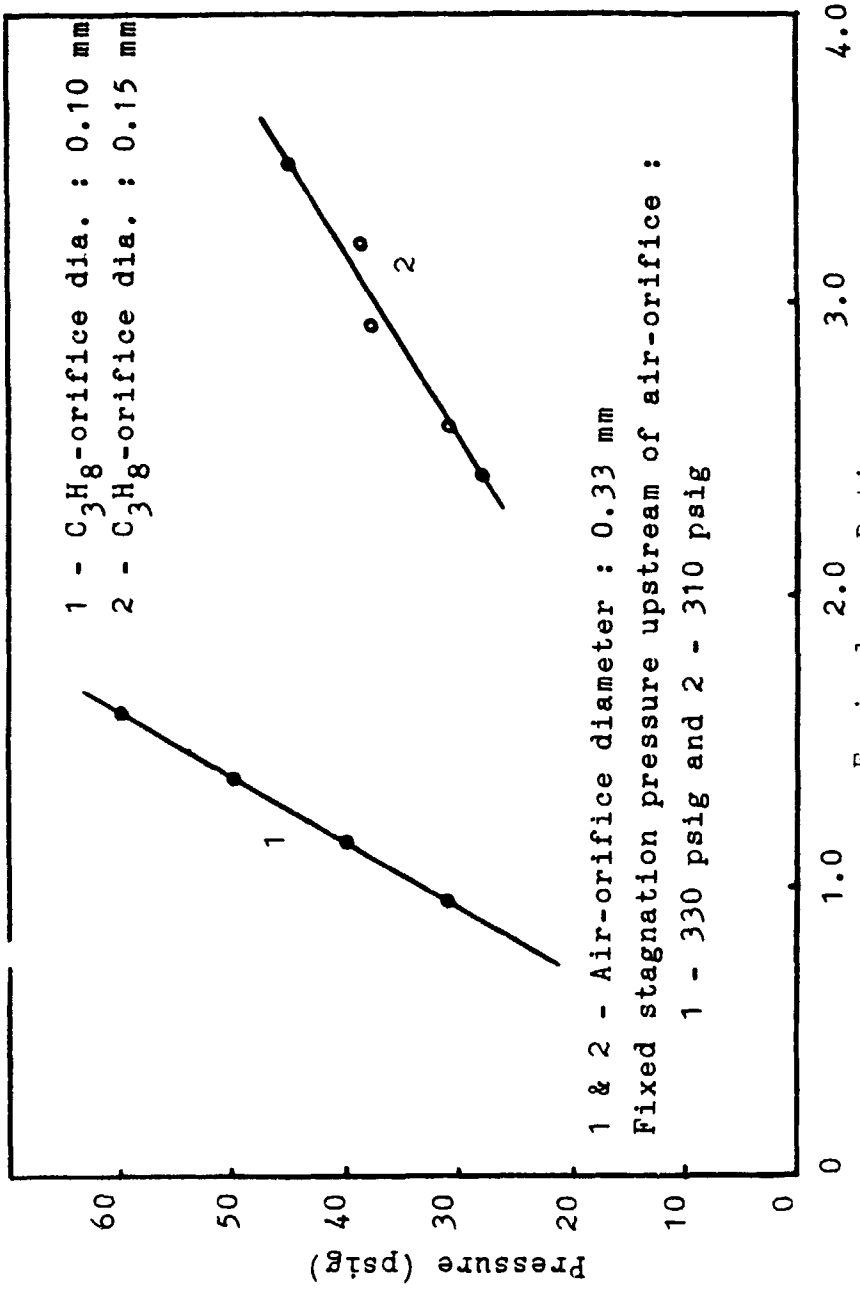

Figure 15

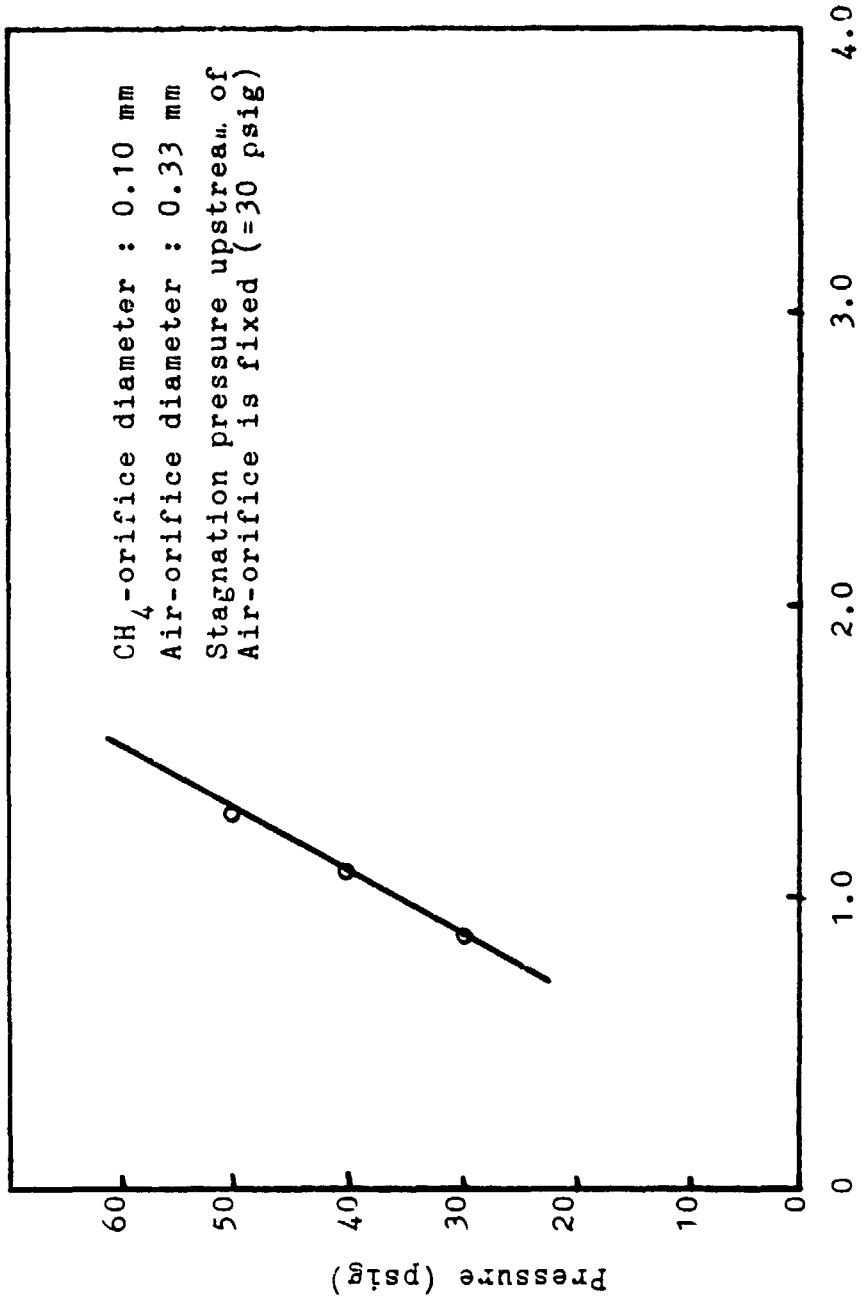

Figure 16

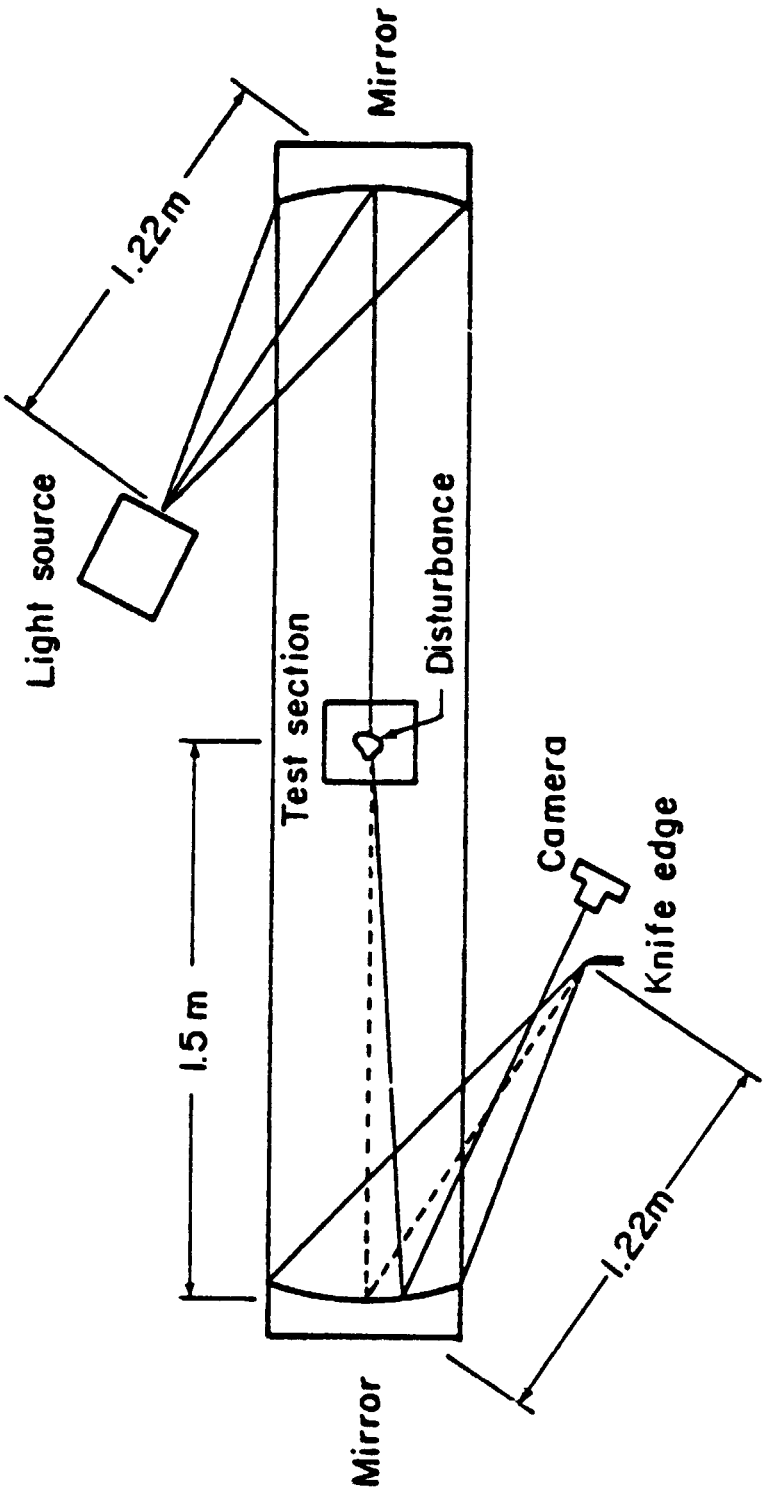

Figure 17

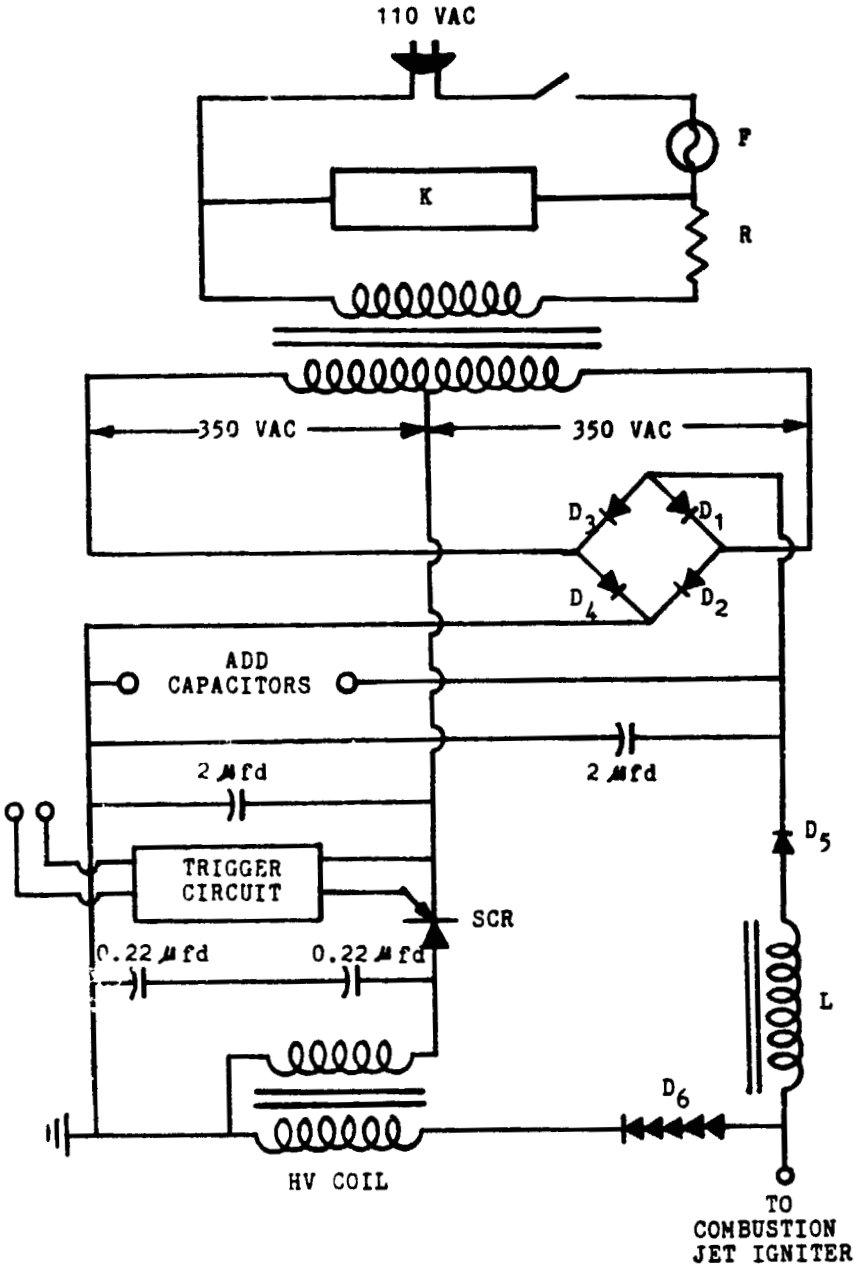

Figure 18

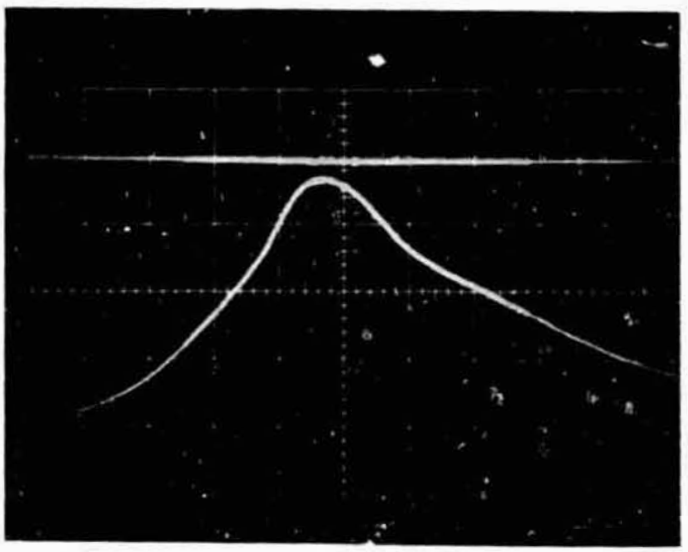

Displacement

Pressure

a

Time Scale : 2 ms/div.
Pressure Scale : 5 psi/div.

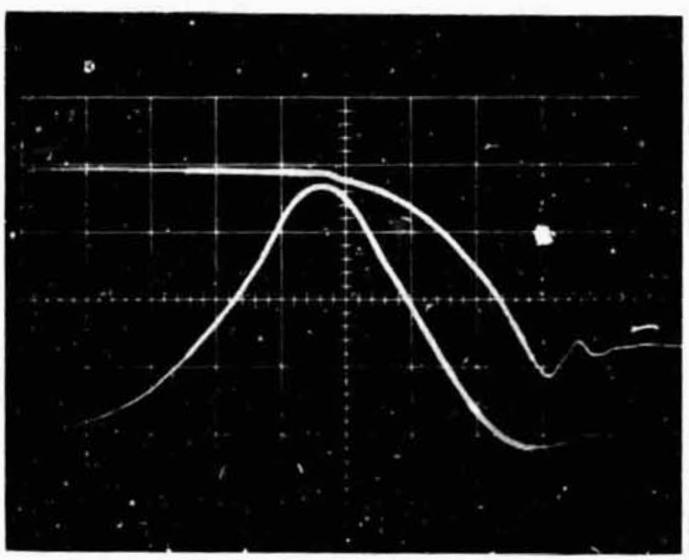

Displacement

Pressure

b

Time Scale : 2 ms/div.
Pressure Scale : 5 psi/div.
Displacement Scale : 1.13 mm/div.

Figure 19

1 ms

2 ms

3 ms

5 ms

Figure 20

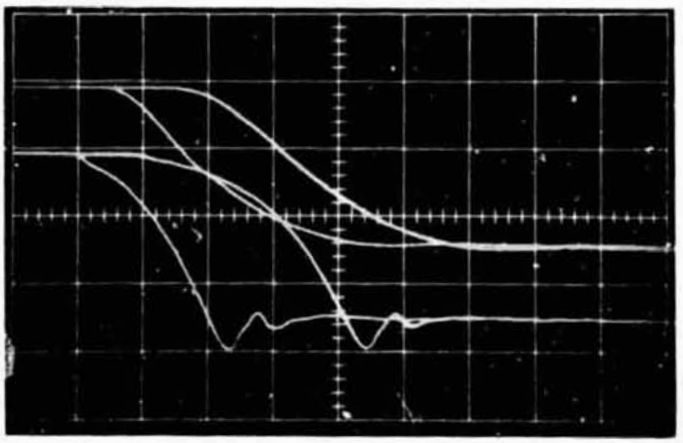

a

Time Scale : 2 ms/div.
Pressure Scale : 10 psi/div.
Displacement Scale : 1.13 mm/div.

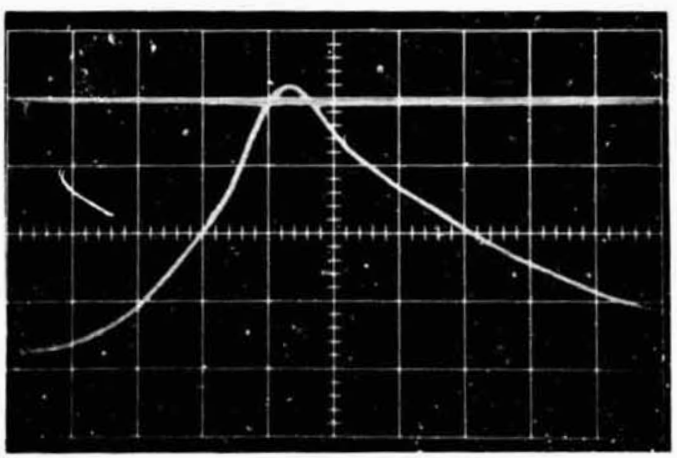

b

Time Scale : 2 ms/div.
Pressure Scale : 5 psi/div.

Figure 21

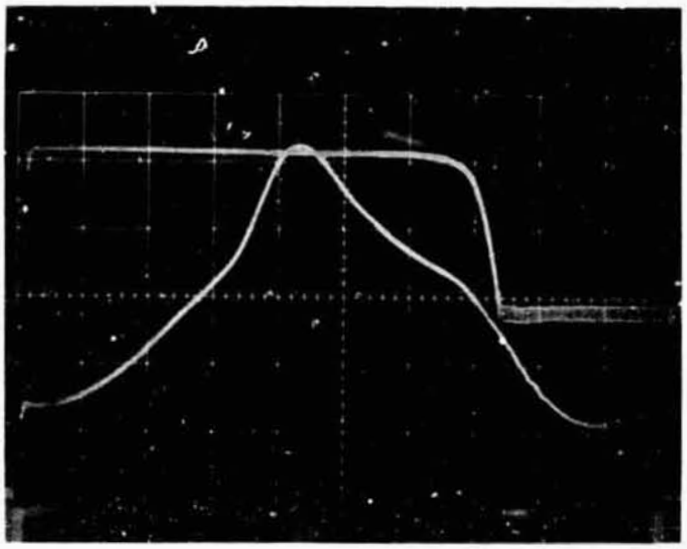

Displacement

Pressure

Time Scale : 2 ms/div.
Pressure Scale : 5 psi/div.
Displacement Scale : 1.13 mm/div.

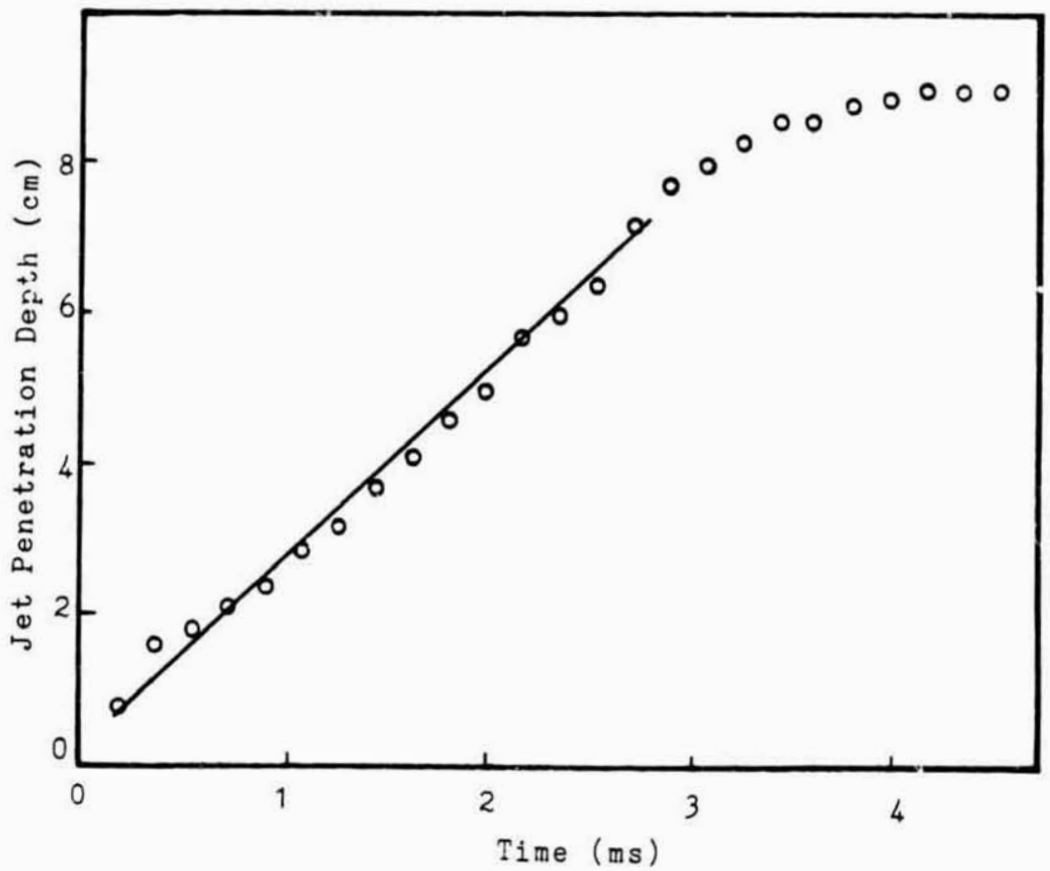

Figure 22

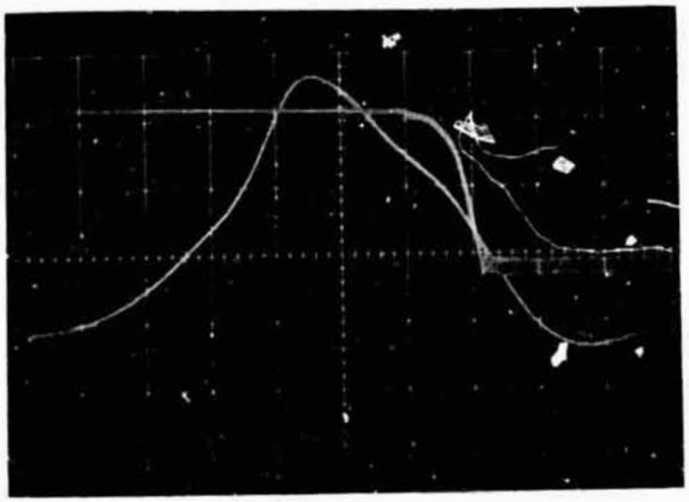

Displacement

Pressure

Time Scale : 2 ms/div.
Pressure Scale : 5 psi/div.
Displacement Scale : 1.13 mm/div.

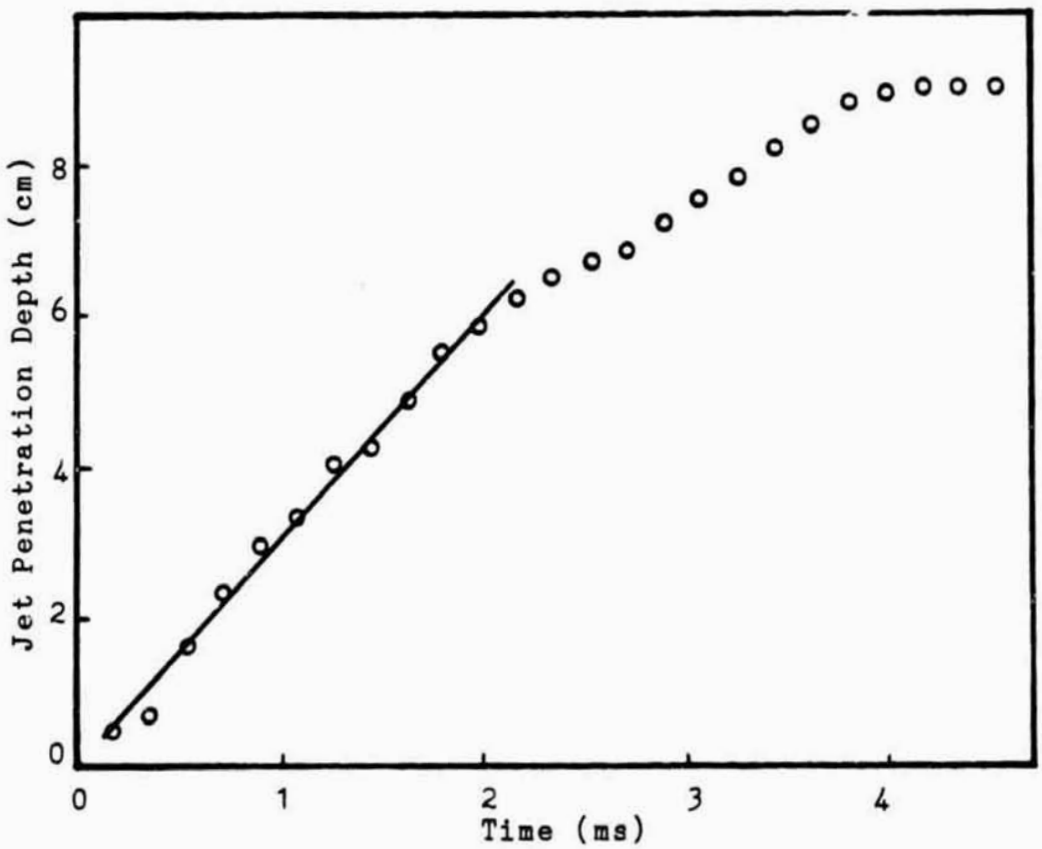

Figure 23

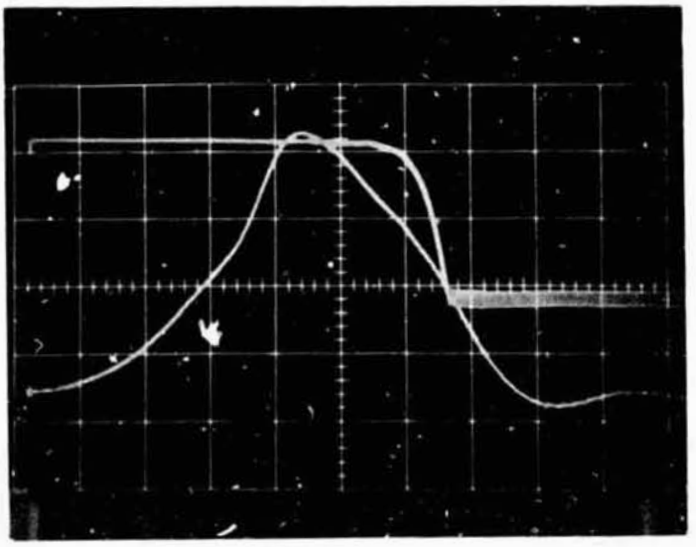

Displacement

Pressure

Time Scale : 2 ms/div.
Pressure Scale : 5 psi/div.
Displacement Scale : 1.13 mm/div.

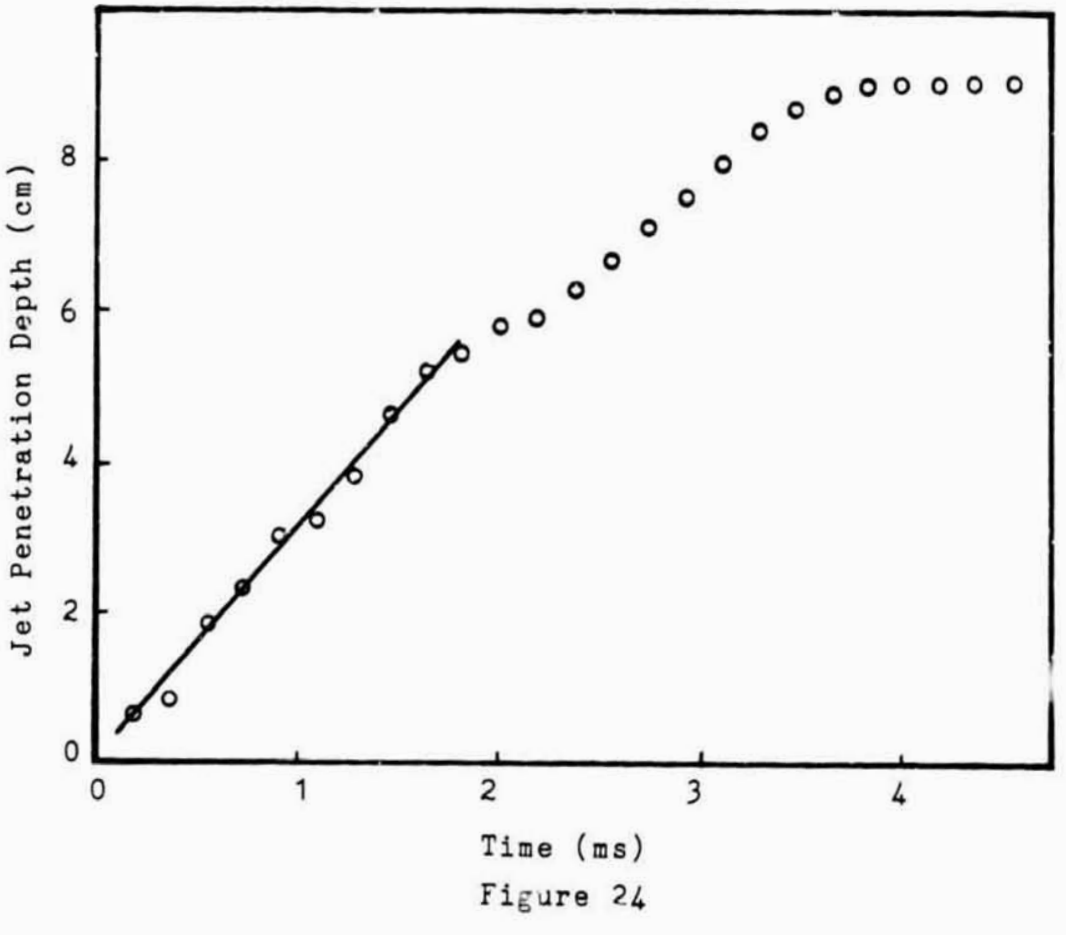

Figure 24

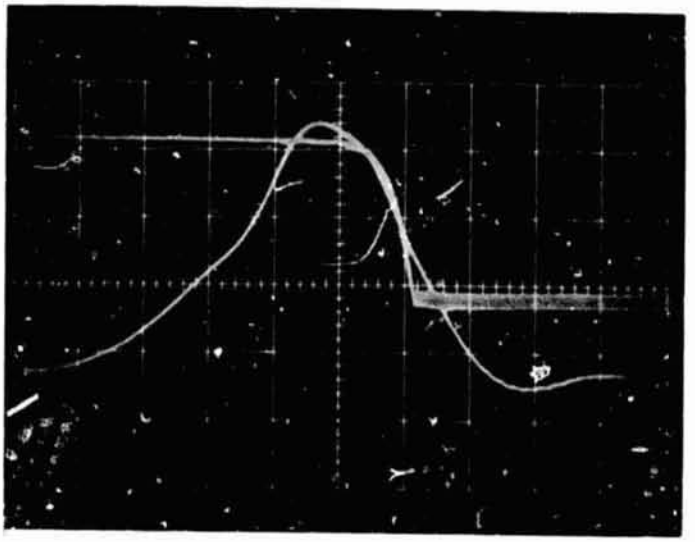

Displacement

Pressure

Time Scale : 2 ms/div.
Pressure Scale : 5 psi/div.
Displacement Scale : 1.13 mm/div.

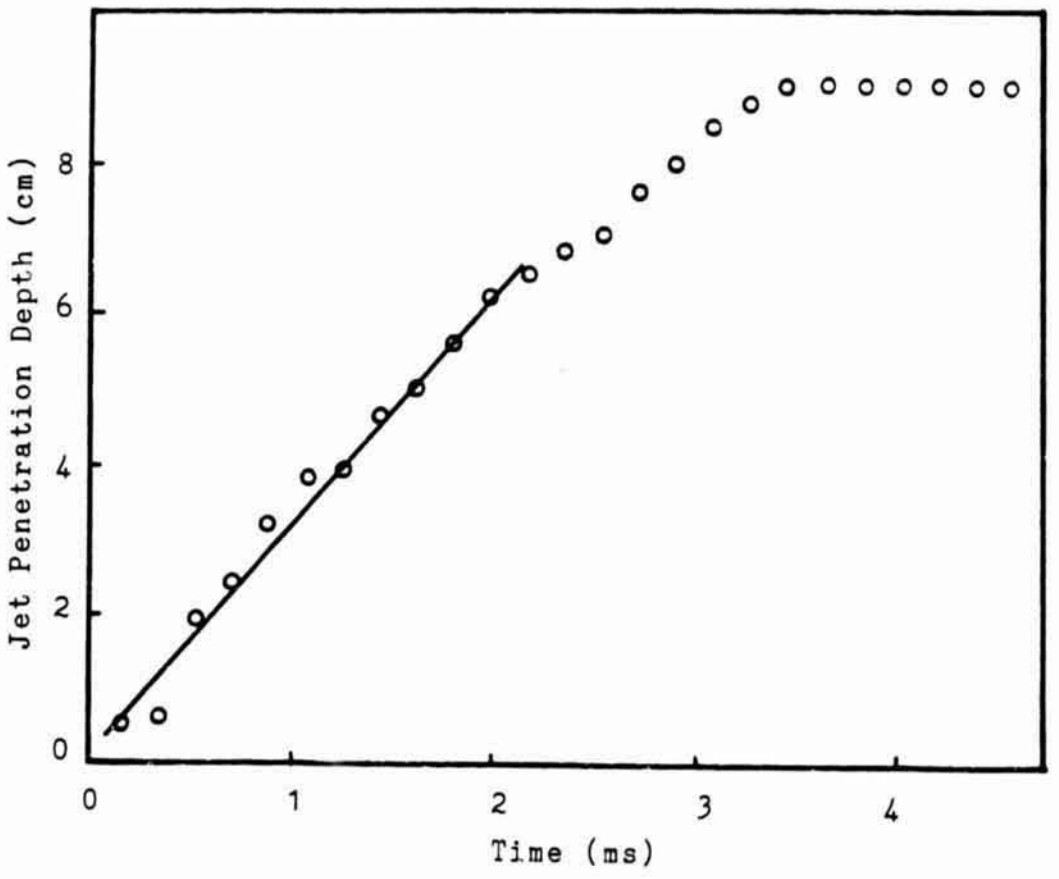

Figure 25

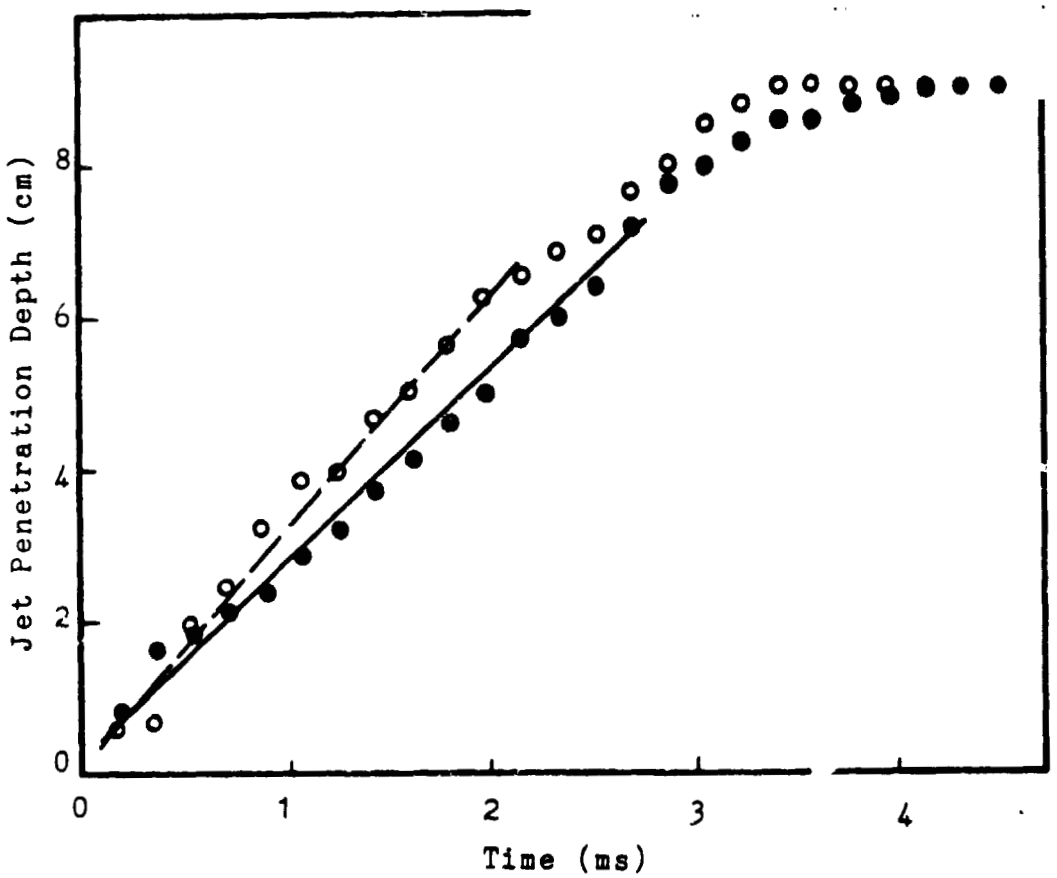

o - Valve opening at peak pressure

● - Valve opening 3 ms after peak pressure

Figure 26

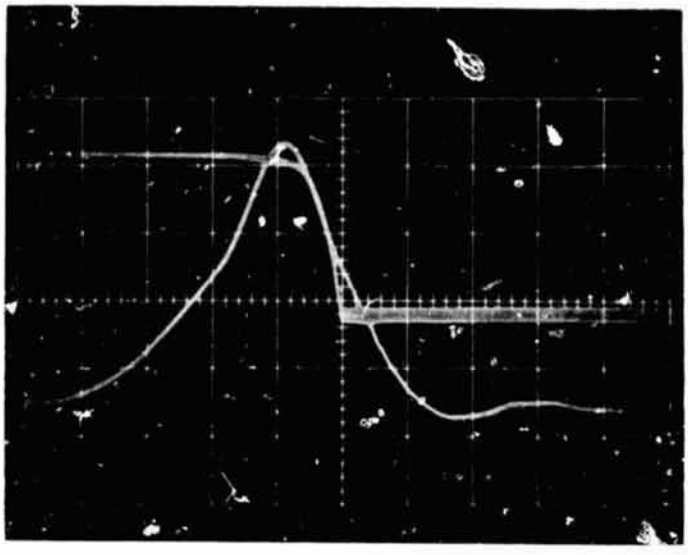

Displacement

Pressure

Time Scale : 2 ms/div.
Pressure Scale : 5 psi/div.
Displacement Scale : 1.13 mm/div.

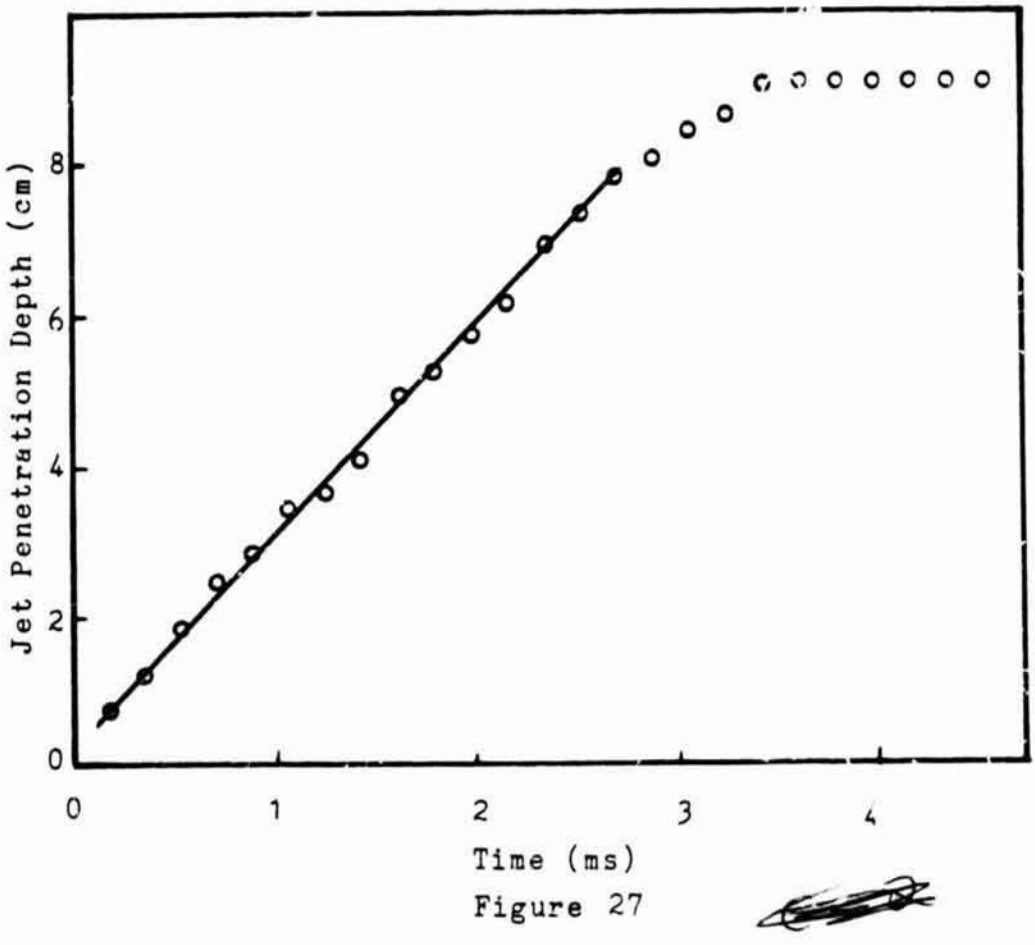

Figure 27

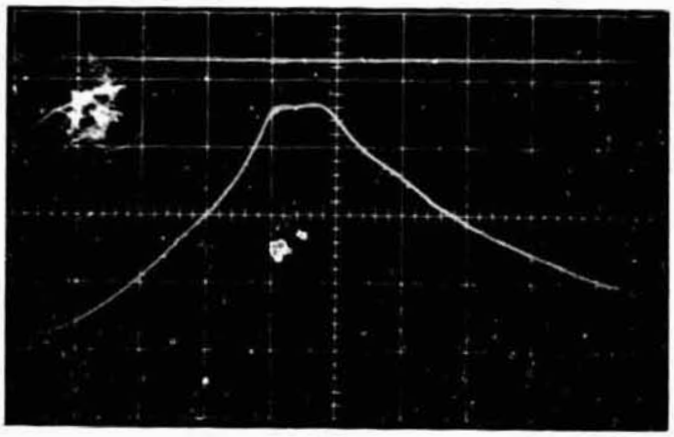

Displacement

Pressure

a

Time Scale : 2 ms/div.
Pressure Scale : 5 psi/div.

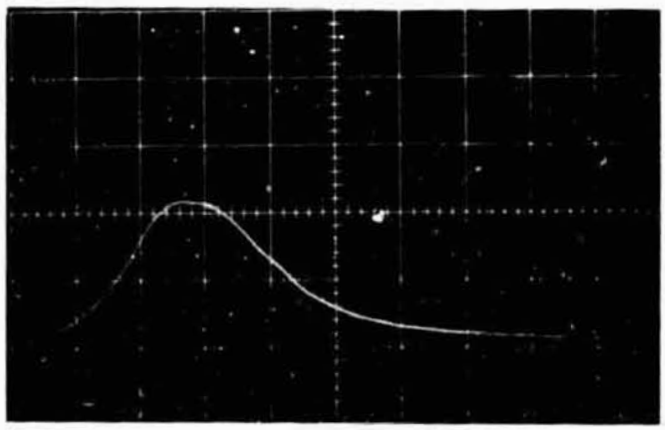

b

Time Scale: 5 ms/div.
Pressure Scale : 5 psi/div.

C-2

Figure 28

.55 ms

1.1 ms

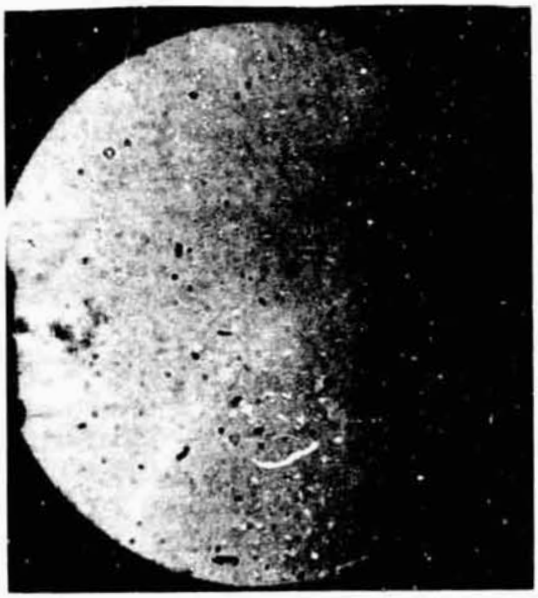

2.0 ms

3.0 ms

Figure 29

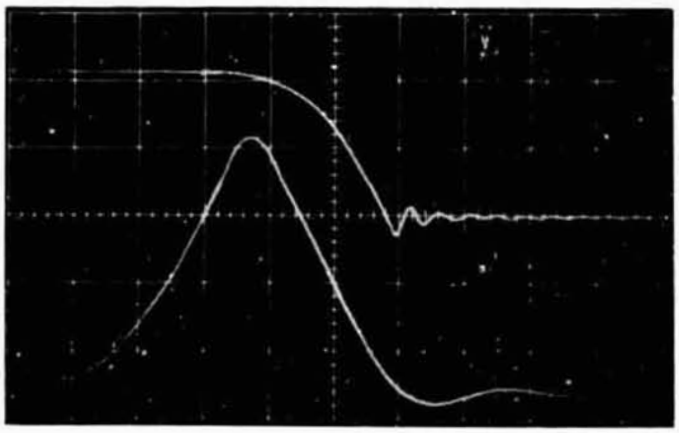

Time Scale : 2 ms/div.
Pressure Scale : 5 psi/div.
Displacement Scale : 1.13 mm/div.

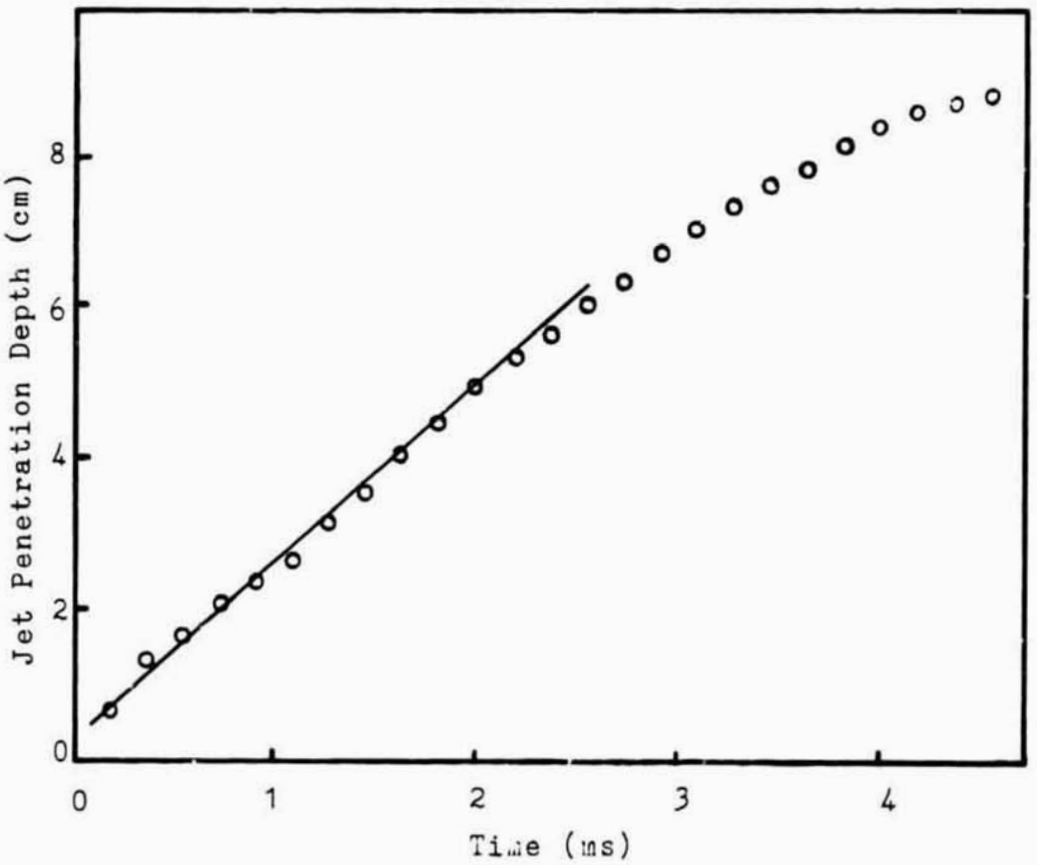

Figure 30

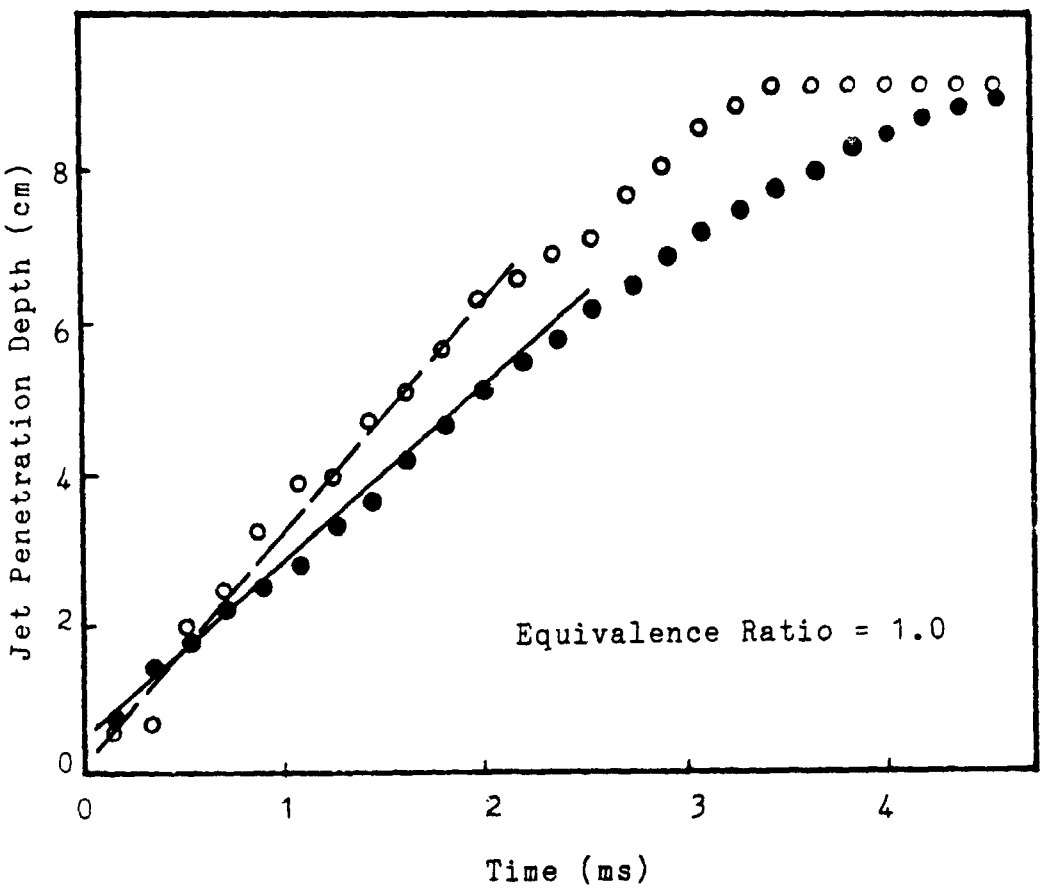

o - C_3H_8/Air mixture

● - CH_4/Air mixture

Figure 31

.63 ms.

1.1 ms

2.C ms

3,0 ms

Figure 32

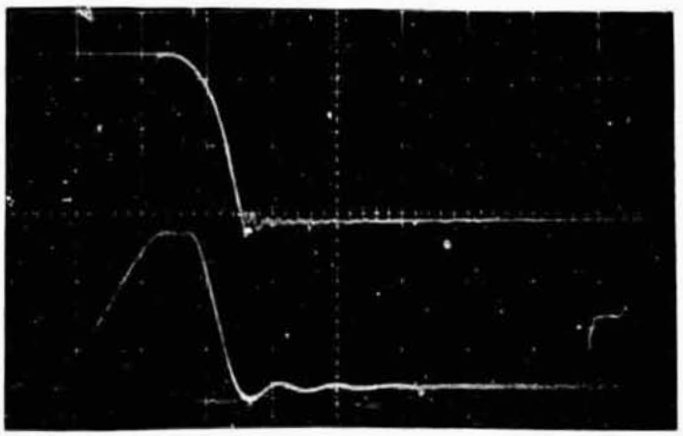

Displacement

Pressure

Time Scale : 5 ms/div.
Pressure Scale : 5 psi/div.
Dispalcement Scale : 1.13 mm/div.

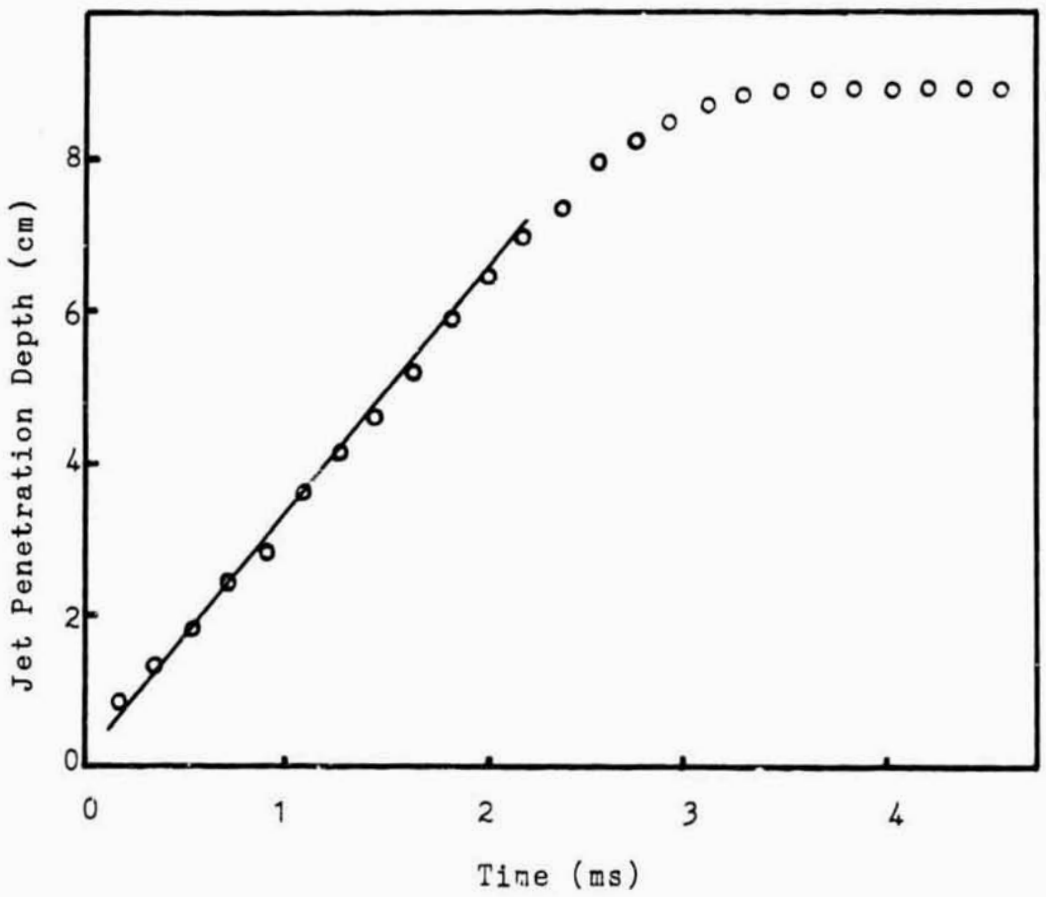

Figure 33

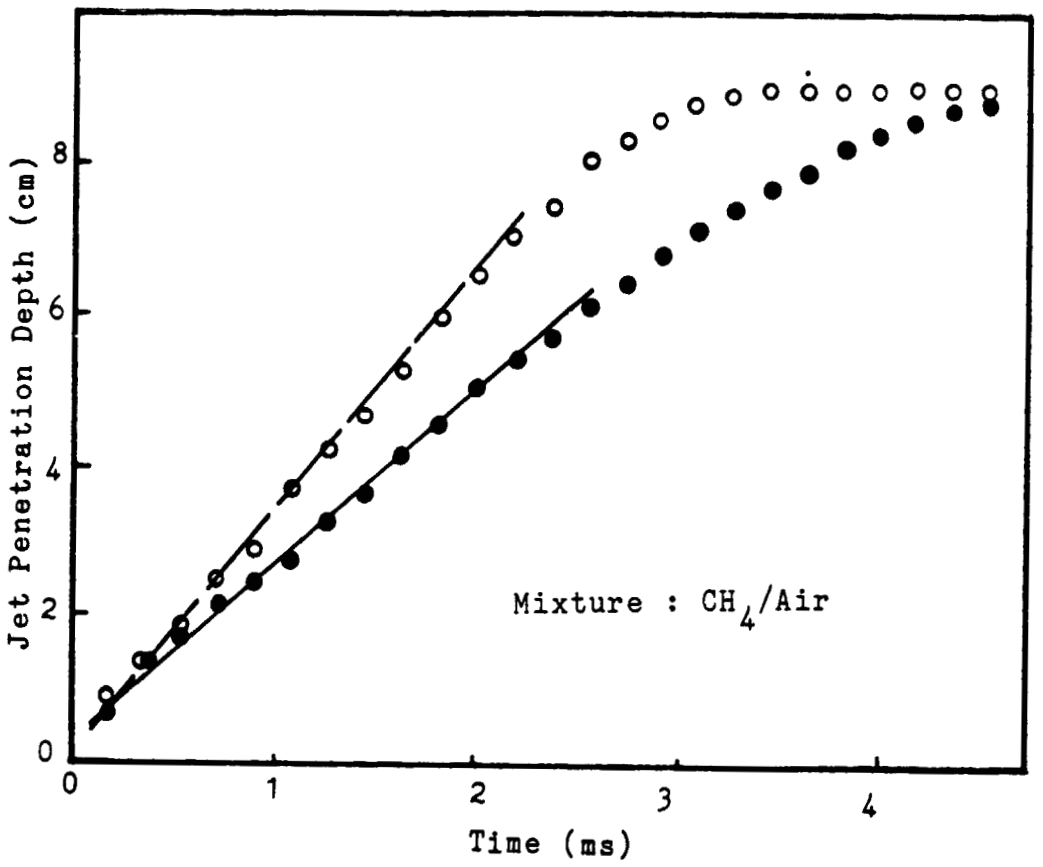

o - Equivalence Ratio : 1.2

● - Equivelence Ratio : 1.0

Figure 34

.59 ms

2.2 ms

3.9 ms

6.5 ms

Figure 35

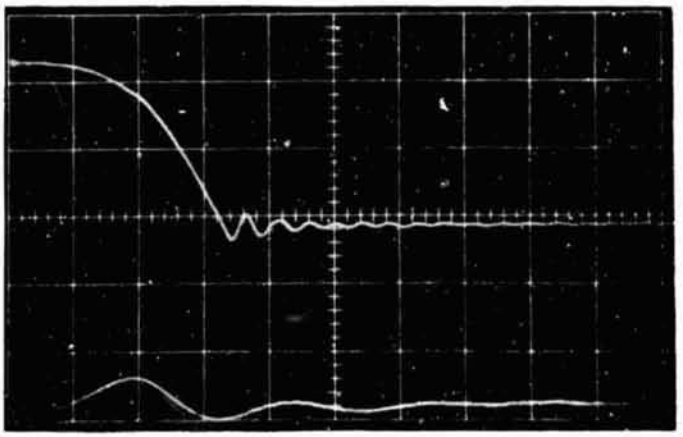

Time Scale : 2 ms/div.
Pressure Scale : 5 psi/div.
Displacement Scale : 1.13 mm/div.

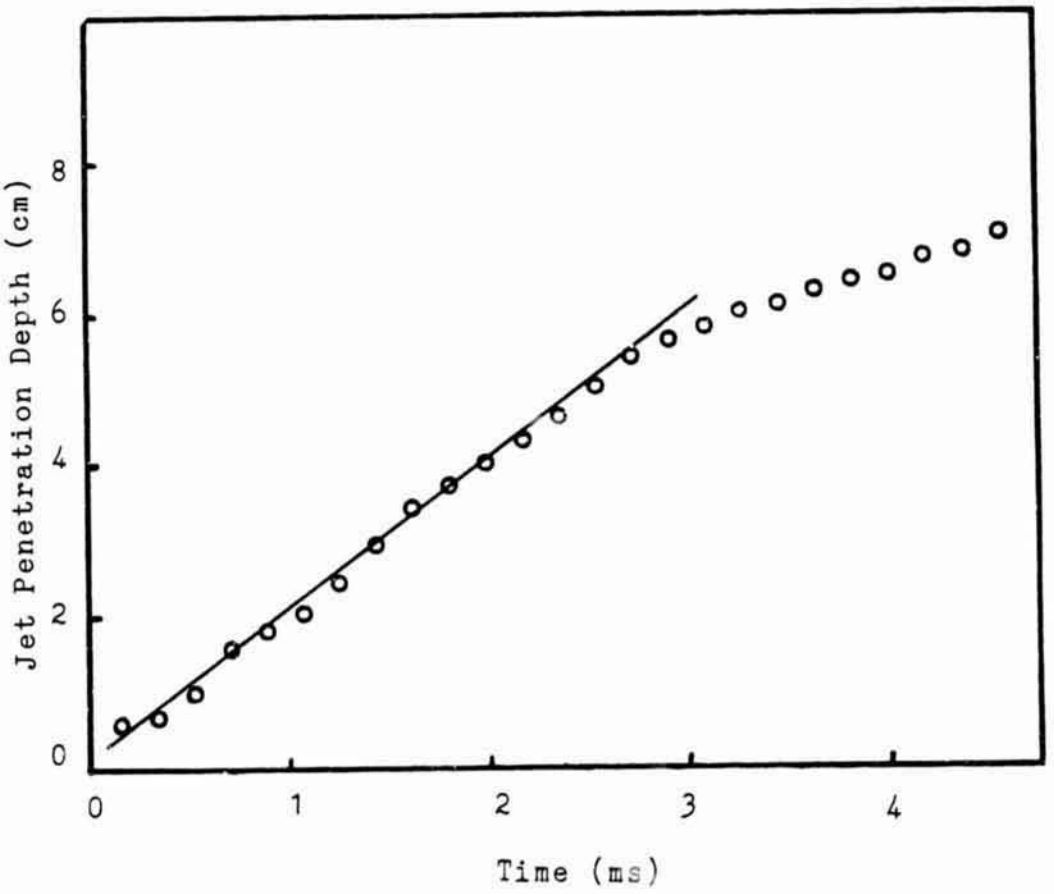

Figure 36

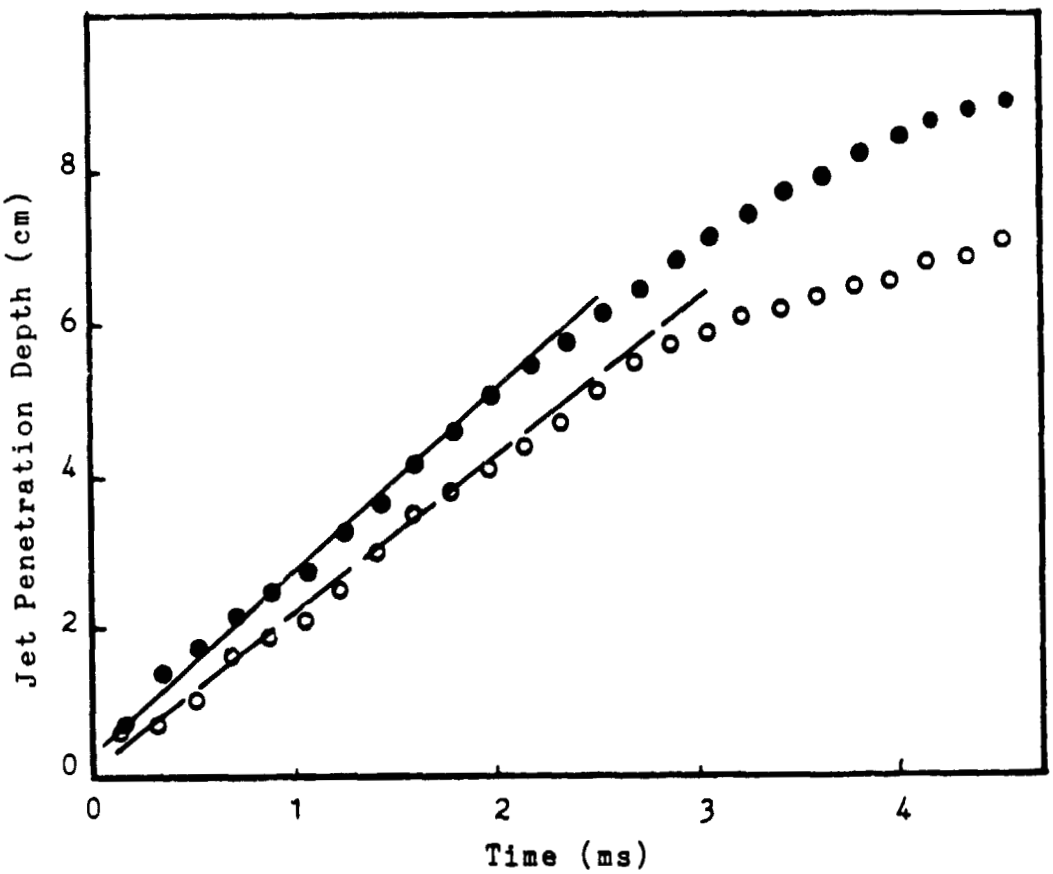

o - Valve opening 1 ms after electric spark

● - Valve opening at peak pressure

Figure 37

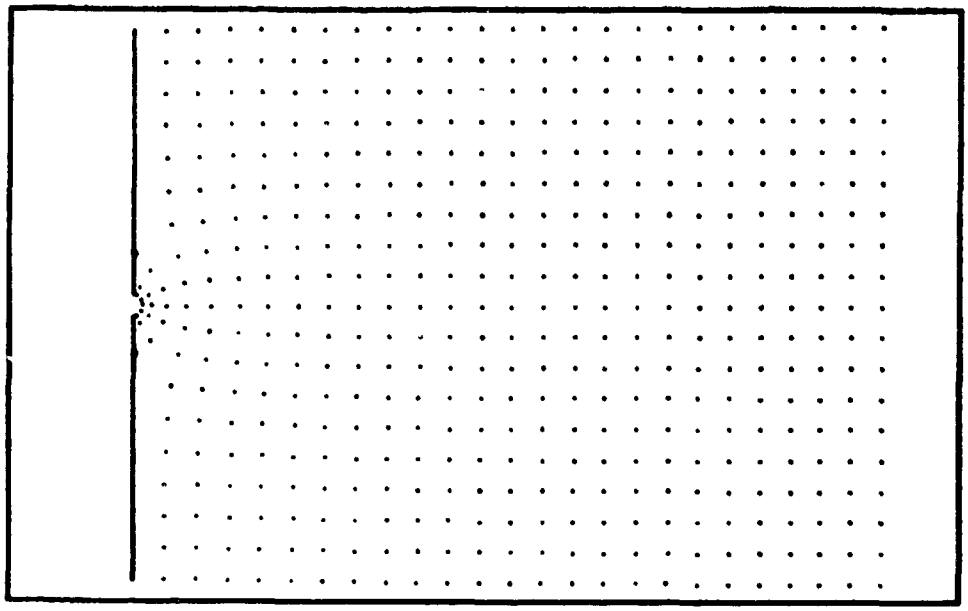

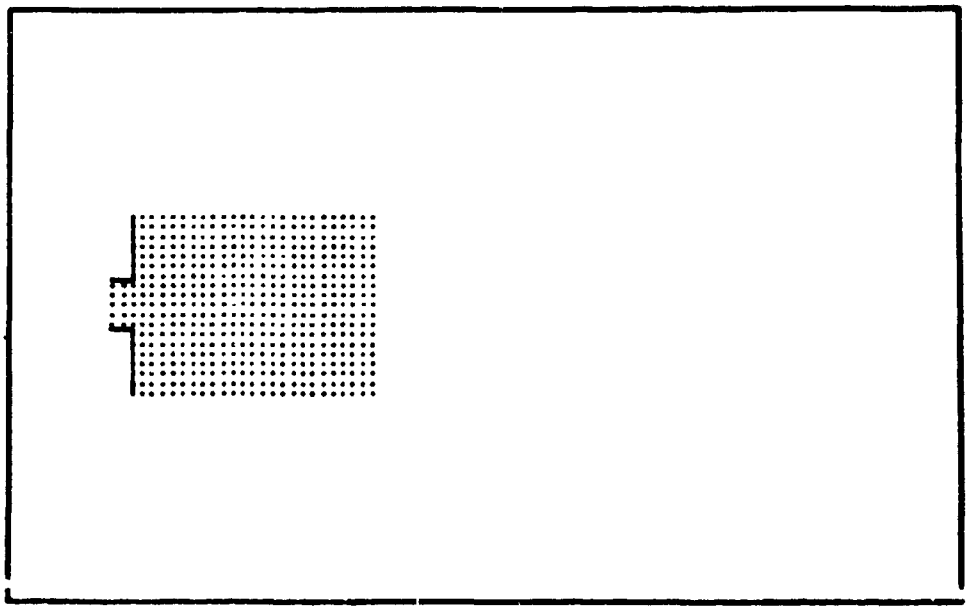

Figure 38

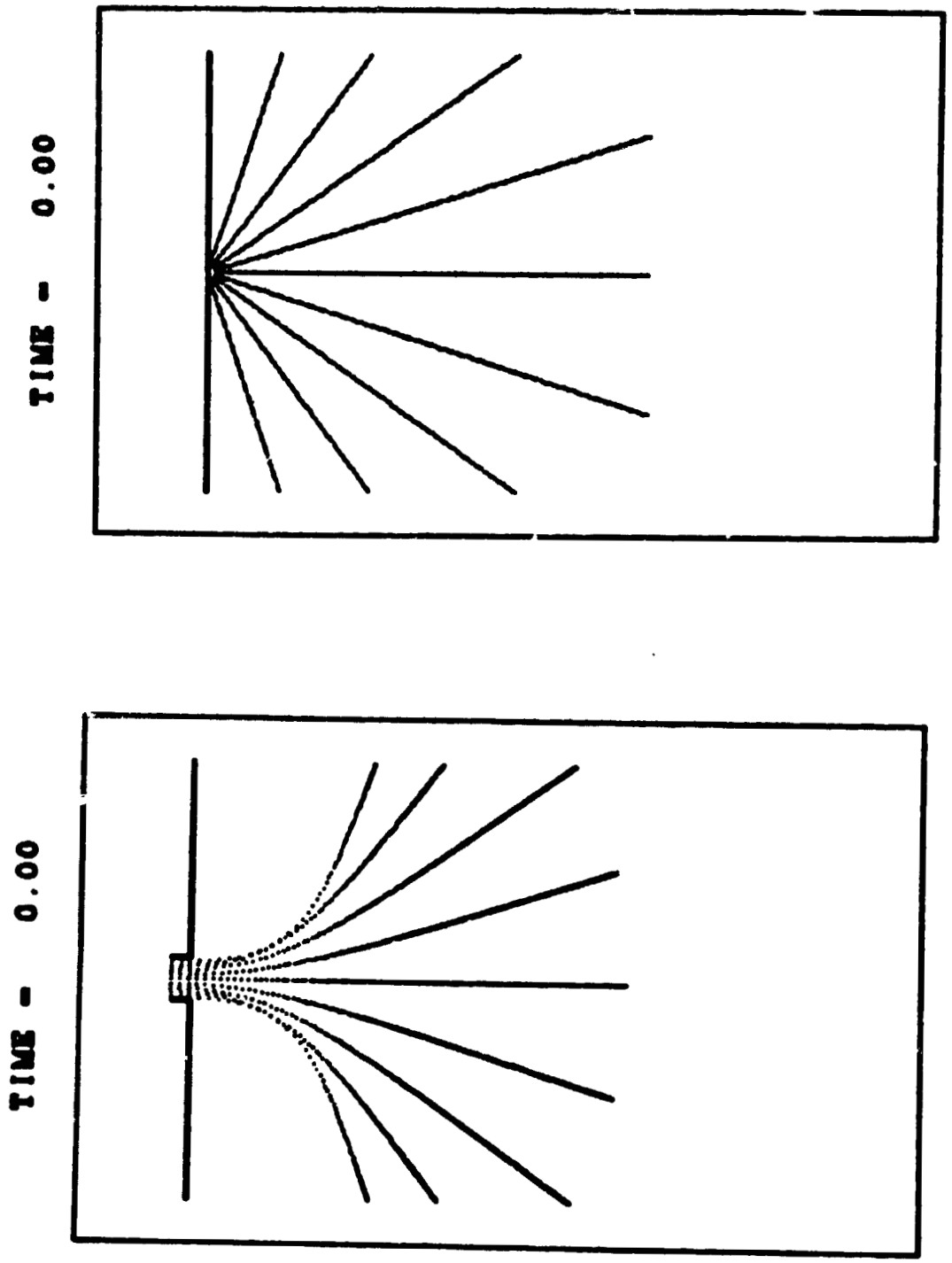

Figure 39

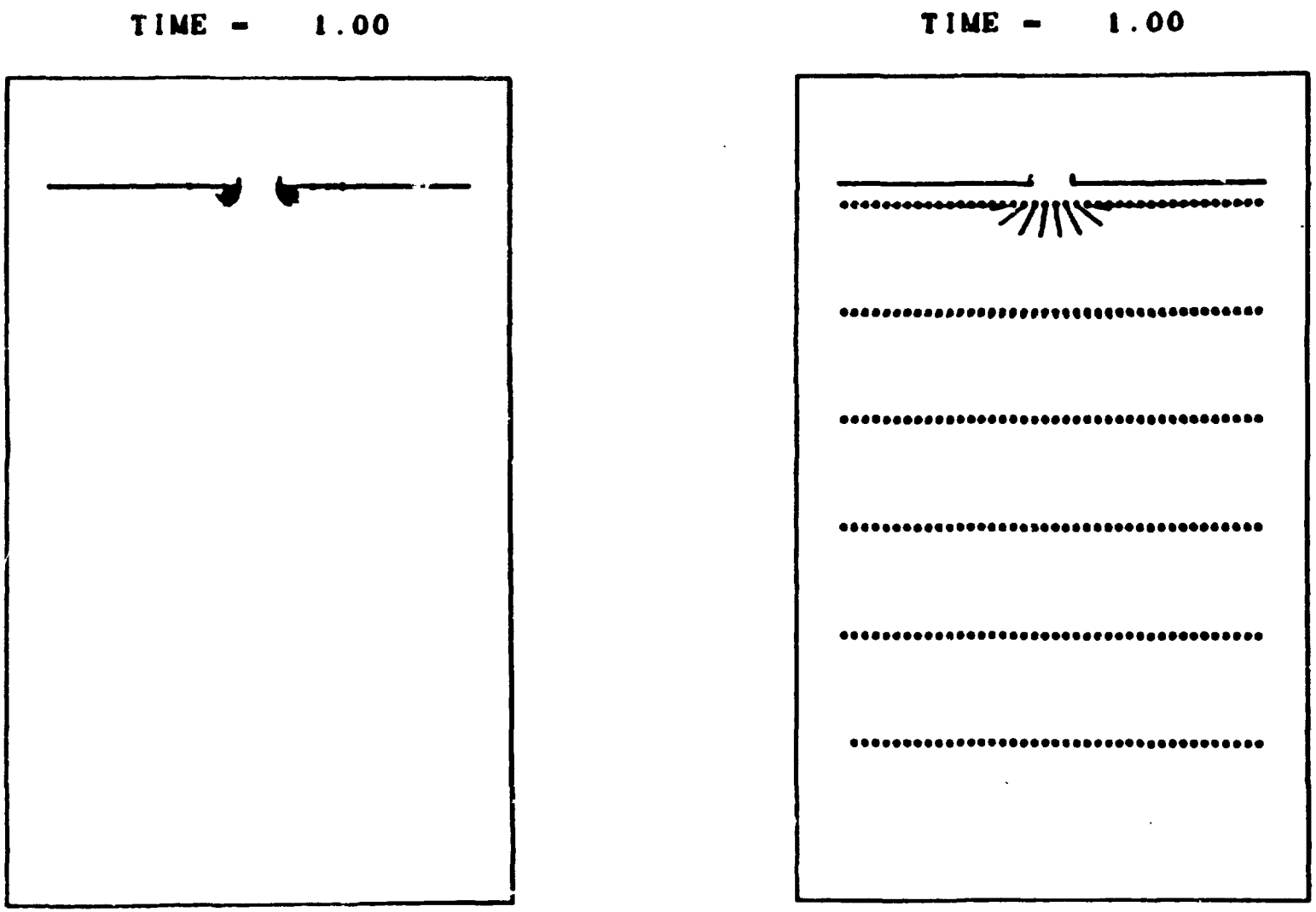

Figure 40 - a

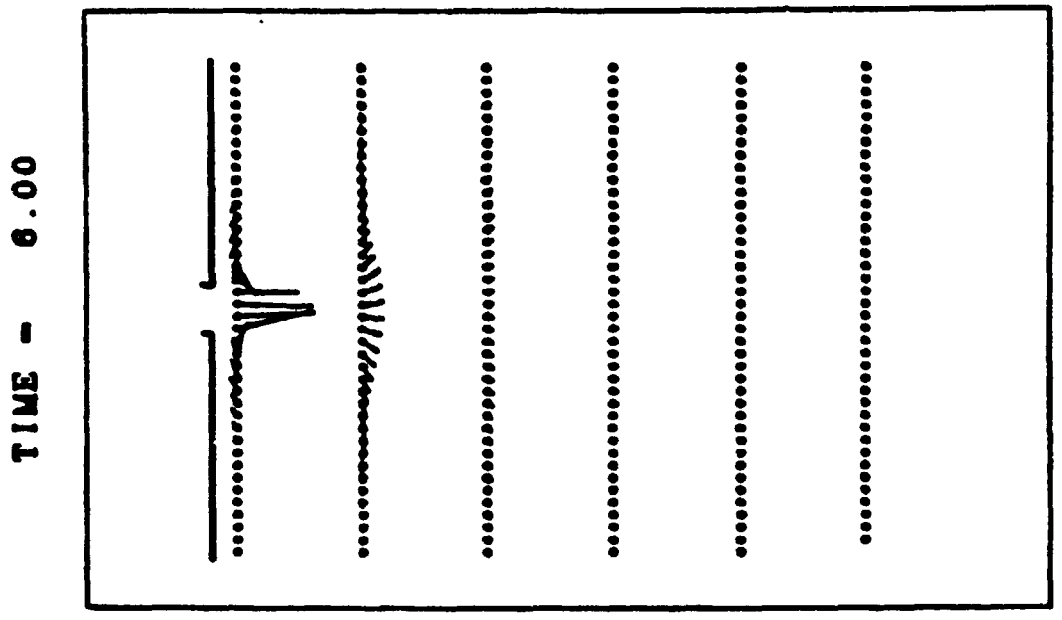

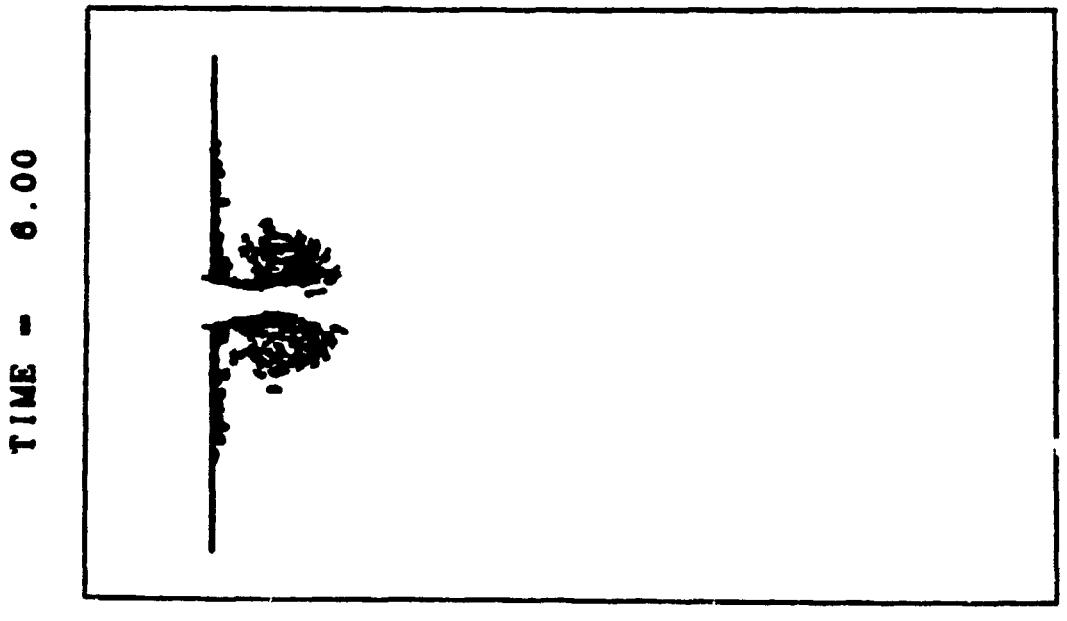

Figure 40 - b

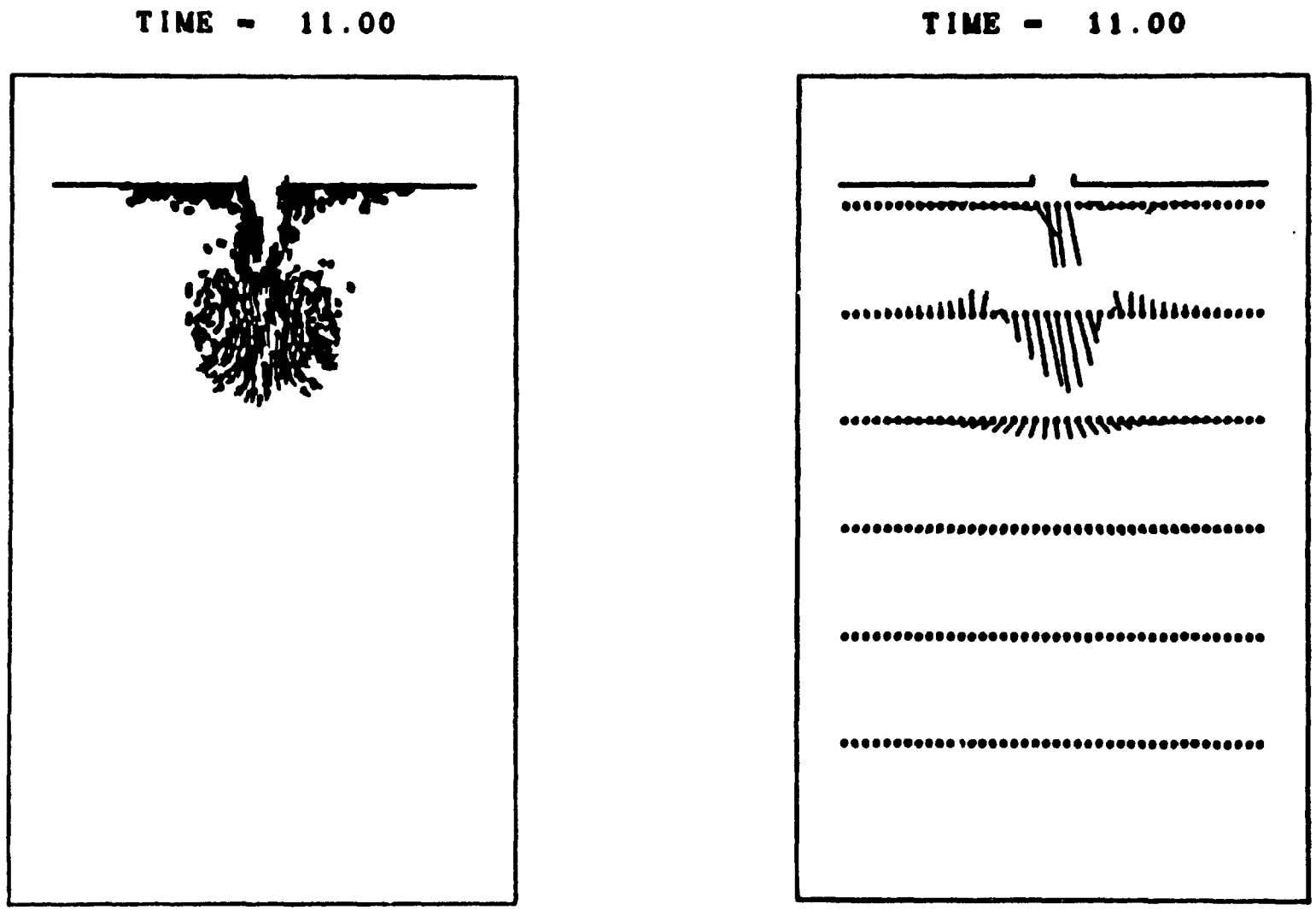

Figure 40 - c

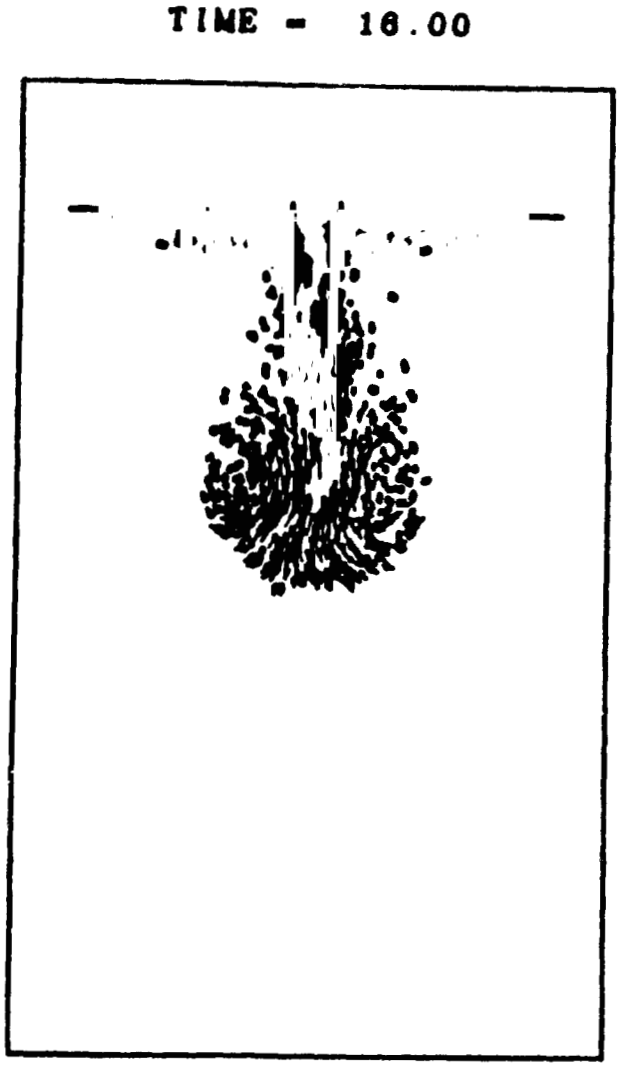

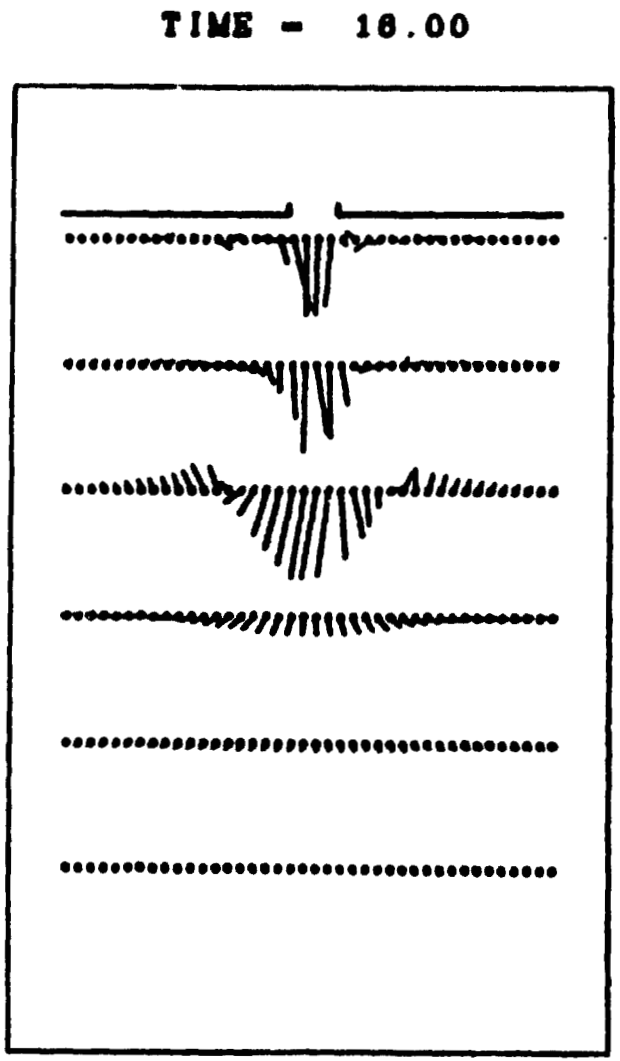

Figure 40 - d

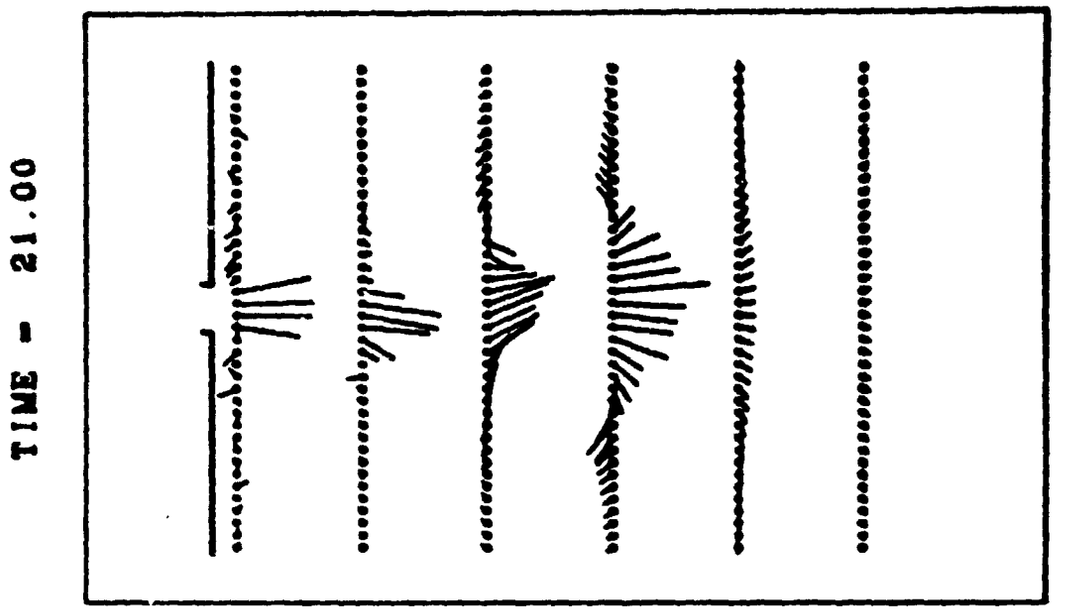

Figure 40 - e

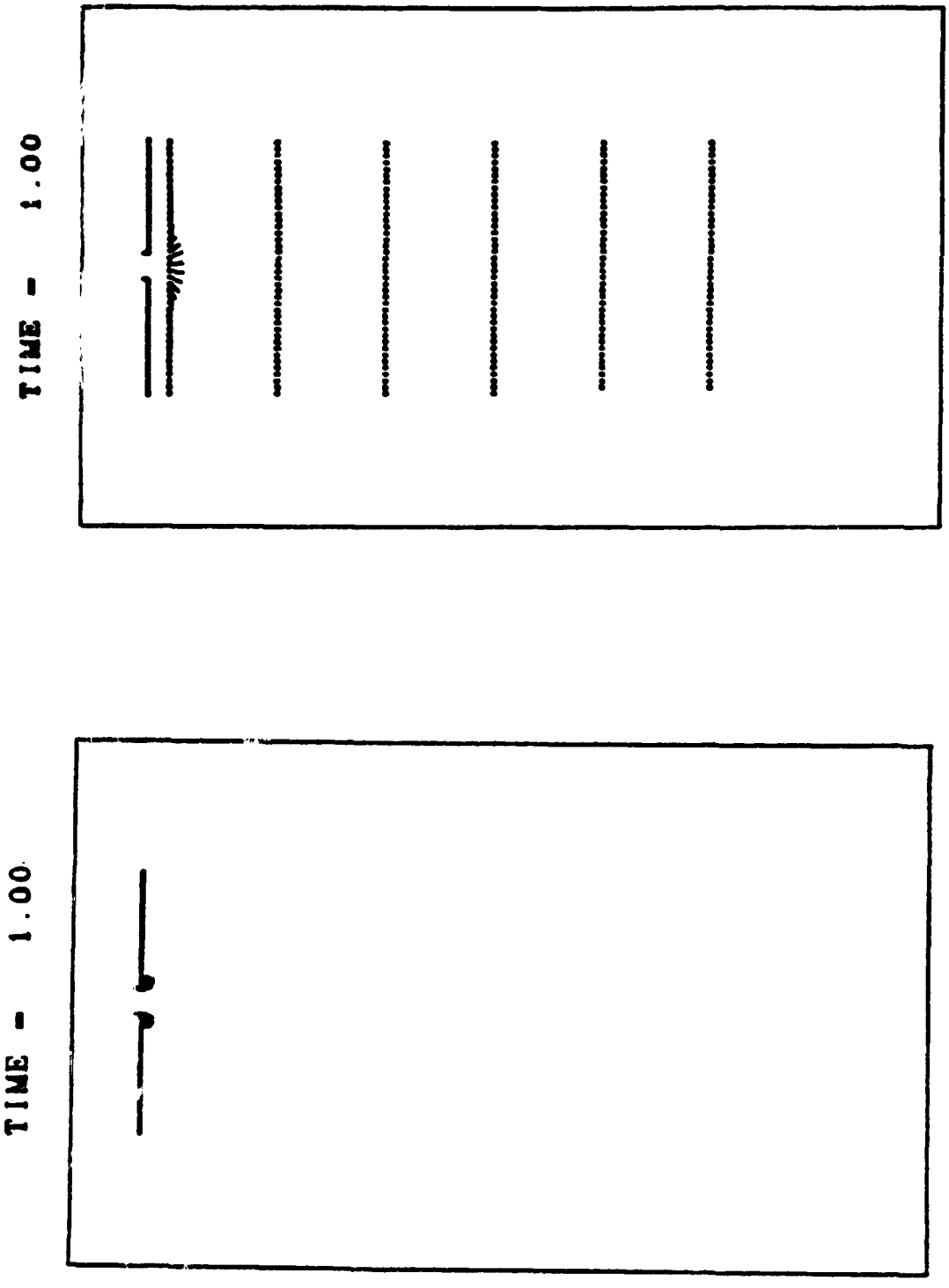

Figure 41 - a

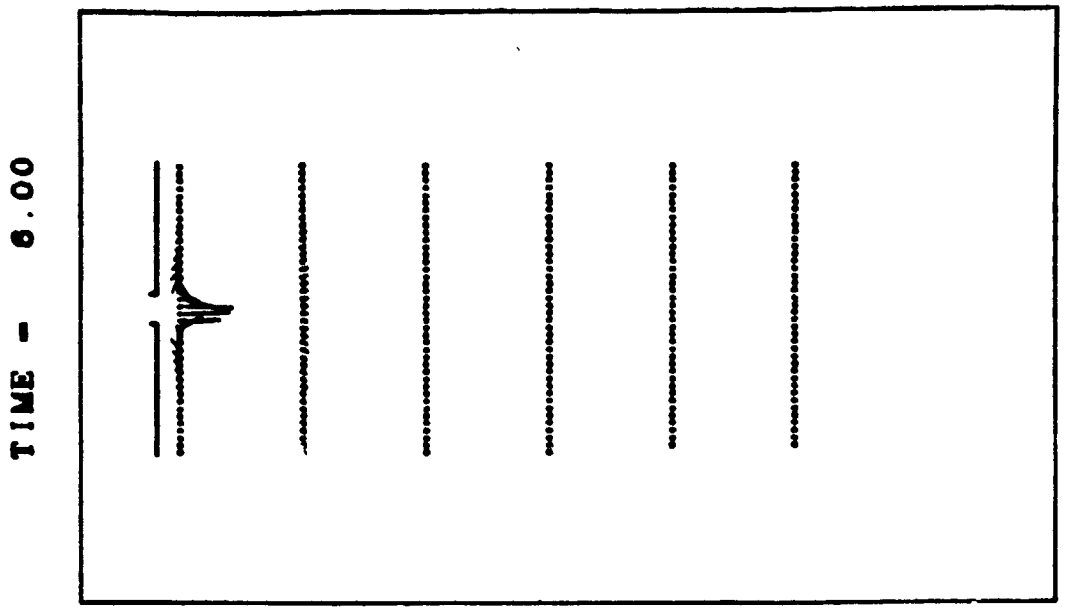

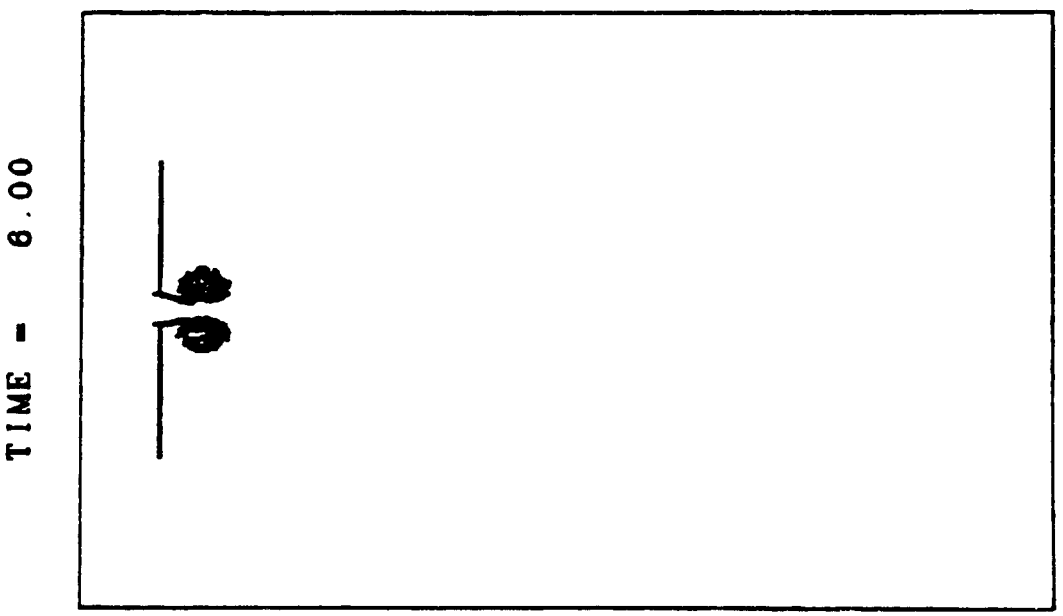

Figure 41 - b

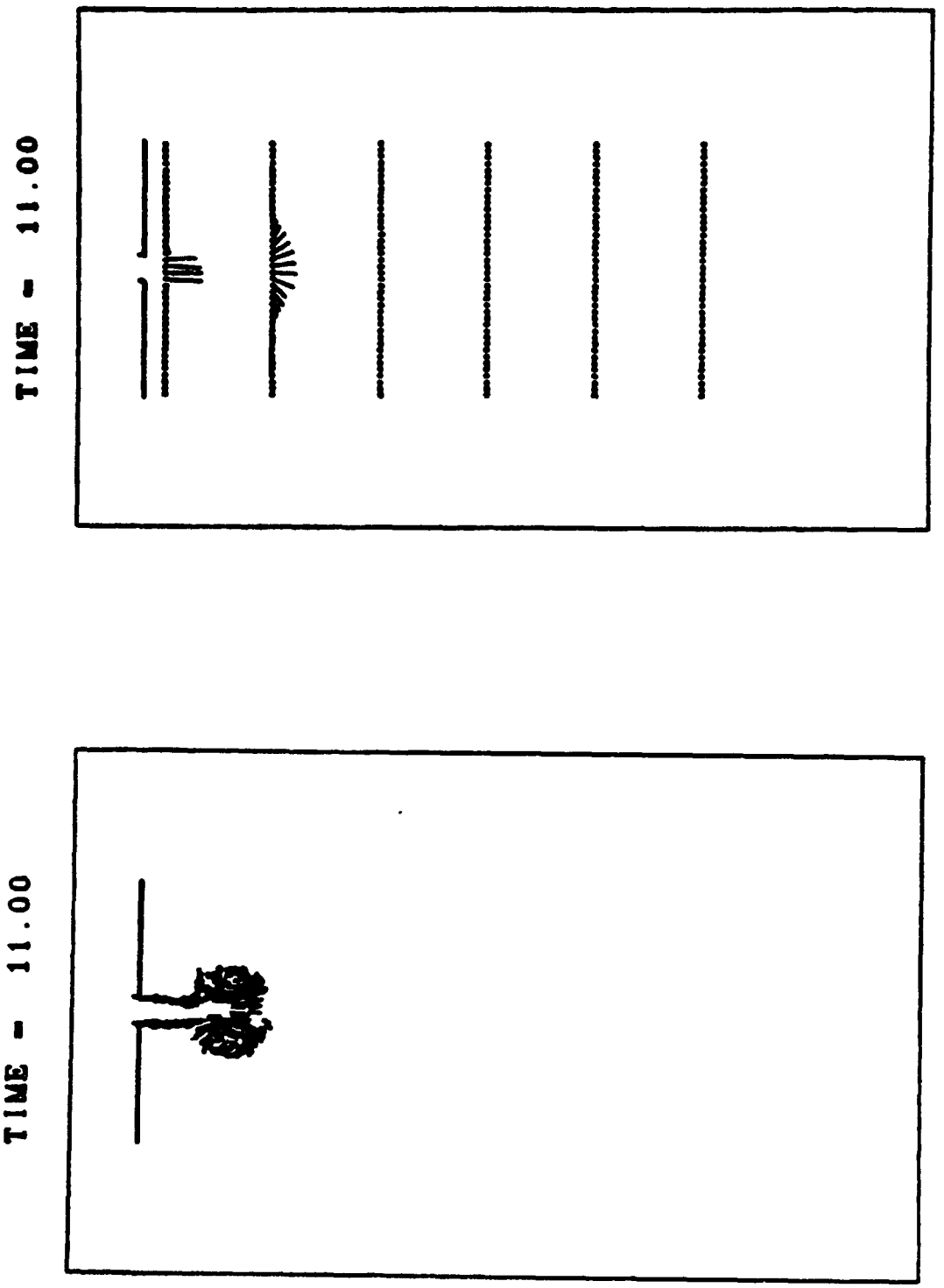

Figure 41 - c

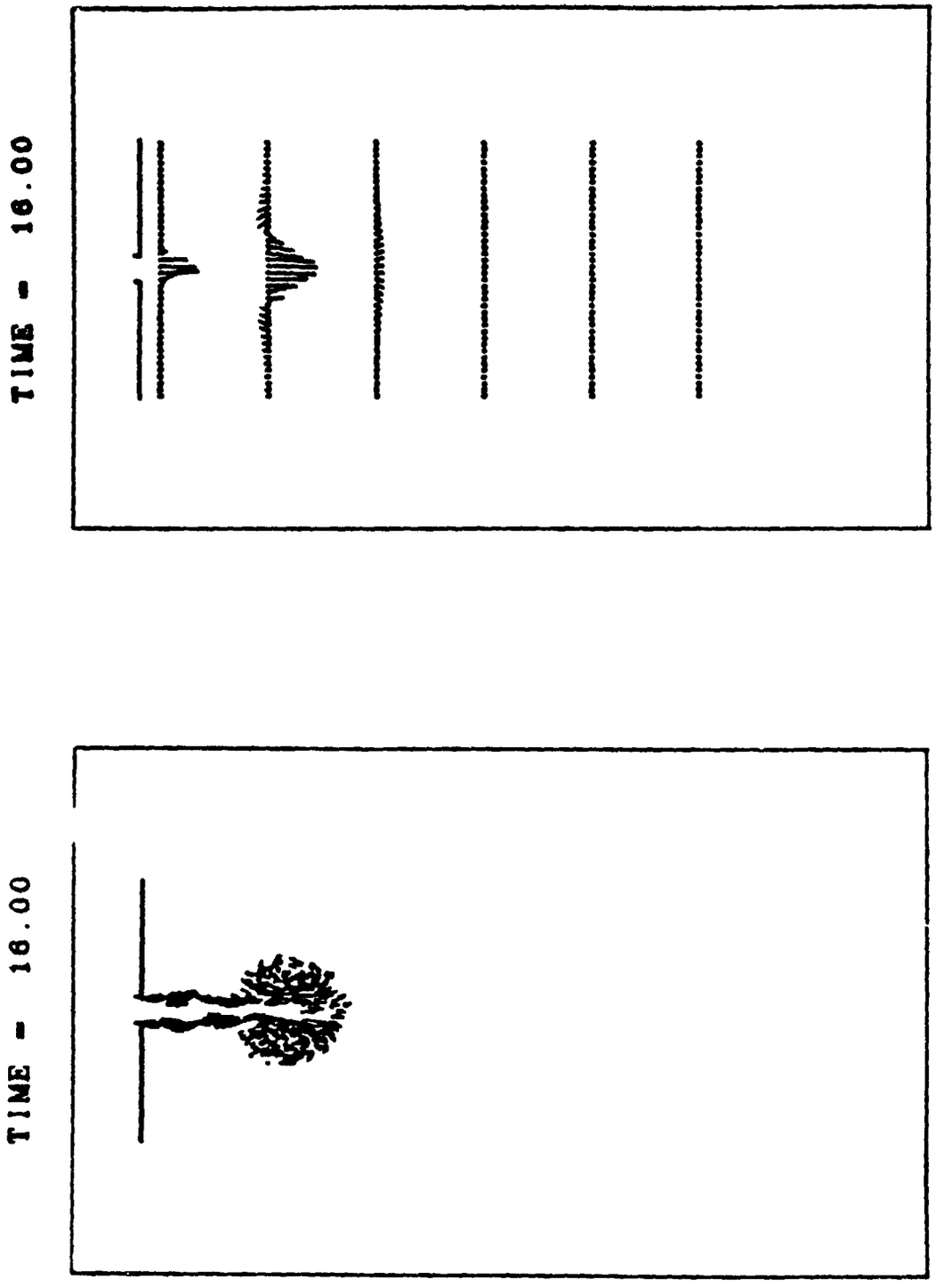

Figure 41 - d

Figure 41 - e

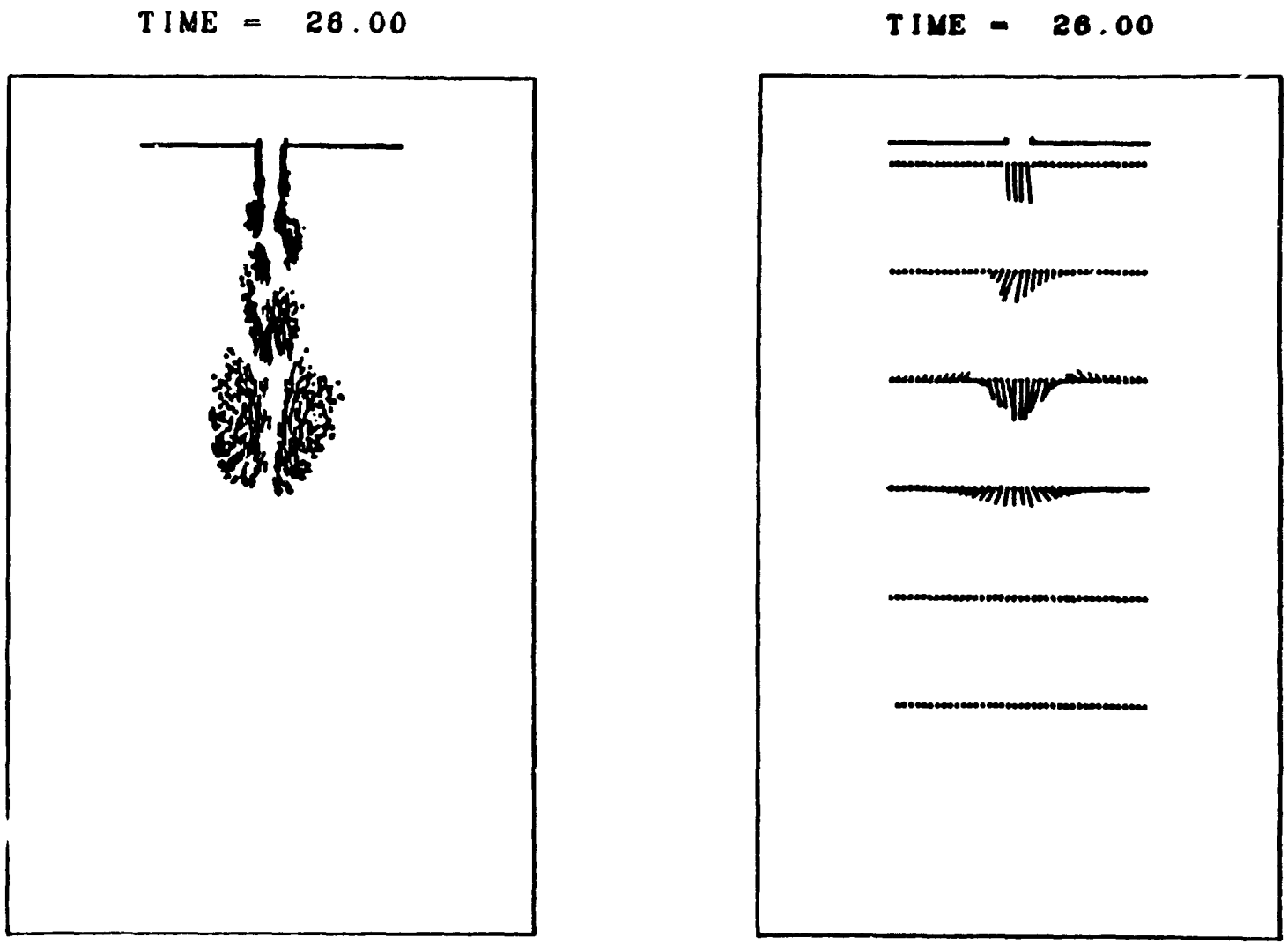

Figure 41 - f

Figure 41 - g

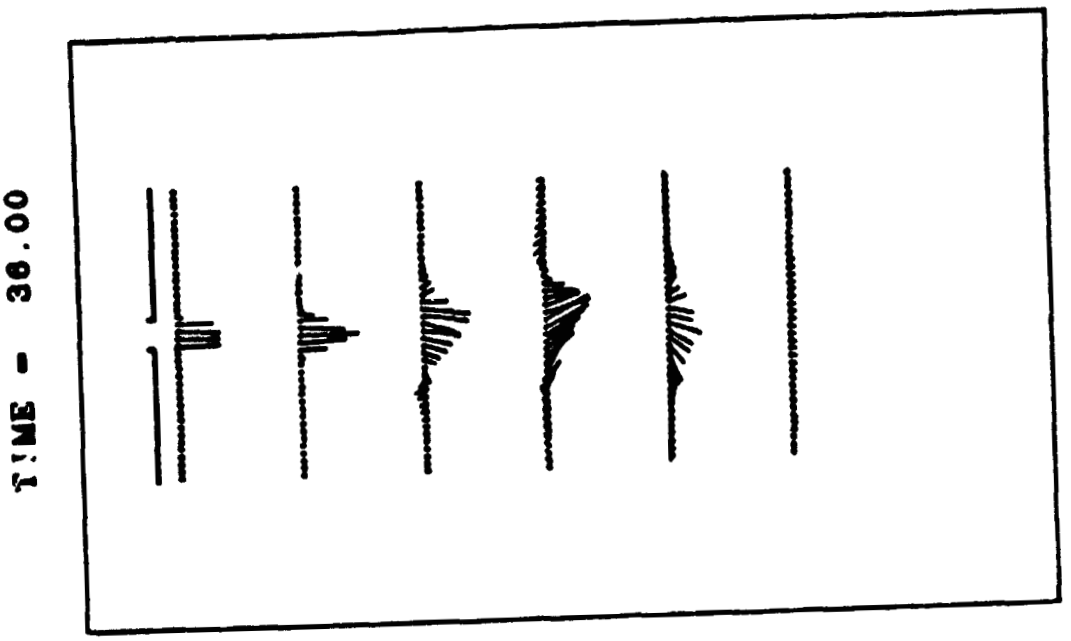

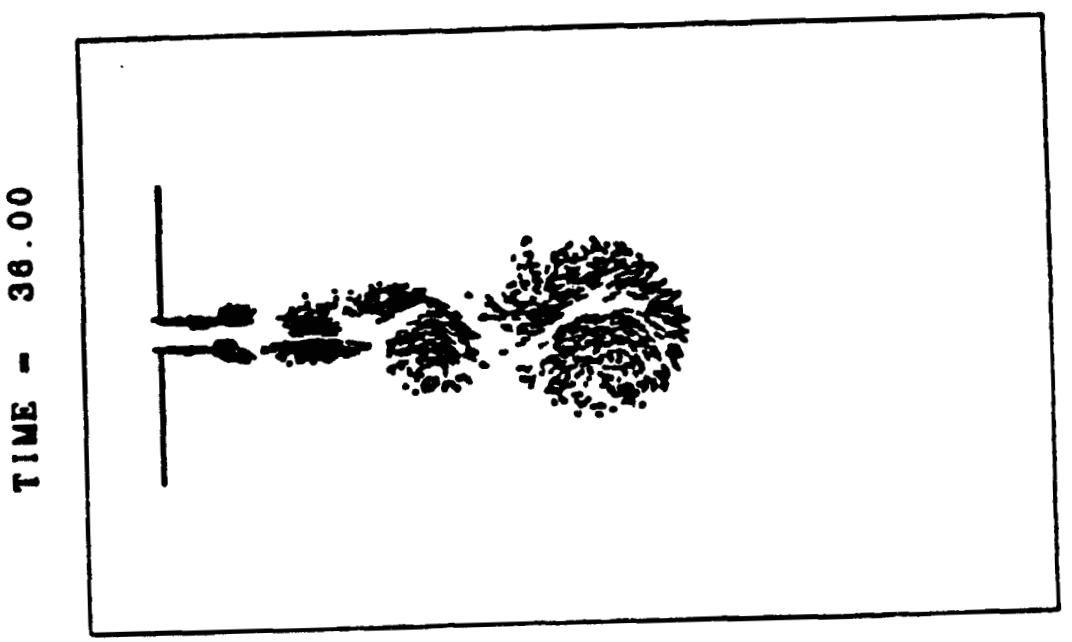

Figure 41 - h

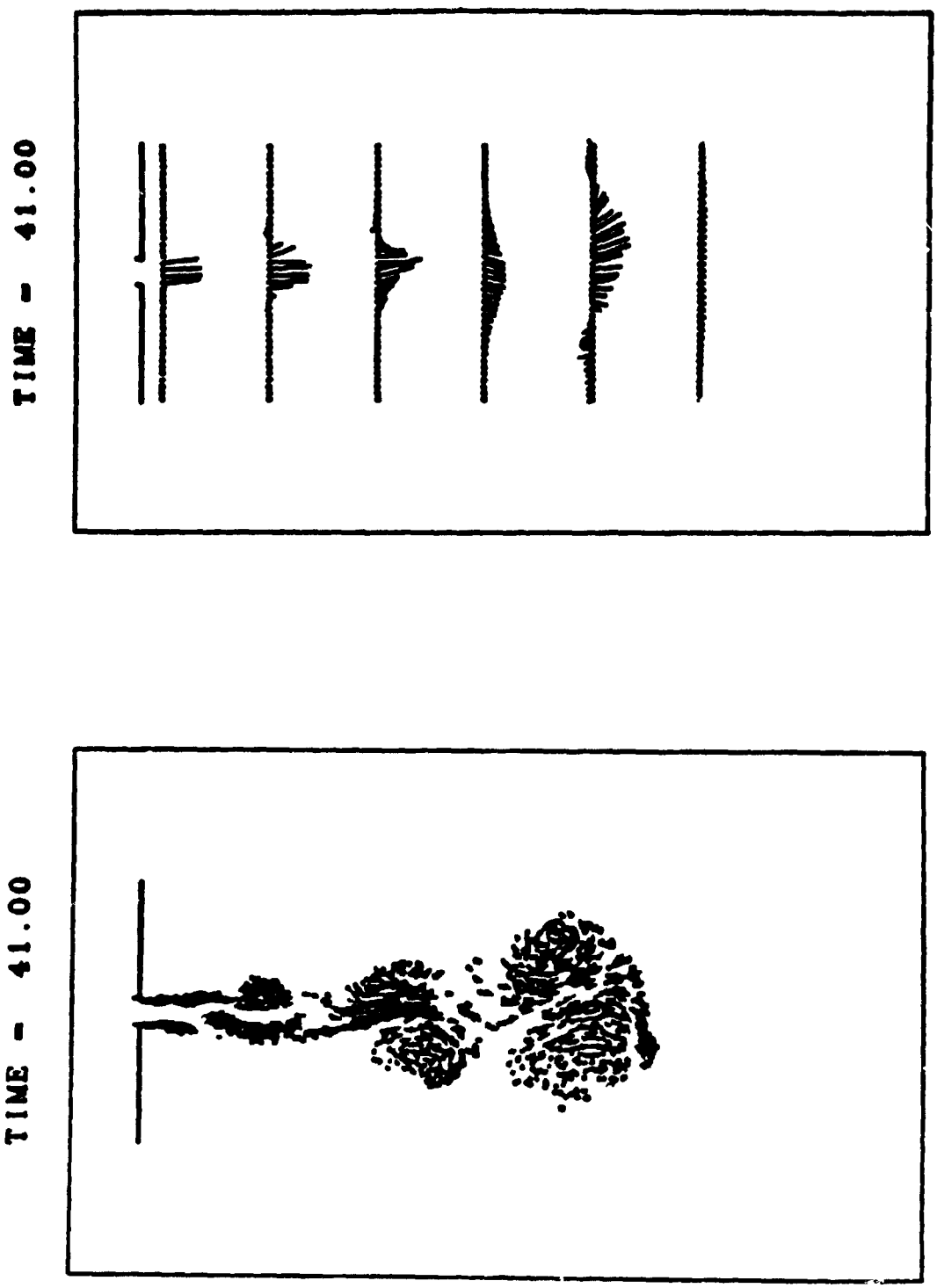

Figure 41 - i

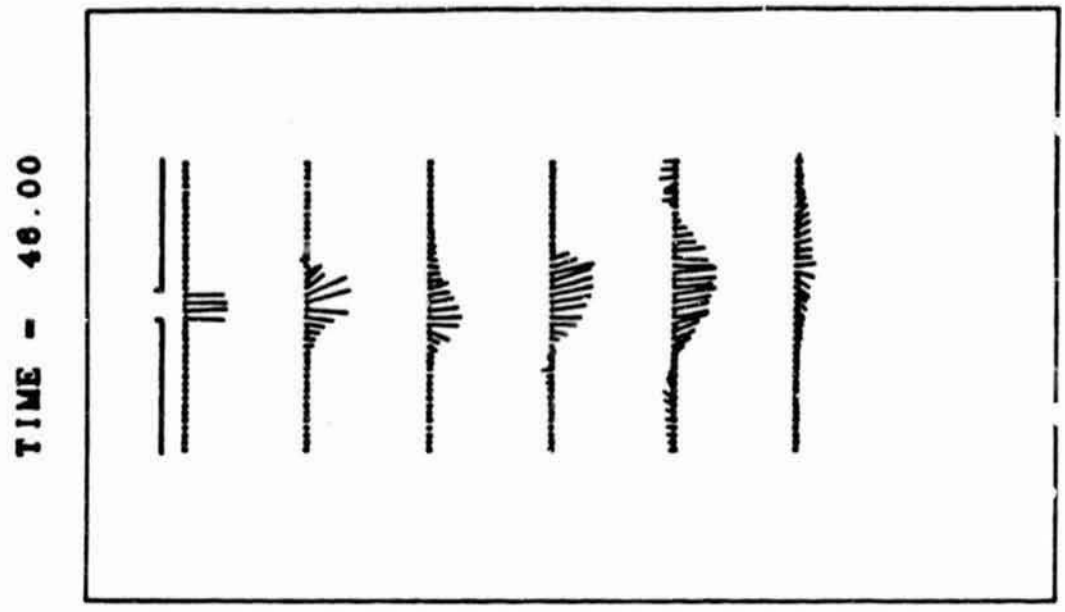

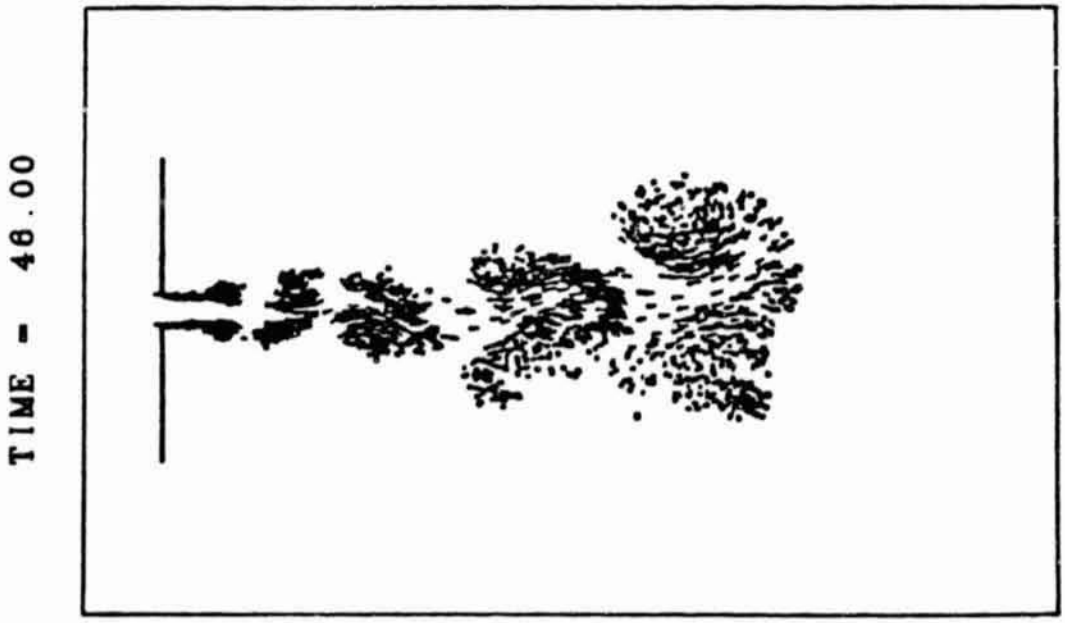

Figure 41 - j

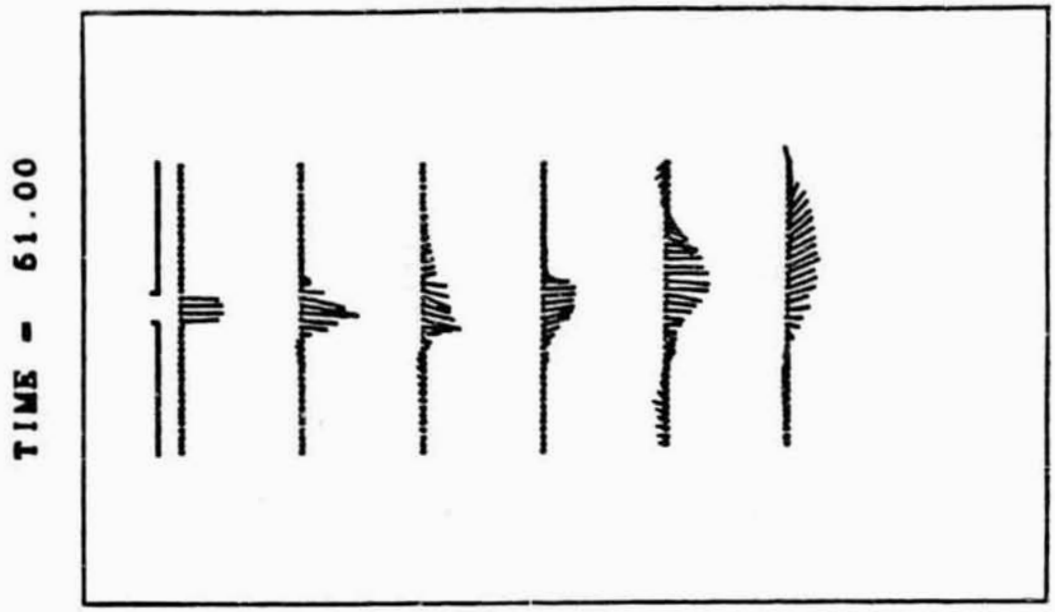

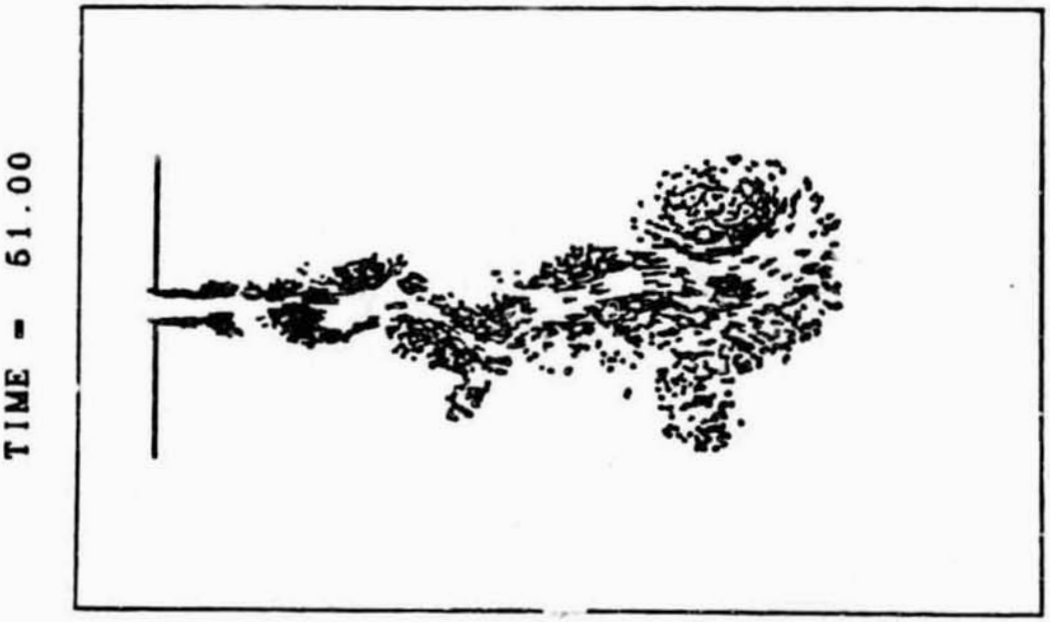

Figure 41 - k

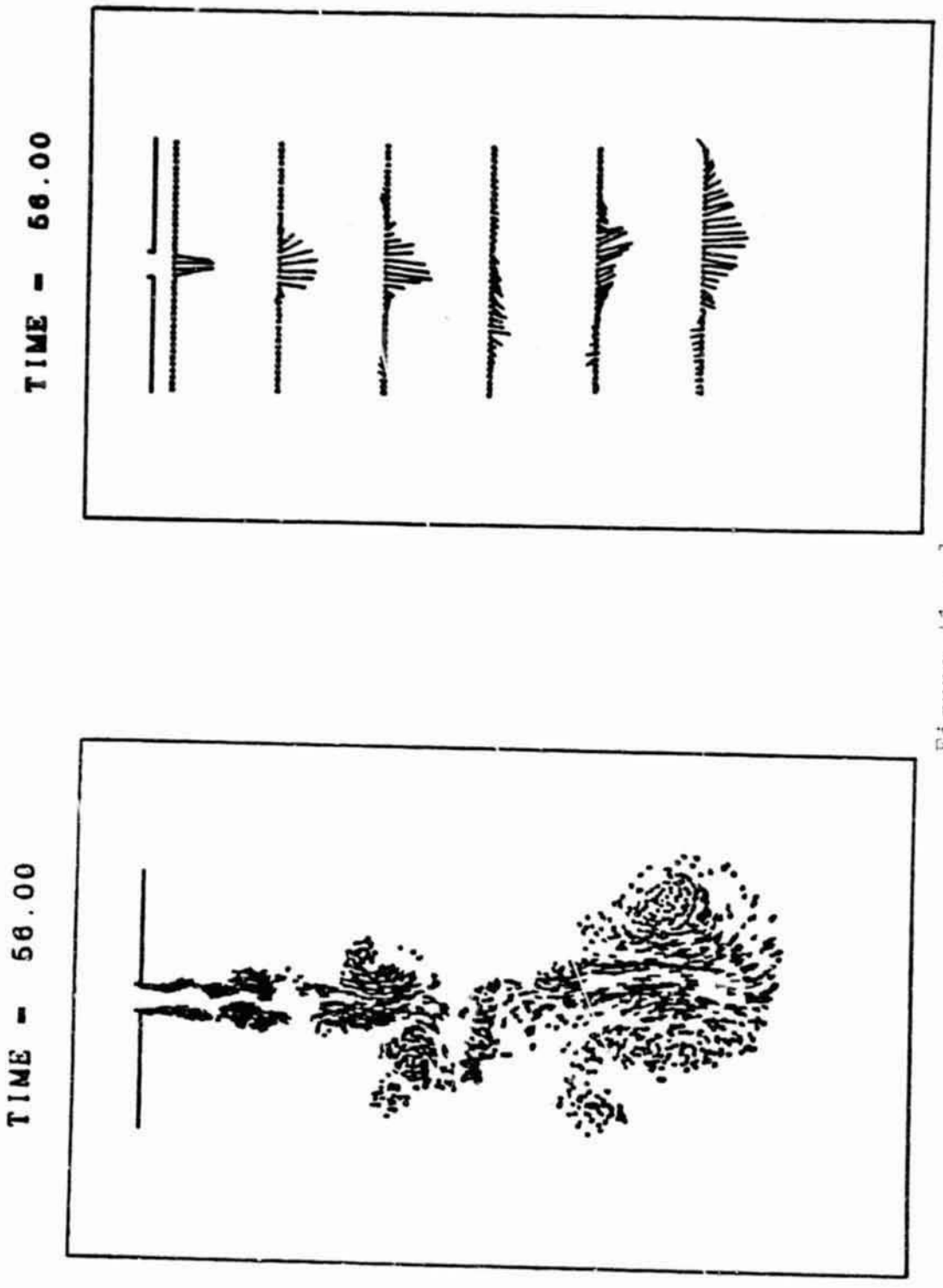

Figure 41 - 1

Figure 41 - m

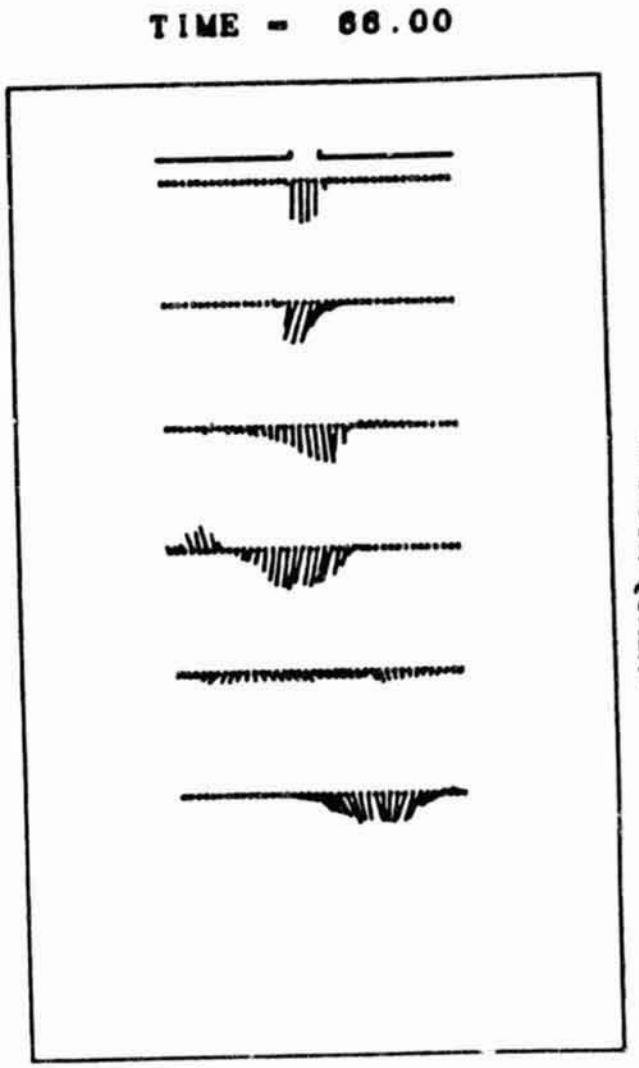

Figure 41 - n

Figure 42 - a

Figure 42 - b

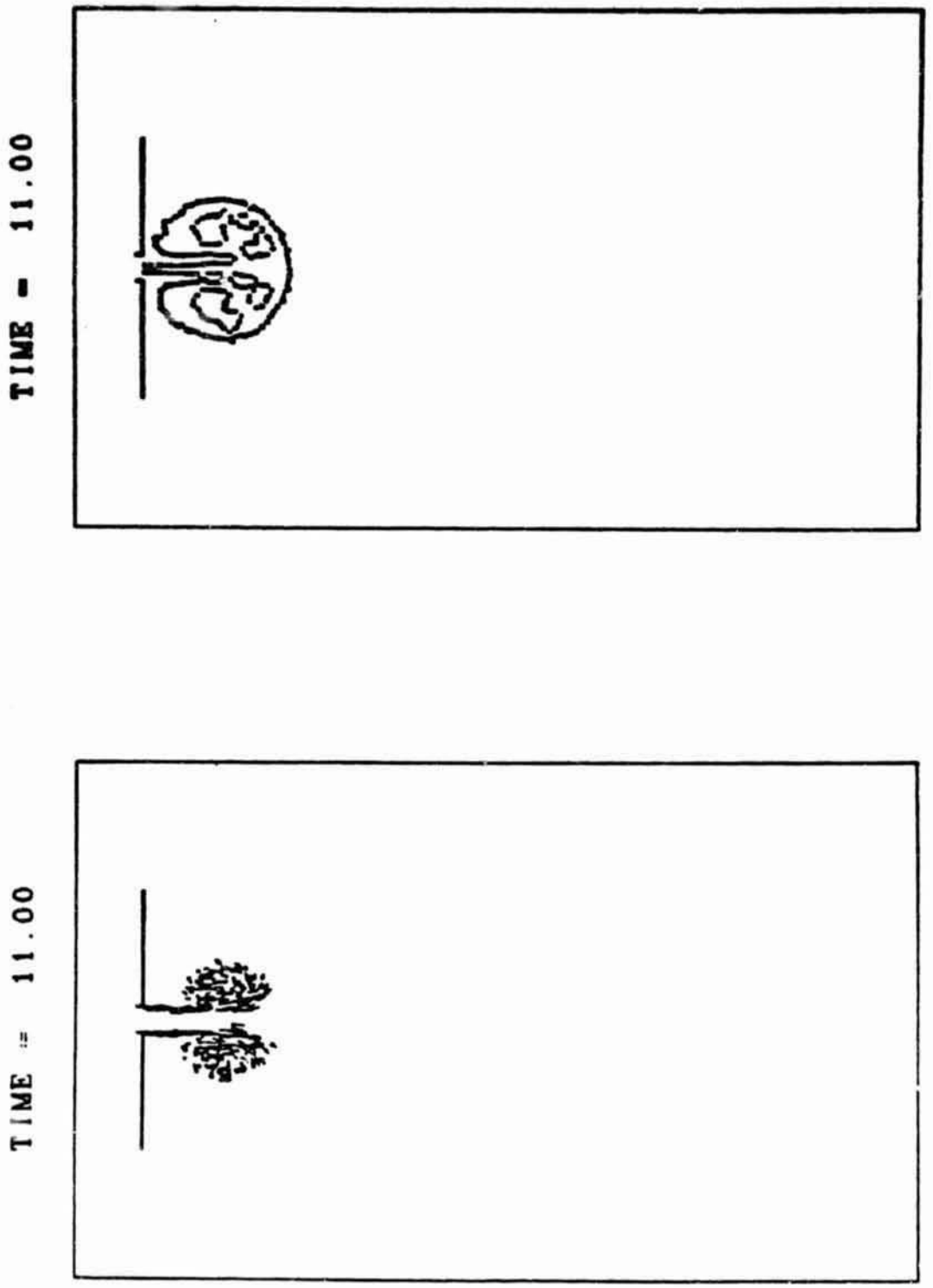

Figure 42 - c

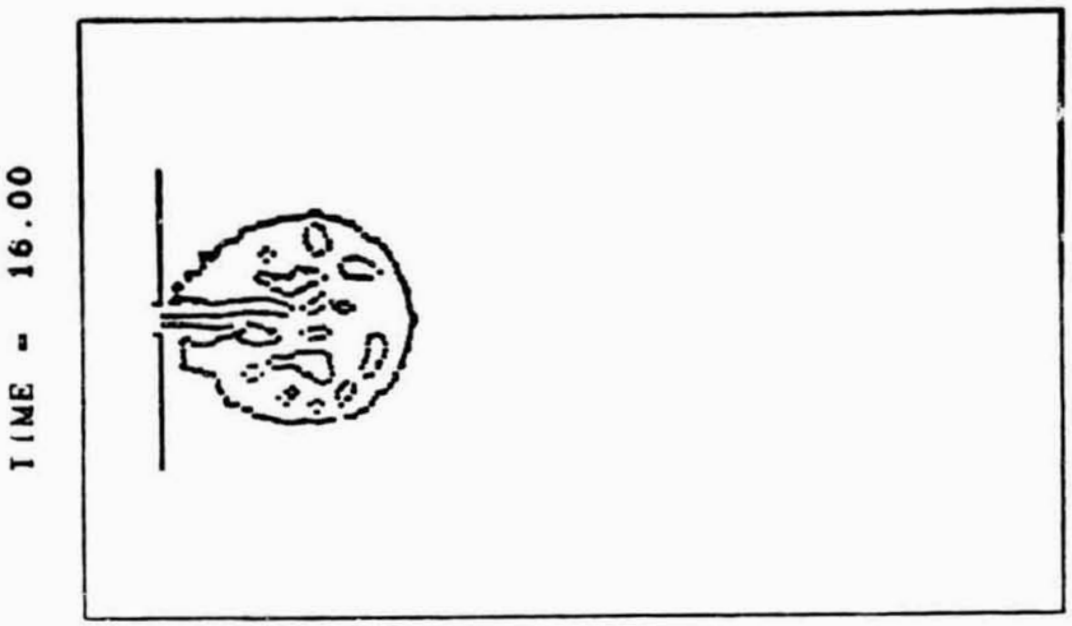

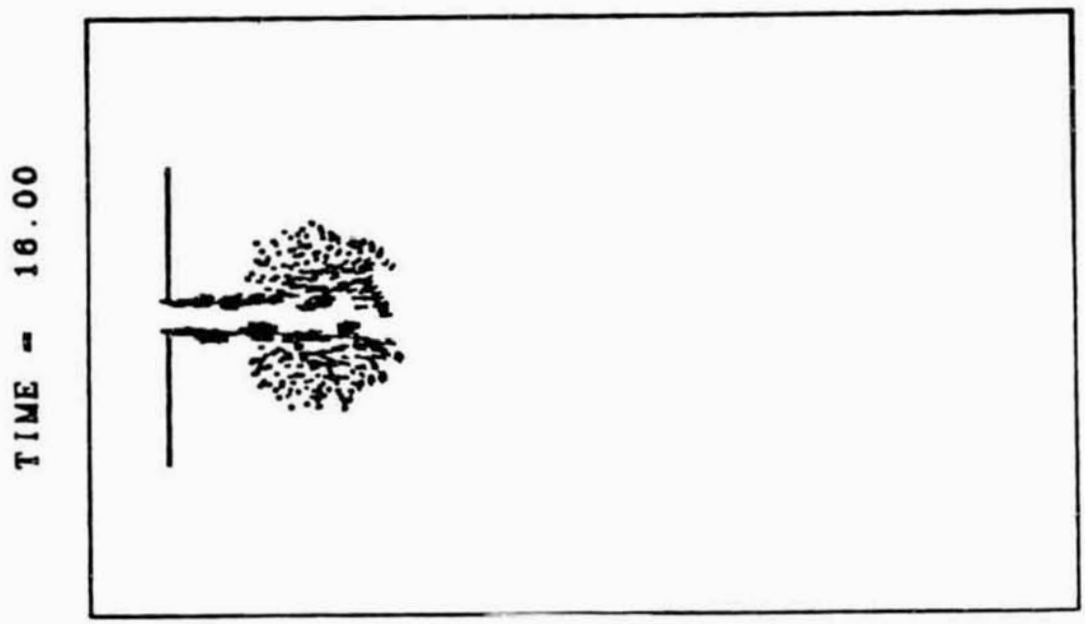

Figure 42 - d

Figure 42 - e

a b

Figure 43

c d

Figure 43

Figure 43

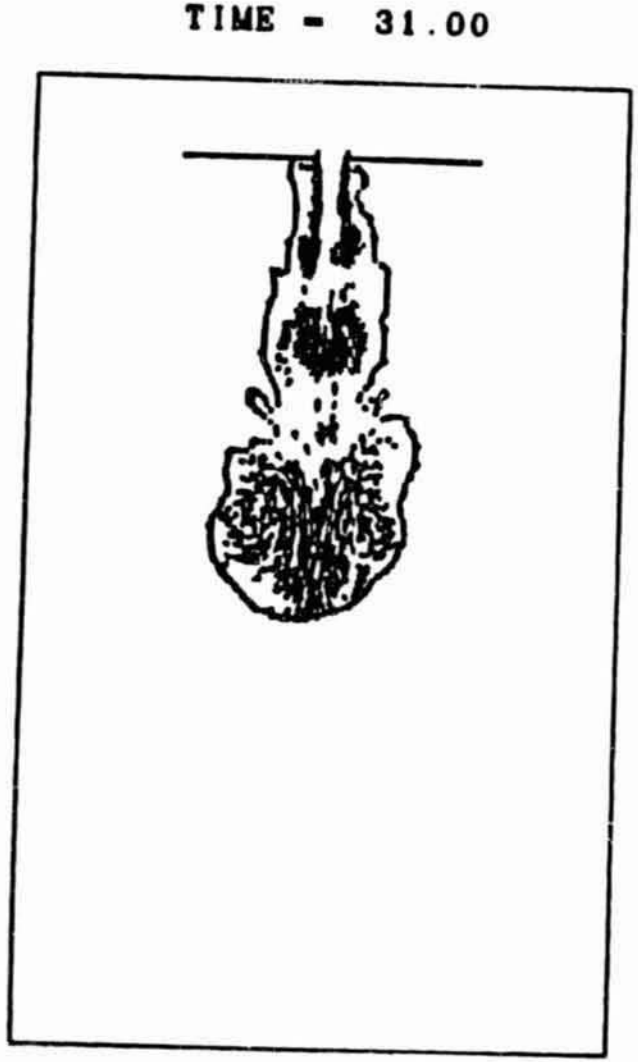

g

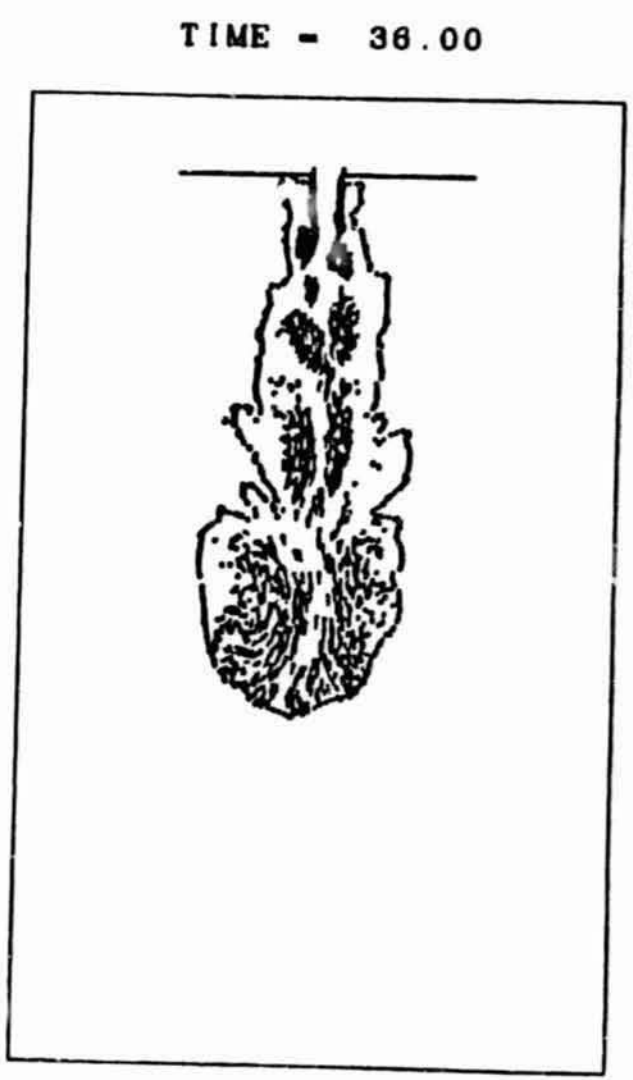

h

Figure 43